NORTHWESTERN UNIVERSITY

Biophysical and Structural Characterization of Particulate Methane Monooxygenase and Methanobactin from *Methylosinus trichosporium* OB3b

A DISSERTATION

SUBMITTED TO THE GRADUATE SCHOOL
IN PARTIAL FULFILLMENT OF THE REQUIREMENTS

for the degree

DOCTOR OF PHILOSOPHY

Field of Chemistry

By

Amanda Sarah Hakemian

EVANSTON, ILLINOIS

June 2008

ABSTRACT

Biophysical and Structural Characterization of Particulate Methane Monooxygenase and Methanobactin from *Methylosinus trichosporium* OB3b

Amanda Sarah Hakemian

Particulate methane monooxygenase (pMMO) is a membrane-bound metalloenzyme that oxidizes methane to methanol in methanotrophic bacteria. The nature of the pMMO active site and the overall metal content are controversial, with spectroscopic and crystallographic data suggesting the presence of a mononuclear copper center, a dinuclear copper center, a trinuclear center, and a diiron center or combinations thereof in various samples. Most studies have focused on pMMO from *Methylococcus capsulatus* (Bath). In this work, pMMO from a second organism, *Methylosinus trichosporium* OB3b, has been purified and characterized by spectroscopic and crystallographic methods. Purified *M. trichosporium* OB3b pMMO contains ~2 copper ions per 100 kDa protomer. Electron paramagnetic resonance (EPR) spectroscopic parameters indicate type 2 Cu(II) is present as two distinct species. Extended X-ray absorption fine structure (EXAFS) data are best fit with oxygen/nitrogen ligands and a Cu-Cu interaction at 2.52 Å.

The crystal structure of *M. trichosporium* OB3b was solved to 3.9 Å resolution. Crystallographic characterization of *M. trichosporium* OB3b pMMO shows that a mononuclear copper center found in the *M. capsulatus* (Bath) pMMO X-ray structure is not present whereas a dinuclear copper center is clearly conserved. Notably, a metal center occupied by zinc in the *M.*

capsulatus (Bath) pMMO structure is occupied by copper in *M. trichosporium* OB3b pMMO. These findings extend previous work on pMMO from *M. capsulatus* (Bath) and provide new insight into the functional importance of the different metal centers.

The oxidation state of copper bound to methanobactin, a small siderophore-like molecule from *M. trichosporium* OB3b, was also investigated. Purified methanobactin loaded with Cu(II) exhibits a weak EPR signal probably due to adventitious Cu(II). The EPR signal intensity increases significantly upon addition of the strong oxidant nitric acid. Features of the X-ray absorption near edge spectrum, including a 1s→4p transition at 8985.5 eV, further indicate the presence of Cu(I). EXAFS data were best fit using a multiple scattering model generated from previously reported crystallographic parameters. These results establish definitively that *M. trichosporium* OB3b methanobactin binds Cu(I) and suggest that methanobactin itself reduces Cu(II) to Cu(I).

ACKNOWLEDGEMENTS

First and foremost, I would like to acknowledge my thesis advisor, Professor Amy Rosenzweig. She has fostered an open and supportive laboratory environment, and provided invaluable guidance over the years. I am especially grateful for her flexibility and support of my decision to seek out additional teaching experience as a graduate student, in spite of the fact that it took me away from the lab.

I am lucky to have worked in such a wonderful laboratory. Dr. Raquel Lieberman deserves credit for not only laying the groundwork for the pMMO project in the lab, but also for being an excellent example of how much a dedicated graduate student can accomplish. Deepak Shrestha taught me everything I know about growing methanotrophs. Christine Tinberg, who worked with me as an undergraduate at NU, did much of the work developing the production and purification of methanobactin, and it has been a pleasure to watch her go on to graduate school and continue to grow as a scientist. I have enjoyed working closely with Stephen Smith, as we pursued parallel and similarly difficult projects, often literally side by side. The other members of the methanotroph subgroup, Uchechi Ukaegbu, Thomas Lawton and Dr. Ramakrishnan Balasubramanian, have been a source of endless discussion and inspiration. Drs. Monika Sommerhalter, Carnie Abajian and Matthew Sazinsky were all gracious in sharing their time and knowledge with me when I was first learning crystallography. Finally, I thank all other Rosenzweig lab members, past and present, for making it a great place to work: Dr. Liliya Yatsunyk, Dr. Shannon Henery, Matthew Traverso, Sorabh Agarwal, and Eliza Zielazinski.

It has been my privilege to work with excellent collaborators throughout this project. Professor Timothy Stemmler generously took the time to teach me to collect and analyze XAS data and Kalyan Kondapalli, a graduate student in his lab, has contributed substantial effort to the XAS characterization of pMMO and methanobactin. Professor Joshua Telser of Roosevelt University has patiently run countless EPR samples and answered numerous questions over the years, and together with Professor Brian Hoffman of Northwestern University has been instrumental in completing this aspect of the project. Qiang Fu and Liang Li in the laboratory of Rustem Ismagilov at The University of Chicago devoted much time and thought to extensively screening pMMO crystallization conditions.

I have benefited greatly from the support and feedback provided by the members of my committee: Professors Brian Hoffman, Jon Widom, Alfonso Mondragón and Thomas O'Halloran. A special thank you is due to Dr. Mondragón, who kindly agreed to serve as a substitute on my defense committee when scheduling problems arose.

Throughout my life, I have been blessed with the love and encouragement of my family. I would especially like to thank my parents, Rick and Peggy Hakemian, my sisters, Victoria and Jillian Hakemian, my grandparents, Robert and Marion Hakemian and Ashby and the late June Kelley, and my in-laws, William and Barbara Miller, who have all been there to cheer me on during my time in graduate school. Most importantly, I thank my husband, Aaron Miller, for his endless love and support, and for being my best friend.

TABLE OF CONTENTS

LIST OF FIGURES

LIST OF TABLES

CHAPTER 1: THE BIOCHEMISTRY OF METHANE OXIDATION

A previous version of this chapter has been published as Hakemian, A. S.; Rosenzweig, A.C. The biochemistry of methane oxidation. *Ann. Rev. Biochem.* **2007,** *76*, 223-241.

ABSTRACT

Methanotrophic bacteria oxidize methane to methanol in the first step of their metabolic pathway. Two forms of methane monooxygenase (MMO) enzymes catalyze this reaction: soluble MMO (sMMO) and membrane-bound or particulate MMO (pMMO). pMMO is expressed when copper is available, and its active site is believed to contain copper. Whereas sMMO is well characterized, most aspects of pMMO biochemistry remain unknown and somewhat controversial. This introduction emphasizes recent advances related to pMMO and to copper uptake and copper-dependent regulation in methanotrophs. The pMMO metal centers have been characterized spectroscopically, and the first pMMO crystal structure has been determined. Significant effort has been devoted to improving in vitro pMMO activity. Proteins involved in sMMO regulation and additional copper-regulated proteins have been identified, and the *Methylococcus capsulatus* (Bath) genome has been sequenced. Finally, methanobactin (mb), a small copper chelator proposed to facilitate copper uptake, has been characterized.

INTRODUCTION

Methanotrophic bacteria utilize methane as their sole carbon and energy source (*1*). Found in a variety of habitats, including extreme environments (*2*), methanotrophs comprise 13 genera within the α and γ Proteobacteria (*3*). These organisms play an important role in the global carbon cycle and are potentially useful in curtailing the contribution of methane emissions to global warming (*1, 4, 5*). Oxidation of methane to methanol, the first step in methane metabolism, is catalyzed by methane monooxygenase (MMO) enzymes, which have attracted much attention for their possible applications in catalyst development (*6*) and/or bioremediation (*7, 8*). There are two forms of MMO, soluble MMO (sMMO) (*9*) and membrane-bound or particulate MMO (pMMO) (*10*). All but one genus of methanotrophic bacteria express pMMO, and a small subset produces both pMMO and sMMO (*3*). In this subset, differential expression of the two MMOs is controlled by the concentration of copper in the growth medium, with sMMO only produced at low copper concentrations (*11-13*). The mechanism of this "copper switch" is not known. Most studies of MMO have focused on enzymes from two organisms in this subset, *Methylococcus capsulatus* (Bath) and *Methylosinus trichosporium* OB3b.

sMMO comprises three components, a hydroxylase (MMOH), which houses the active site, a reductase (MMOR), which shuttles electrons from NADH to the active site of MMOH, and a regulatory protein (MMOB) that is required for activity (*9*). MMOH consists of three polypeptides arranged as an $\alpha_2\beta_2\gamma_2$ dimer (*14*). Methane and dioxygen bind at a carboxylate-bridged diiron center, similar to diiron centers found in the ribonucleotide reductase R2 protein (*15*), the stearoyl acyl-carrier protein Δ9 desaturase (*16*), and a growing family of bacterial multicomponent monooxygenases (BMMs) that includes toluene monooxygenases, phenol

hydroxylases, and alkene monooxygenases (*17*). A number of recent reviews have focused on structural (*18*), mechanistic (*19*), and evolutionary (*17*) aspects of sMMO and the BMM family. Because sMMO has a wide substrate specificity, oxidizing alkanes, alkenes, and aromatics (*20*), it has been a favored target for bioremediation applications (*8*). pMMO is more practical for in situ bioremediation for two reasons, however. First, only a few methanotrophs produce sMMO (*3*), and second, sMMO expression is repressed at the high levels of copper found in polluted environments (*21*).

Although pMMO is much more prevalent than sMMO in nature, less is known about its biochemistry, owing to difficulties working with an integral membrane protein. pMMO is composed of three subunits, α, β and γ, also known as pmoB, pmoA, and pmoC, respectively (*10, 22*). Ammonia monooxygenase (AMO), a pMMO homolog and the only enzyme other than sMMO and pMMO known to oxidize methane, has a similar polypeptide composition (*23, 24*). The metal content of pMMO has been controversial, but the active site is generally believed to contain copper ions (*10, 25*). pMMO has a more limited substrate specificity than sMMO (*26*), a property that could potentially be altered for bioremediation purposes once the active site has been characterized.

Whereas sMMO was the main focus in the field of methane oxidation biochemistry 10–20 years ago, interest in pMMO has been increasing over the past decade. This chapter focuses on recent advances in biological methane oxidation related to pMMO and to copper uptake and copper-dependent regulation in methanotrophs. Significant discoveries in the past two to three years include completion of the *M. capsulatus* (Bath) genome, identification and characterization of proteins involved in regulation of sMMO, detection of additional proteins that are copper

regulated, more complete spectroscopic characterization of the pMMO metal centers, the first crystal structure of pMMO, improved activity for isolated pMMO, and detailed characterization of a novel copper chelator called methanobactin (mb). We highlight these advances, which were reported after the last comprehensive pMMO review (*10*), in the context of previous work with an emphasis on key unresolved issues.

GENETICS AND REGULATION

The genome of *M. capsulatus* (Bath) was completed and was the first methanotroph genome to become available. Proteins that may participate in the regulation of sMMO as well as additional copper-regulated genes have been identified recently.

The M. capsulatus *(Bath) Genome*

The *M. capsulatus* (Bath) genome comprises 3.3 megabases and includes 51 identifiable insertion elements and two putative prophages (*27*). As determined previously (*28, 29*), the genes encoding pMMO are present in multiple copies with two complete copies of the *pmoCAB* operon and a third copy of *pmoC*, *pmoC3*, located adjacent to three genes of unknown function. Mutants of *M. capsulatus* (Bath) in which one of the two copies of the *pmoCAB* operon is disrupted grow on methane, although they show decreased methane oxidation rates compared to wild-type bacteria. If both gene copies are disrupted, the cells are not viable, however. Interestingly, researchers were unable to isolate mutants in which *pmoC3* is disrupted, indicating this gene may play an essential role in methanotroph growth (*29*). Redundancy is also observed for other enzymes in the metabolic pathway, including methanol dehydrogenase and formate dehydrogenase. By contrast, the genes encoding sMMO occur only once. A transposase is present in some clones between the *mmoB* and *mmoZ* genes, which encode the regulatory protein

B and the γ subunit of MMOH, respectively (*30*). Beyond the genes encoding enzymes in methane-dependent metabolism, genome analysis suggests the ability of methanotrophs to utilize sugars, oxidize chemolithotrophic hydrogen and sulfur, and exist under conditions of low oxygen tension (*27*). This proposed metabolic flexibility is not necessarily consistent with known methanotroph physiology and requires further study (*31*).

Copper trafficking proteins encoded by the genome may be of importance in the copper-regulated expression of the two MMOs or copper delivery to pMMO. Three homologs of the P_{1B}-type copper transporting ATPases are encoded (MCA0705, MCA0805, MCA2072) (*32*) as are homologs of soluble copper chaperones in the Atx1/CopZ (MCA0611) (*33, 34*) and PcoC/CopC (MCA0808, MCA2170) (*35, 36*) families. There is also a putative metal responsive transcription factor (MCA1339), annotated as a mercuric resistance operon regulatory protein. Finally, it should be noted that the genome encodes two putative nonribosomal peptide synthetases (MCA1883, MCA2107), which could be involved in the biosynthesis of the copper chelator mb (*37*) (*vide infra*).

Regulation of sMMO

In methanotrophs that express both forms of MMO, sMMO is expressed at < 0.8 μM copper in the growth medium, whereas at 4 μM copper, pMMO is expressed and extensive intracytoplasmic membranes develop (*12, 13, 38*). In *M. capsulatus* (Bath), the concentrations of the three pMMO polypeptides and of the pmoA transcript increase proportionally with copper levels in the medium, up to 60 μM copper, after which a decrease in the amounts of pMMO is observed (*38*). Candidate regulatory proteins for pMMO expression have not yet been identified. Addition of copper to both *M. capsulatus* (Bath) and *M. trichosporium* OB3b leads to a decrease

in sMMO mRNA (*39, 40*), consistent with the existence of a copper-binding repressor protein (*11, 41*). Copper-responsive transcriptional repressors or activators have not been identified, but some progress has been made toward understanding regulation of sMMO.

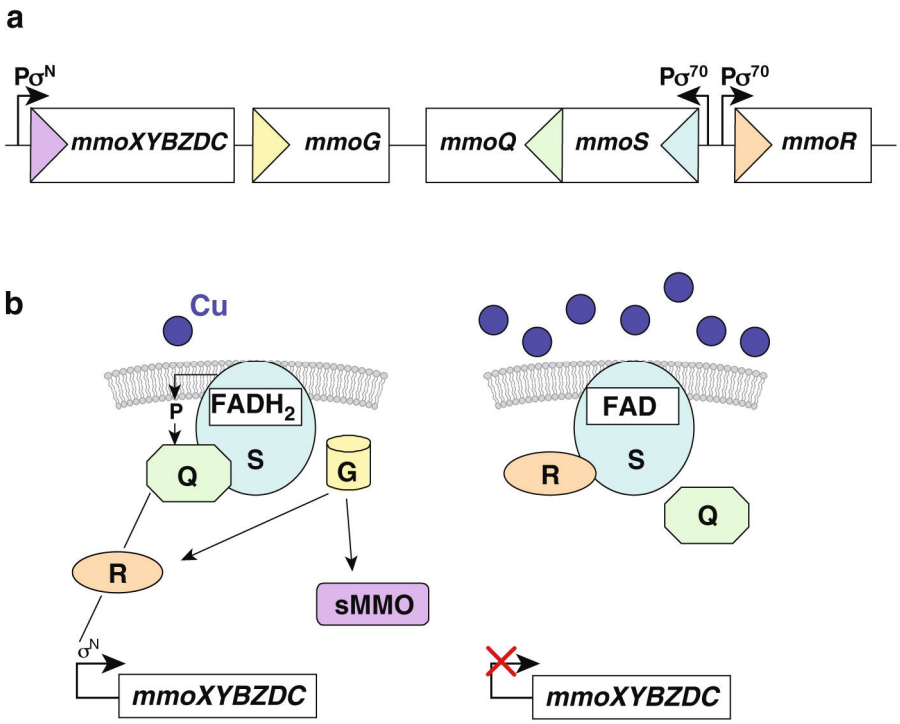

Figure 1.1. Regulation of sMMO
(a) In *M. capsulatus* (Bath), the regulatory genes *mmoG*, *mmoQ*, *mmoS*, and *mmoR* are found downstream of the *mmoXYBZDC* operon, which encodes the sMMO proteins. (b) Model for regulation of sMMO expression. (left) Low copper levels; (right) high copper levels. Abbreviations: FAD, flavin adenine dinucleotide; FADH2, reduced flavin adenine dinucleotide; G, MmoG; Q, MmoQ; R, MmoR; S, MmoS; $P\sigma^N$, σ^N-dependent promoter; $P\sigma^{70}$, σ^{70}-dependent promoter.

Four genes located immediately downstream (3') of the *M. capsulatus* (Bath) sMMO operon, *mmoG*, *mmoQ*, *mmoS*, and *mmoR* (*42*), may be involved in regulation (Figure 1.1a). The *mmoG* and *mmoR* genes are also present in *M. trichosporium* OB3b, but are located upstream (5') of the sMMO structural genes (*43*). According to the results of marker-exchange mutagenesis, both

MmoG and MmoR are required for sMMO transcription. It should be noted that MmoR is not to be confused with MMOR, the reductase in the sMMO enzyme system. MmoG is predicted to be a GroEL homolog and may function in proper folding of MmoR or assembly of the sMMO complex (*42, 43*). MmoG might alternatively act as a coregulator together with MmoR, which is predicted to be a σN-dependent transcriptional activator that activates sMMO expression when copper levels are low (*42*). The MmoR sequence contains no obvious copper-binding motifs, however, suggesting that additional proteins might sense copper and transmit the signal to MmoR (*42*).

The proteins encoded by the *mmoQ* and *mmoS* genes could be involved in the copper-sensing mechanism. These proteins are homologous to two-component signaling systems in which a sensor protein detects an environmental stimulus, autophosphorylates a histidine residue within its histidine kinase domain, and then transfers the phosphoryl group to an aspartic acid residue in the response regulator protein, activating an effector domain (*44, 45*). MmoS resembles the sensor protein, and MmoQ corresponds to the regulator. The N-terminal sensing region of MmoS includes two predicted PAS-PAC domains. Because PAS-PAC domains detect changes in redox potential, light, or concentrations of small ligands (*46, 47*), MmoS is a reasonable candidate for participating in the copper switch, either directly or indirectly (*42*). MmoS lacking the N-terminal transmembrane domain has been characterized biochemically (*48*). Purified MmoS is a 480-kDa tetramer containing one flavin adenine dinucleotide (FAD) cofactor per monomer that is localized in the PAS-PAC domains. No evidence for copper binding has been obtained, indicating that MmoS does not sense copper directly. The properties of MmoS, including a redox potential of MmoS-bound FAD of –290 ± 2 mV at pH 8.0 and 25 °C, are quite

similar to those of the sensor protein, NifL, from diazotrophic bacteria. NifL senses oxygen or fixed nitrogen via an FAD cofactor and subsequently inhibits the ability of the NifA protein to activate transcription of genes involved in nitrogenase biosynthesis (*49*).

Several models have been proposed for sMMO regulation by these proteins. In *M. trichosporium* OB3b, MmoR is proposed to be inactivated by a copper signal, either directly or through MmoG. The inactive MmoR then cannot activate transcription of the sMMO genes (*43*). In *M. capsulatus* (Bath), an unknown copper sensor is proposed to transmit a signal to MmoS, which transfers a phosphoryl group to MmoQ. MmoQ then regulates sMMO expression via an interaction with MmoR (*42*). A more detailed variation of this model takes into account the possible redox-sensing ability of the FAD cofactor in MmoS (*48*) (Figure 1.1b). In this third scenario, the MmoS FAD cofactor is present at low copper levels as reduced flavin adenine dinucleotide ($FADH_2$). This form of MmoS phosphorylates MmoQ, which interacts with MmoR and promotes MmoS transcription. At higher copper levels, $FADH_2$ is oxidized to FAD, causing a conformational change in MmoS that allows it to interact directly with MmoR, preventing MmoR from activating transcription. It is unclear exactly how copper concentrations might change the redox state of the FAD cofactor. The latter two models remain subject to the caveat that it has not yet been demonstrated that MmoS and/or MmoQ are essential for copper-dependent sMMO regulation. In addition, no evidence for the protein-protein interactions invoked in these models has been reported.

Additional Copper-Regulated Genes

In addition to the two MMOs, multiple other proteins are differentially expressed as a function of copper concentrations in the growth medium. Several of these proteins were

identified using sodium dodecyl sulfate-polyacrylamide gel electrophoresis and N-terminal sequencing prior to completion of the *M. capsulatus* (Bath) genome. In *M. capsulatus* (Bath), at least two formaldehyde dehydrogenases (FalDH) are regulated by copper, with a dye-linked FalDH expressed in the presence of copper and an $NAD(P)^+$-linked FalDH expressed under low-copper conditions (*50*). The copper-dependent expression of the different FalDHs is consistent with the way each MMO may be linked to the electron transport chain. The $NAD(P)^+$-linked FalDH is expressed under the same conditions as sMMO, which couples to the electron transport chain through NADH. The dye-linked FalDH, expressed with pMMO, is coupled to the electron transport chain through the cytochrome bc_1 complex, consistent with electron flow from the cytochrome bc_1 complex to pMMO (*22*).

Proteins of unknown function repressed by copper include CorA, an 28.5-kDa membrane-bound protein from *Methylomicrobium albus* BG8 (*51*), and MopE, a cell surface-associated protein from *M. capsulatus* (Bath) (*52, 53*). Deletion of CorA affects cell growth, which cannot be rescued by copper addition (*51*). MopE exists in two forms, a 66-kDa cell surface-associated protein ($MopE^C$) and a 46-kDa protein, comprising the C-terminal part of $MopE^C$, which is secreted from the bacteria into the growth media (MopE*). Both $MopE^C$ and MopE* are copper repressible (*53*), and MopE* is similar in sequence to *M. albus* BG8 CorA (*52*). Both proteins may play a role in copper uptake (*51, 53*), but neither sequence contains obvious copper-binding motifs. Additional biochemical and genetic studies are required to define the functions of MopE and CorA.

Immediately upstream of *mopE* in the *M. capsulatus* (Bath) genome is another copper-repressible gene (MCA2590), which encodes a protein homologous to the bacterial diheme

cytochrome *c* peroxidase (BCCP) family (*54*). Unlike other members of the BCCP family, this protein is localized to the external surface of the outer membrane, rather than the periplasm. The sequence contains two heme-binding motifs, and *c*-type heme has been detected. Interestingly, an unannotated ORF in *M. albus* BG8, found immediately downstream of the gene encoding CorA, is 50% identical to the N-terminus of this heme protein (*54*). The physiological role of the MCA2590 gene product has not been determined, although it has been suggested, based on the proximity of the genes and their similar expression profile, that its function is linked with that of MopE (*54*).

The effects of copper concentration on protein expression in *M. capsulatus* (Bath) have also been investigated by a proteomics approach using cleavable isotope-coded affinity technology (*55*). This study was conducted while the genome sequencing was in progress. Of 682 proteins identified, 60 were upregulated and 68 were downregulated by copper. Most of the proteins exhibiting differential expression were biosynthetic enzymes. Notably, a hemerythrin, also identified independently by two-dimensional gel electrophoresis (*56*), was expressed at high copper levels. Hemerythrins are oxygen carriers found in marine invertebrates and are characterized by a dinuclear iron center housed within a four-helix bundle. Sequence analysis, combined with spectroscopic characterization of the purified protein, indicates that the *M. capsulatus* (Bath) hemerythrin is the first example of a prokaryotic hemerythrin. On the basis of these data, it probably binds oxygen, and a role in providing oxygen specifically to pMMO has been postulated (*55, 56*).

OVERALL STRUCTURE OF PMMO

Structural characterization of pMMO has been challenging due to the difficulty of working

with an integral membrane protein. In this section, structural insights provided by the 2.8 Å resolution crystal structure and the 23 Å resolution cryoelectron microscopy structure, both published in 2005, are discussed.

The 2.8 Å Resolution Crystal Structure

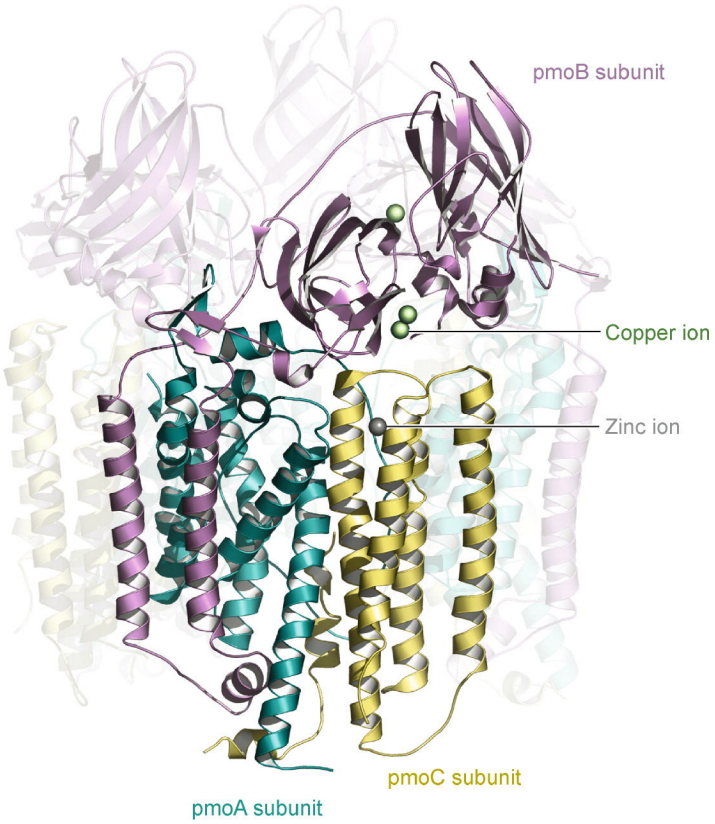

Figure 1.2. The pMMO trimer
The crystal structure of *M. capsulatus* (Bath) is shown with one protomer highlighted.

The crystal structure of pMMO from *M. capsulatus* (Bath) has been determined to 2.8 Å resolution (*57-59*). pMMO is a trimer, approximately 105 Å long and 90 Å in diameter, composed of three copies of each subunit in an $\alpha_3\beta_3\gamma_3$ polypeptide arrangement (Figures 1.2 and 1.3). The soluble region, which extends ~45 Å from the membrane, is composed of six

cupredoxin-like β barrels, two from each copy of the pmoB subunit. Each pmoB subunit also contains two transmembrane helices, which together with seven helices from each pmoA subunit and five from each pmoC subunit add up to a total of 42 transmembrane helices. Each αβγ protomer houses three metal centers (*vide infra*). There is an opening at the center of the pMMO trimer, ~11 Å wide in the soluble region and ~22 Å within the membrane (Figure 1.3a). In the soluble region, this central cavity is lined with charged residues and likely contains solvent, although no water molecules could be modeled at 2.8 Å resolution. In the transmembrane region, this opening is lined with hydrophobic residues and is probably occupied by disordered detergent molecules, also not discernible in the crystal structure. The $\alpha_3\beta_3\gamma_3$ trimeric structure was unexpected because prior biochemical studies suggested either a monomeric αβγ (*60*) or a dimeric $\alpha_2\beta_2\gamma_2$ (*61*) arrangement (*10*).

Cryoelectron Microscopy Structure

Electron microscopy (EM) has also been used to determine the pMMO structure. Early electron micrographs of pMMO from *M. capsulatus* (strain M) revealed particles with a hexagonal shape, approximately 9 nm in diameter (*62*). Each particle had six maxima of protein density, interpreted to indicate a hexameric structure (*62*). In light of the crystal structure, it is probable that these six maxima correspond to the six β barrels in the soluble region of pMMO. More recent electron micrographs of catalytically active pMMO-containing membranes reveal a threefold symmetry (*63*). Moreover, a 23 Å resolution structure of *M. capsulatus* (Bath) pMMO determined by EM and single-particle analysis reveals a complex consistent in size and shape with the crystallographic model (*63*) (Figure 1.3c). Taken together, these EM data strongly suggest that the trimeric arrangement observed in the crystal structure is physiologically relevant.

The EM structure includes several features not observed in the crystal structure (*63*) (Figure 1.3c). First, there is a "belt" of density around the transmembrane region that is interpreted as a ring of detergent molecules, specifically dodecyl-β-D-maltoside, which was used to prepare the samples. Electron density attributed to detergent also fills the central opening at the transmembrane end of pMMO. Second, there are regions of low density or "holes" in the soluble domains. These regions together with the central opening may represent sites of substrate entry or product egress.

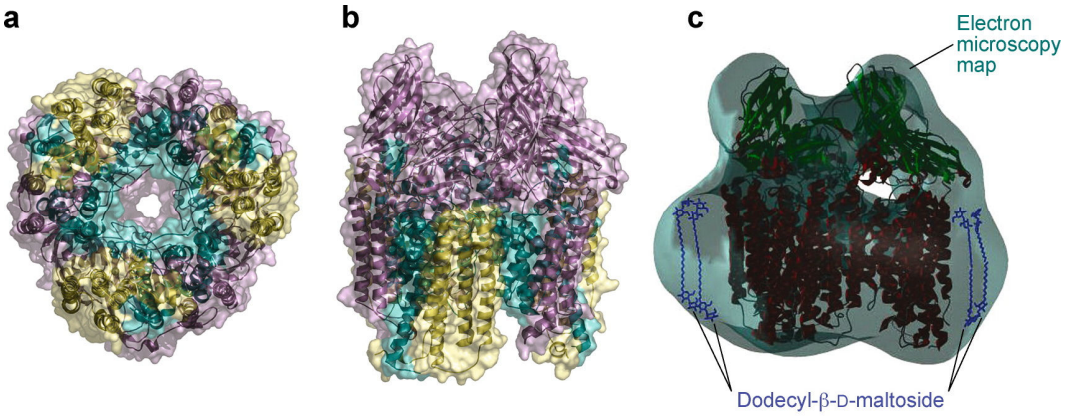

Figure 1.3. Surface representations of pMMO
The crystal structure of pMMO viewed (a) perpendicular to and (b) parallel to the membrane normal and (c) the pMMO crystallographic coordinates and four molecules of dodecyl-β-D-maltoside docked into the electron microscopy map. Panel (c) was kindly provided by Dr. A. Kitmotto (University of Manchester, U. K.)

THE PMMO METAL CENTERS

Many laboratories have investigated the metal centers in pMMO by spectroscopic methods. In this section, these results are summarized in the context of the metal centers observed in the *M. capsulatus* (Bath) pMMO crystal structure.

Metal Content

Although it is generally accepted that pMMO is a metalloenzyme, the nature of the metal center(s) has been the subject of much debate. All researchers find copper associated with pMMO, but a wide range of stoichiometries has been reported and has been tabulated previously (*10*). In brief, copper contents for membrane-bound pMMO range from 4–59 copper ions per 100 kDa. For purified *M. capsulatus* (Bath) pMMO, four different laboratories report varied stoichiometries: 2 copper ions (*64*), 2–3 copper ions (*61*), 8–10 copper ions (*38*), and 15–20 copper ions (*60, 65*). The first three values can be considered similar because the 8–10 copper ions include 6–8 molecules of mb (*vide infra*), which are not present in the first two preparations, and 2 copper ions per 100 kDa pMMO. Consistent with this stoichiometry for the *M. capsulatus* (Bath) enzyme, purified pMMO from *M. trichosporium* OB3b contains 2 copper ions per 100 kDa (*66*). The origin of the higher values reported by Chan and coworkers remains unclear. Recently, it has been suggested that many of these additional copper ions reside in the C-terminal β barrel of pmoB, which is proposed to act as a "Cu(I) sponge" (*67*). In addition to copper, iron is found in some, but not all (*60, 66*), preparations of both membrane-bound and purified pMMO. The reported stoichiometries are 0.75–2.5 iron ions per 100 kDa purified *M. capsulatus* (Bath) pMMO (*22, 38, 61, 64*).

Spectroscopic Studies

The pMMO copper centers in both membrane-bound and purified *M. capsulatus* (Bath) pMMO have been studied extensively by electron paramagnetic resonance (EPR) spectroscopy. On the basis of the hyperfine splitting pattern of a broad isotropic signal at $g \sim 2.1$ and redox potentiometric studies, Chan and coworkers (*68, 69*) have proposed the presence of a

ferromagnetically coupled trinuclear Cu(II) cluster. They also observed a type 2 Cu(II) signal, assigned to a second trinuclear cluster in which two of the three Cu(II) ions are antiferromagnetically coupled (*70*). By contrast, researchers in four other laboratories have observed only the type 2 signal using a variety of samples from three different organisms (*22, 38, 61, 64, 71*). This type 2 signal is not attributed to a trinuclear cluster and accounts for 40–50% of the total copper present (*61, 64*). Alternative assignments for the signal interpreted as a trinuclear cluster include mb (*22*), superposition of a radical signal with that from the type 2 center (*72*), $CuFe(CN)_6^{2-}$ (*73*), or adventitiously bound copper ions (*64*).

X-ray absorption spectroscopic (XAS) data also provide insight into the pMMO metal centers (*61, 74*). The X-ray absorption near edge spectra (XANES) of as-isolated samples, containing 2–3 copper ions per 100 kDa, demonstrate that the copper centers can undergo redox chemistry. A feature at 8984 eV, attributable to a Cu(I) 1s→4p transition, increases in intensity upon chemical reduction with dithionite, indicating that some, but not all, of the copper ions are present as Cu(I) in purified pMMO. Treatment with H_2O_2 diminishes this peak, suggesting that some oxidation can occur, although complete oxidation has not been achieved. Extended X-ray absorption fine structure (EXAFS) data are best fit with two shells of backscatterers. The first shell is best fit with two Cu-O/N ligand environments with Cu-O/N distances ranging from 1.93 to 2.22 Å, depending on the sample and oxidation state. A second scattering interaction, observed in all samples, is best fit with a Cu-Cu interaction at 2.51 Å for as-isolated and oxidized pMMO and 2.65 Å for reduced pMMO. These data are the only direct spectroscopic evidence of a multinuclear copper cluster. The possibility of a Cu-Fe center with a short metal-metal distance was ruled out by Fe XAS data, which indicate the presence of Fe(III), but with no Fe-

metal scattering in the 2.5–2.65 Å range. The Fe EXAFS parameters, combined with the optical spectrum of purified pMMO (*61*) and the observation of an EPR signal characteristic of high-spin heme, suggest that the iron is due to heme contaminants (*74*). Heme is not observed in some iron-containing preparations, however (*38*), leaving the possibility of a functional iron center. In support of this hypothesis, a recent Mössbauer study of *M. capsulatus* (Bath) pMMO revealed spectral properties similar to the antiferromagnetically coupled diiron(III) cluster found in sMMO (*75*).

Crystallographic Data

Three metal centers were found in the crystal structure of *M. capsulatus* (Bath) pMMO (*57, 58*) (Figure 1.4). A dinuclear copper center is located in the N-terminal β barrel of the pmoB subunit ~10 Å above the membrane interface. The copper ions are coordinated by His 33, His 137, and His 139 (Figure 1.4a). Notably, His 33 is the N-terminal residue of pmoB and ligates one of the copper ions through both its side chain δ nitrogen and the N-terminal amino nitrogen. The two copper ions are separated by ~2.6 Å, similar to the Cu-Cu distance obtained from EXAFS. The three histidine ligands are strictly conserved in pmoB and the related amoB subunit of AMO (Figures 1.5 and 1.6a), consistent with an important role for this metal center. Two second-sphere ligands, Glu 35 and Gly 152, which are hydrogen bonded to the coordinating histidines, are also highly conserved.

A mononuclear copper center is also found in the soluble region of pmoB, ~25 Å above the membrane. The copper ion is coordinated by the δ nitrogens of His 48 and His 72 (Figure 1.4b). Residue His 48 is not conserved (Figures 1.5 and 1.6a). In many methanotrophs, an asparagine residue is found at this position, and in most AMOs, the histidine is replaced with a glutamine.

The second ligand, His 72, is conserved among most pmoB and amoB sequences, but in a few species of nitrifying bacteria, the corresponding residue is an arginine. An adjacent glutamine, Gln 404, which was proposed to hydrogen bond to solvent ligands not observed in the crystal structure (*58*), is not conserved at all (Figure 1.5). At 2.8 Å resolution, exogenous ligands were not detected at either copper center, but the EXAFS data indicate a coordination number of 2–4 for the O/N ligands, which is more than the two ligands to each copper ion in the crystal structure (*74*). The oxidation states of the copper ions present in the crystal structure are not known, but multiple scenarios have been considered. The scheme most consistent with the spectroscopic data is that the mononuclear site is Cu(I) and the dinuclear site is a completely localized, mixed valence Cu(I)Cu(II) site (*74*).

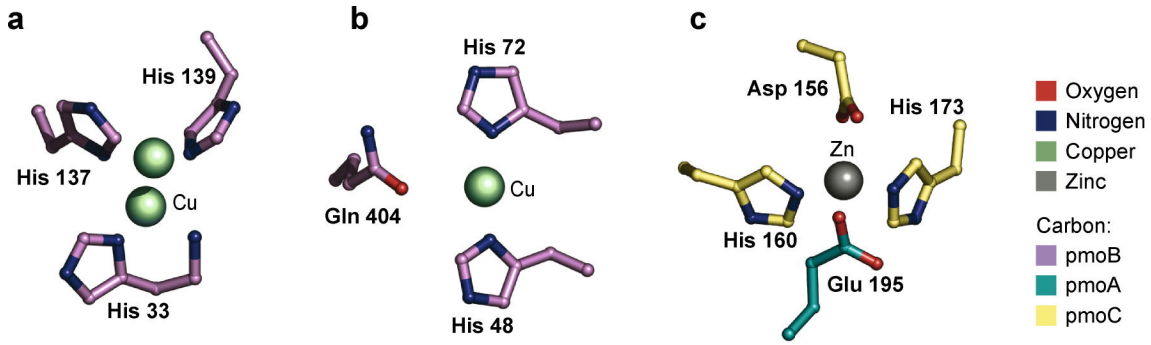

Figure 1.4. The metal centers of *M. capsulatus* (Bath) pMMO
The dicopper (a), monocopper (b), and zinc (c) sites modeled in the pMMO crystal structure. Data reported in Reference (*57*).

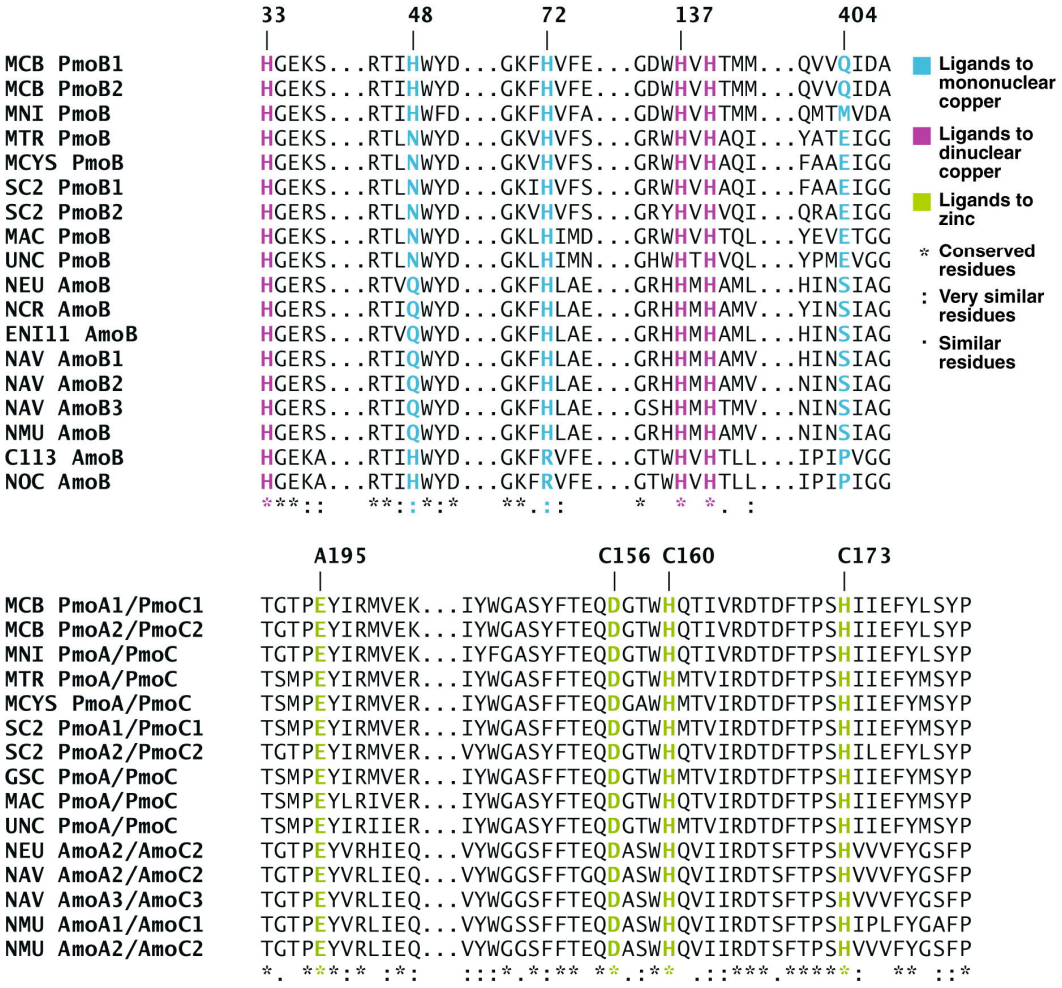

Figure 1.5. Multiple sequence alignments of pMMO and AMO subunits showing the ligands to the metal centers in the *M. capsulatus* (Bath) pMMO structure

Numbers above the alignment correspond to copy 2 of pMMO in *M. capsulatus* (Bath). Abbreviations: MCB, *M. capsulatus* (Bath); MNI, *Methylomicrobium* sp. NI; MTR, *M. trichosporium* OB3b; MCYS, *Methylocystis* sp. M; SC2, *Methylocystis* sp. SC2; MAC, *Methylocapsa acidiphila*; UNC, uncultured methanotroph; NEU, *Nitrosomonas europaea*; NCR, *Nitrosomonas cryotolerans*; ENI11, *Nitrosomonas* sp. ENI-11; NAV, *Nitrosospira* sp. NpAV; NMU, *Nitrosospira multiformis* ATCC 25196; C113, *Nitrosococcus* sp. C-113; NOC, *Nitrosococcus oceani*; GSC, *Methylocystis* sp. GSC357. GenBank accession numbers and alignments of the full subunit sequences can be found in Appendix A.

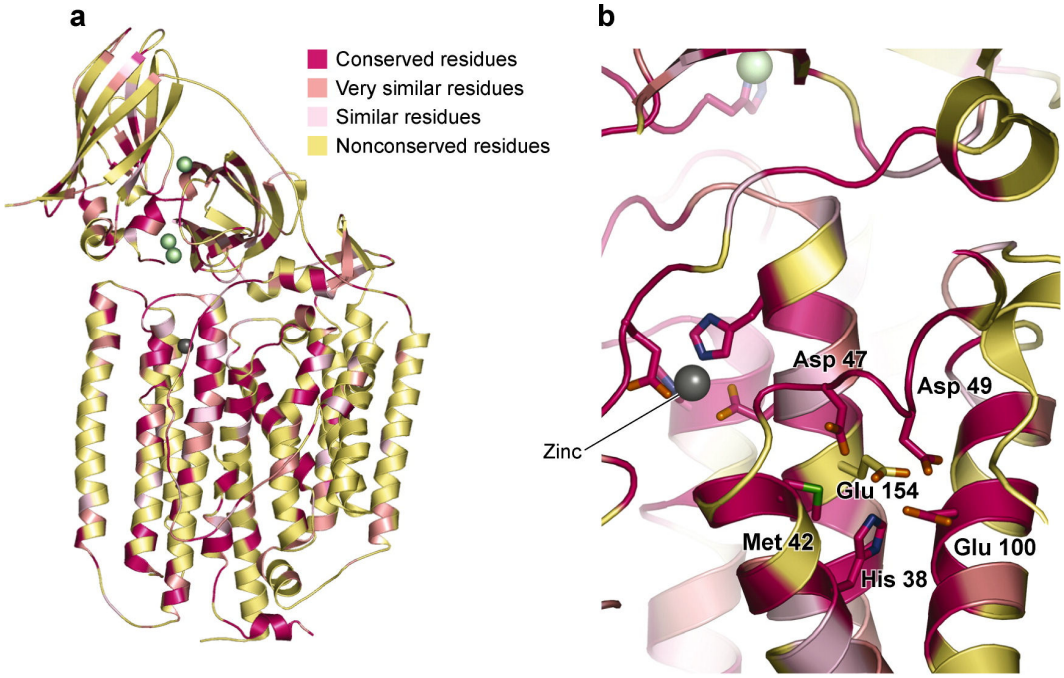

Figure 1.6. Multiple sequence alignments mapped to the pMMO crystal structure
(a) The pMMO protomer with conserved residues, very similar residues, and similar residues shown. (b) A conserved patch of hydrophilic residues adjacent to the zinc center that may represent an additional metal-binding site.

A third metal center, occupied in the structure by zinc from the crystallization buffer, is located within the membrane. A single zinc ion is coordinated by Asp 156, His 160, and His 173 from the pmoC subunit and Glu 195 from the pmoA subunit (Figure 1.4c). All four of these residues are strictly conserved, strongly suggesting that this site is functionally important (Figures 1.5 and 1.6b). Because purified pMMO contains less than 0.2 zinc ions per monomer (*57*), this site may be occupied by copper or iron in vivo. One possibility is a carboxylate-bridged diiron center, like that found in the active site of MMOH (*57*), and recent Mössbauer spectroscopic data suggest that this model is plausible (*75*).

Although the spectroscopic and crystallographic data have provided much information on the

pMMO metal centers, their functions remain unclear, and the active site has not yet been identified. On the basis of sequence alignments, the mononuclear copper center seems unlikely to play an essential role. The dinuclear copper site is an attractive candidate for the active site because the residues are strictly conserved and because there is an adjacent hydrophobic pocket (*57*). Other dinuclear copper centers, such as that in tyrosinase (*76*), are capable of hydroxylation chemistry, but these sites have longer Cu-Cu distances and six rather than three coordinating histidine residues (*77*). The zinc center is also a reasonable option, depending on what metal ion or ions occupy this site in vivo. A third possibility is that the active site is metal depleted in the crystal structure. There is one region of hydrophilic residues within the membrane ~13 Å from the zinc site, composed of strictly conserved His 38, Met 42, Asp 47, Asp 49, and Glu 100 from pmoA and Glu 154 from pmoC (Figure 1.6b). It is conceivable that a metal-binding site could be assembled by some combination of these residues.

PMMO AND CATALYSIS

The conditions necessary for the isolation of catalytically active pMMO have been researched extensively, but remain unclear. In this section, progress toward understanding the catalytic activity and mechanism of pMMO is summarized.

Isolation and Activity

pMMO can oxidize alkanes and alkenes up to five carbons in length, but unlike sMMO, it cannot oxidize cyclic or aromatic hydrocarbons (*8, 26*). Obtaining purified pMMO that retains activity has been a significant issue in the field. Using the propylene oxidation assay (*20*) with either NADH or duroquinol (*78*) as a reductant, specific activities for *M. capsulatus* (Bath) pMMO of ~10–200 nmol propylene oxided (mg protein · min)$^{-1}$ for the membrane-bound

enzyme and 2–126 nmol propylene oxided (mg protein · min)$^{-1}$ for purified preparations have been reported (*22, 38, 61, 64, 65, 79, 80*). For purified *M. trichosporium* OB3b pMMO, a specific activity of ~3–4 nmol propylene oxided (mg protein · min)$^{-1}$ has been reported (*66*). These values were obtained using a variety of purification procedures, which have been described in detail previously (*10*). A comparison of the different protocols suggests that several factors influence pMMO activity.

First, the concentration of copper in the growth medium is important. Addition of excess copper beyond that needed to switch from sMMO to pMMO expression increases the activity of pMMO in cell-free extracts, with reports of optimal concentrations ranging from 30 to 80 μM (*12, 22, 38, 60*). In addition, continuous addition of copper to the culture improves activity in purified pMMO (*38*), as does the use of fast-growing cells with doubling times < 5 hr (*64*). Some iron in the growth medium is also necessary to obtain reasonable activity (*38*). Second, anaerobicity might have an effect. The highest reported specific activity for membrane-bound pMMO, 290 nmol propylene oxided (mg protein · min)$^{-1}$, was obtained for pMMO isolated under anaerobic conditions (*38*), but another report indicated that anaerobic purification resulted in little to no activity (*64*). Third, activity is dependent on the solubilization procedure. All reported pMMO solubilization protocols employ dodecyl-β-D-maltoside, but different amounts are used. DiSpirito and coworkers (*38*) determined that the optimal detergent/protein ratio (w/w) is 1–1.25 mg dodecyl-β-D-maltoside per mg protein and observed a loss of the metal ions at nonoptimal detergent concentrations. Furthermore, increasing the detergent concentration in purified pMMO after solubilization resulted in inactivation (*38*). Because each laboratory purifying pMMO handles these variables in a different fashion (*10*), the discrepancies in activity

and metal content are not surprising.

Physiological Reductant

The issue of pMMO activity is further complicated because the physiological reductant of pMMO is not known. It may be that disruption of the electron transport chain during purification contributes to problems maintaining pMMO activity (*81*). For membrane-bound pMMO, NADH can serve as a reductant for in vitro activity assays. Once pMMO is solubilized, however, only quinols produce activity (*22, 61, 64*), with duroquinol yielding the best results (*78*). Improved specific activities for pMMO have been obtained either by adding another protein back to purified pMMO or by partially purifying a pMMO sample that contains additional proteins. For example, addition of purified type 2 NADH:quinone oxidoreductase (NDH-2) together with NADH and duroquinol increased specific activity in purified pMMO samples by up to 35% (*38*). Alternatively, Dalton and coworkers (*64*) reported that copurification with two polypeptides of molecular masses 63 and 8 kDa was necessary to obtain activity with duroquinol. No activity was observed in the absence of these proteins, and reconstitution of the complex gave only 10% of the original activity. The 63-kDa component is likely methanol dehydrogenase (*64*).

These observations have led to several proposals for the electron transfer pathway. In one scenario, NDH-2 uses NADH generated by oxidation of formate and formaldehyde to reduce endogenous quinones, which then reduce pMMO either directly or through an additional reductase. This model is consistent with the observation that the NDH-2 inhibitor diphenyliodonium inhibits NADH-dependent membrane-bound pMMO activity (*81*). The activity observed in the presence of the putative 63-kDa methanol dehydrogenase suggests a role

for methanol dehydrogenase in electron transfer, but neither methanol nor formaldehyde enhanced activity, perhaps owing to loss of a cytochrome component (*64*). Finally, the cytochrome bc_1 complex may donate electrons to pMMO, perhaps through ubiquinone 8. This model is consistent with the coexpression of pMMO and the dye-linked FalDH (*50*). It is not known whether any of these proteins interact directly with pMMO in vivo. Interestingly, the crystal structure reveals a negatively charged patch on the pMMO surface, which could represent a docking site for a partner reductase (*57*).

Mechanistic Studies

Some attempts have been made to address the pMMO chemical mechanism using membrane preparations. Experiments with chiral alkanes, which have provided insight into the sMMO mechanism (*19*), suggest a concerted mechanism, rather than the involvement of radical or cation intermediates (*80, 82*). No carbon kinetic isotope effect was observed for propane oxidation, which was interpreted as indicating little or no structural change at the carbon center during transition state formation in the rate-limiting step (*83*). When oxidizing multicarbon compounds, pMMO was shown to oxidize the C-2 position preferentially (*84*). On the basis of these limited studies, Chan and coworkers (*80*) have proposed that the C-H bond of the substrate is presented to a "hot" oxygen species, resulting in the formation of a nonlinear C···O···H transition state. Using density functional theory calculations on model complexes, they have further argued that a trinuclear bis(μ_3-oxo)Cu(II, II, III) center is best suited to this chemistry (*85*). Considering the absence of such a cluster in the crystal structure, the fact that these mechanistic studies were carried out on membrane preparations, and the discrepancy in metal ion content and activity among various pMMO preparations, these conclusions remain speculative. A more detailed

discussion of possible mechanisms and active site locations can be found in Reference (*86*).

COPPER UPTAKE AND METHANOBACTIN

Because of the importance of copper in both the regulation and chemistry of pMMO, it is likely that methanotrophs possess a specialized copper acquisition system. Methanobactin (mb), a copper-chelating, siderophore-like molecule, is believed to play an important role in this uptake system, as well as possibly contributing to pMMO activity.

Methanobactin Structure and Properties

Initial evidence for a copper uptake system in methanotrophs was derived from studies of *M. trichosporium* OB3b mutants that constitutively express sMMO and do not express active pMMO or produce intracytoplasmic membranes. The extracellular media from these mutants also have an unusually high concentration of copper (*21, 87*). According to the prevailing hypothesis, this phenotype results from a defect in a copper-complexing agent, reminiscent of an iron siderophore (*87*). Candidate molecules for this copper chelator were later detected in the spent media of *M. trichosporium* OB3b (*88, 89*) and *M. capsulatus* (Bath) (*22*) grown at low copper concentrations. These compounds, referred to as copper-binding compounds or ligands, range in molecular mass from 382 to 1217 Da and bind a single copper ion with high affinity. Further characterization was hindered, however, by degradation and difficulties determining the sequence and chemical composition. These issues were resolved recently, and the crystal structure of the *M. trichosporium* OB3b copper-binding compound was determined. This molecule, renamed methanobactin (mb), has a molecular weight of 1217 Da and the sequence *N*-2-isopropylester-(4-thionyl-5-hydroxyimidazolate)-Gly^{1}-Ser^{2}-Cys^{3}-Tyr^{4}-pyrrolidine-(4-hydroxy-5-thionylimidazolate)-Ser^{5}-Cys^{6}-Met^{7} (*37, 90*). The crystal structure reveals a pyramid-like

structure, with a single copper ion coordinated by an N_2S_2 donor set at the base of the pyramid (*37*) (Figure 1.7).

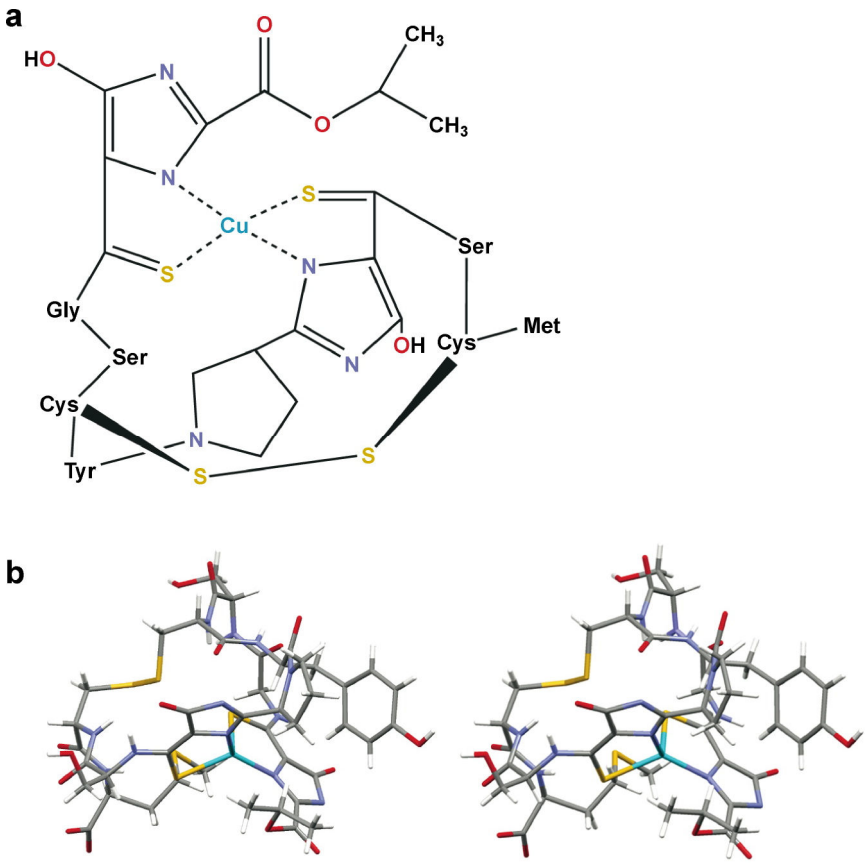

Figure 1.7. Methanobactin structure
Shown (a) schematically and (b) in stereo as a ball-and-stick representation. Data reported in Reference (*37*).

The oxidation state of the chelated copper ion in mb was suggested to be Cu(I) on the basis of X-ray photoelectron spectroscopy and was confirmed by XAS and EPR analysis. The XANES spectrum of *M. trichosporium* OB3b copper-bound mb (Cu-mb) exhibits a 1s→4p transition at 8985 eV indicative of Cu(I) and lacks features attributable to Cu(II) (*91*). The EPR spectrum of Cu-mb only shows weak signals with $g_{\|}$ and $A_{\|}$ values that are characteristic of copper with N_xO_{4-x} ligands, as would be expected from adventitiously bound Cu(II) (*22, 88, 91*).

Furthermore, EPR signals attributable to Cu(II) with sulfur ligation typically disappear < 10 min after Cu(II) addition to mb (*92*). Thus, mb itself is capable of reducing Cu(II) to Cu(I). The optical spectrum of Cu-mb also lacks features characteristic of Cu(II) (*90*). Spectral and kinetic data suggest that mb initially binds Cu(II) as a dimer with coordination by 4-hydroxy-5-thionylimidazolate and possibly tyrosine, followed by reduction to Cu(I) and coordination by 4-thionyl-5-hydroxyimidazolate (*93*).

Possible Functions of Methanobactin

Several lines of evidence suggest that mb is involved in copper uptake. When *M. trichosporium* OB3b or *M. capsulatus* (Bath) cells are grown under copper-limited conditions, mb is present in the spent media. After copper supplementation, the level of mb in the medium decreases (*22, 88, 89*), and Cu-mb is found associated with the membranes (*22, 88*). The addition of stoichiometric quantities of mb and copper to the growth medium when *M. trichosporium* OB3b cells are switched from copper-starved to copper-rich conditions also decreases the lag time and stimulates growth (*90*).

Cu-mb is also proposed to play a role in pMMO activity. DiSpirito and coworkers have reported that an irreversible loss of pMMO activity occurs upon dissociation of Cu-mb from pMMO (*22, 38, 92*). Other preparations lacking Cu-mb do exhibit reasonable activity, however (*63, 64, 66*). In support of a role in activity, addition of *M. trichosporium* OB3b Cu-mb to *M. capsulatus* (Bath) cells expressing pMMO or to *M. capsulatus* (Bath) membrane fractions enhances activity. The specific activity of membrane-bound pMMO is increased by 35% (*92*). Addition of Cu(II) alone also increases activity, but only by 20%. These data should be considered with two caveats. First, Cu-mb and pMMO from two species were combined because

procedures for isolating Cu-mb from *M. trichosporium* OB3b and pMMO from *M. capsulatus* (Bath) are best developed. It is not known whether mb has the same chemical composition in both organisms, however. Second, the effects of adding Cu(I) to the activity assay were not reported. It may be that Cu-mb acts as a copper chaperone, increasing activity by delivering Cu(I) to the catalytic metal center.

The effect of Cu-mb on pMMO activity may be indirect. Cu-mb exhibits superoxide dismutase activity and thus may protect pMMO in cell-free extracts from oxidative damage (*38*). Alternatively, Cu-mb may interact with pMMO directly. This possibility has been probed by EPR spectroscopy (*92*). Addition of *M. trichosporium* OB3b Cu-mb to high activity membrane-bound *M. capsulatus* (Bath) pMMO resulted in an almost complete loss of the type 2 Cu(II) signal and the appearance of a free radical signal at $g = 2.005$. Addition of oxygen resulted in reappearance of the type 2 signal and an increase in intensity of the radical signal. Addition of methane and oxygen also resulted in reappearance of the type 2 signal, but the radical signal was no longer present. This radical signal disappeared upon purification (*61*), however, suggesting that it may not be relevant to pMMO. When these experiments were repeated on lower activity membrane preparations, the effects of Cu-mb were less pronounced. In some preparations, addition of Cu-mb resulted in the loss of the superhyperfine structure associated with the type 2 signal. Taken together, these EPR spectral changes were interpreted as evidence of an interaction between Cu-mb and the type 2 Cu(II) center of pMMO. Further studies using purified pMMO and Cu-mb from the same organism are clearly necessary.

SUMMARY POINTS

1. The genome of *M. capsulatus* (Bath) has been sequenced and offers the opportunity to investigate protein expression as a function of copper concentration.
2. The copper switch mechanism governing differential expression of sMMO and pMMO is not yet understood, but the sMMO regulatory proteins MmoR, MmoG, MmoS, and MmoQ may be involved.
3. Spectroscopic data indicate that pMMO contains a mixture of Cu(I) and Cu(II), of which some is present as a copper-containing cluster with a short Cu-Cu distance. Several pMMO preparations also contain iron.
4. The crystal structure of *M. capsulatus* (Bath) pMMO reveals a trimer, also observed by cryo-EM studies. A mononuclear copper center, a dinuclear copper center, and a mononuclear zinc site are present.
5. The specific activity of isolated pMMO is variable and depends on growth conditions as well as solubilization and purification protocols. The physiological reductant has not been identified.
6. Methanobactin, a 1217-Da Cu(I) chelator, likely functions in copper uptake and may also modulate pMMO activity.

FUTURE ISSUES

1. The specific factor(s) that sense copper and promote the switch from sMMO to pMMO expression need to be identified.

2. Additional crystal structures and spectroscopic data are required to establish the pMMO metal composition in vivo, the detailed coordination geometries of the metal centers, and, most importantly, the nature of the active site.
3. The in vivo function of methanobactin remains to be determined, and the biosynthetic enzymes and receptors involved in its handling should be investigated.
4. Once the pMMO active site is identified and high activity preparations of purified enzyme are obtained routinely, detailed mechanistic studies should be initiated.

CHAPTER 2: GROWTH, PURIFICATION AND BIOPHYSICAL CHARACTERIZATION OF PARTICULATE METHANE MONOOXYGENASE FROM *METHYLOSINUS TRICHOSPORIUM* OB3B

Portions of this chapter will be published as Hakemian, A. S.; Kondapalli, K. C.; Telser, J.; Hoffman, B. M.; Stemmler, T. L.; Rosenzweig, A. C. *Biochemistry* submitted.

ABSTRACT

The nature of the pMMO active site and the overall metal content are controversial, with spectroscopic and crystallographic data suggesting the presence of a mononuclear copper center, a dinuclear copper center, a trinuclear center, and a diiron center or combinations thereof in various samples. Most studies have focused on pMMO from *Methylococcus capsulatus* (Bath). The purification and biophysical characterization of pMMO from a second organism, *Methylosinus trichosporium* OB3b, is presented in this chapter. Purified *M. trichosporium* OB3b pMMO contains ~2 copper ions per 100 kDa protomer. Electron paramagnetic resonance (EPR) spectroscopic parameters indicate type 2 Cu(II) is present as two distinct species. Extended X-ray absorption fine structure (EXAFS) data are best fit with oxygen/nitrogen ligands and a Cu-Cu interaction at 2.52 Å.

INTRODUCTION

Methanotrophs are eubacteria capable of utilizing methane as their only carbon and energy source. Methanotrophs are divided into several classes on the basis of their cell morphologies, membrane arrangements, and pathways for carbon assimilation. The two most widely studied organisms are the type X methanotroph *Methylococcus capsulatus* (Bath) and the type II methanotroph *Methylosinus trichosporium* OB3b (*1*). The first step of their metabolic pathway is the conversion of methane to methanol by the enzyme methane monooxygenase (MMO), which exists in both a well-studied, but rarely expressed, soluble iron-containing form (sMMO) (*9*) and a membrane-bound particulate form (pMMO) (*9, 94*). Although the active site and chemistry of sMMO are well established, the nature of the pMMO catalytic center remains controversial, particularly regarding the number and types of metal ions present.

pMMO comprises three subunits: pmoB or α (47 kDa), pmoA or β (24 kDa), and pmoC or γ (22 kDa). Several laboratories have reported that purified *M. capsulatus* (Bath) pMMO contains 2–3 copper ions per 100 kDa αβγ protomer (*38, 61, 64*). Similarly, *M. trichosporium* OB3b pMMO was found to contain 2 copper ions per αβγ protomer (*66*). By contrast, Chan and coworkers have reported 15–20 copper ions per *M. capsulatus* (Bath) pMMO protomer (*60, 65*). This large number of copper ions is proposed to be arranged in trinuclear clusters based on the interpretation of a broad isotropic electron paramagnetic resonance (EPR) signal at $g \sim 2.1$ and on redox potentiometric studies (*68, 69*). However, other investigators observe only a type 2 Cu(II) EPR signal for pMMO from several different organisms (*22, 38, 61, 64, 71, 94*). The iron content of pMMO is also contentious. Samples of iron-free pMMO have been obtained from both *M. capsulatus* (Bath) (*60*) and *M. trichosporium* OB3b (*66*). Other preparations of *M.*

capsulatus (Bath) pMMO contain 0.75–2.5 iron ions per 100 kDa (*22, 38, 61, 64*).

The crystal structure of *M. capsulatus* (Bath) pMMO revealed that pMMO is an $\alpha_3\beta_3\gamma_3$ trimer, of which each $\alpha\beta\gamma$ protomer houses three metal centers (*57, 58*). Two of the metal centers in the structure contain copper: a dinuclear copper center for which the three histidine ligands are strictly conserved and a mononuclear copper center that includes two histidine ligands, of which one is not conserved in other pMMOs and the related ammonia monooxygenase (*94*). The third metal site, composed of strictly conserved ligands, is occupied by a zinc ion in the crystal structure, most likely derived from the crystallization buffer. The physiological metal content of this site is unknown. One possibility is a diiron center (*57*), and recent Mössbauer spectroscopic data suggest that this model is plausible (*75*). Additional metal binding sites depleted during crystallization may exist as well, and a potential transmembrane metal binding site identified in the crystal structure (*57*) has been proposed to house a tricopper cluster (*68*). To further investigate the composition and functional relevance of the pMMO metal centers, pMMO from *M. trichosporium* OB3b has been characterized for its enzymatic activity and metal ion content and by ultraviolet-visible-near-infrared (UV-VIS-NIR), electron paramagnetic resonance (EPR) and x-ray absorption (XAS) spectroscopies.

MATERIALS AND METHODS

Bacterial Growth

M. trichosporium OB3b cultures were obtained from the laboratories of Jeremy Semrau (University of Michigan) and John Lipscomb (University of Minnesota). Fermentations were conducted in a 15 L bioreactor (New Brunswick Scientific, Edison, NJ) using previously described culture media (*95*) with the addition of 50 μM copper sulfate. As cells grew very

poorly on plates and in small flasks, the fermentor was inoculated with approximately 10 g frozen cell paste from previous growths, which was first thawed in a small amount of culture media and added directly to the fermentor. Cells were grown at 30 °C and an agitation rate of 300–400 rpm, and were purged with a 3:1 methane:air mixture at 1.2–1.6 L/min total gas flow. The pH in the fermentor was maintained at 7.0 by addition of 1 N NaOH (aq) and 1 N H_2SO_4 (aq).

Cells were harvested at an OD_{600} between 6.0 and 10.0 to ensure that they had not entered stationary phase, and typically 2 L were retained in the bioreactor and sterile media added to start another growth. Harvested cells were centrifuged at 3,000 × *g* for 20 min, washed two or three times with 10 mM PIPES, pH 7.0, frozen in liquid nitrogen, and stored at –80 °C.

Membrane Isolation and Protein Purification

Cells were suspended in lysis buffer (25 mM PIPES, pH 7.0, and 250 mM NaCl) which was degassed on a vacuum line and back filled with argon gas prior to use and supplemented with 500 μM $CuSO_4$. After lysis by sonication, cell debris was removed by centrifugation at 24,000 × *g* for 2 h. The membrane fraction was isolated by ultracentrifugation for 1 h at 160,000 × *g*. Membranes were rinsed twice with degassed lysis buffer using a Dounce homogenizer for resuspension. After the final wash, membranes were resuspended in lysis buffer to a concentration of ~20 mg/mL and frozen in liquid nitrogen. Membrane aliquots were stored at –80 °C until needed.

For solubilization, 1.5 mg dodecyl-ß-D-maltoside (DDM, Anatrace, Maumee, OH) was added to the membranes for every 1 mg protein, usually as a stock of 10% (w/v) DDM, but sometimes as a solid (usually only for large samples). The protein concentration of the membrane sample

was measured using the D_c Assay (Bio-Rad Laboratories, Richmond, CA). The sample was incubated with the detergent, gently rocking or stirring at 4 °C for ~15 min. Before loading onto a Source 15Q (GE Healthcare, Piscataway, NJ) anion exchange column, solubilized membranes were diluted four- or five-fold with buffer A (50 mM Tris, pH 8.5, 0.5% (w/v) DDM), degassed as described above. After loading the protein onto the column and rinsing with two column volumes of buffer A, pMMO was eluted with a 0–50% gradient of degassed buffer B (50 mM Tris, pH 8.5, 2.0 M NaCl, 0.5 % (w/v) DDM). The purification was performed in a 4 °C cold room. During the column run, the buffers were kept anaerobic by suspending balloons filled with argon gas above the bottles (Figure 2.1) to maintain a blanket of argon gas between the buffers and the air.

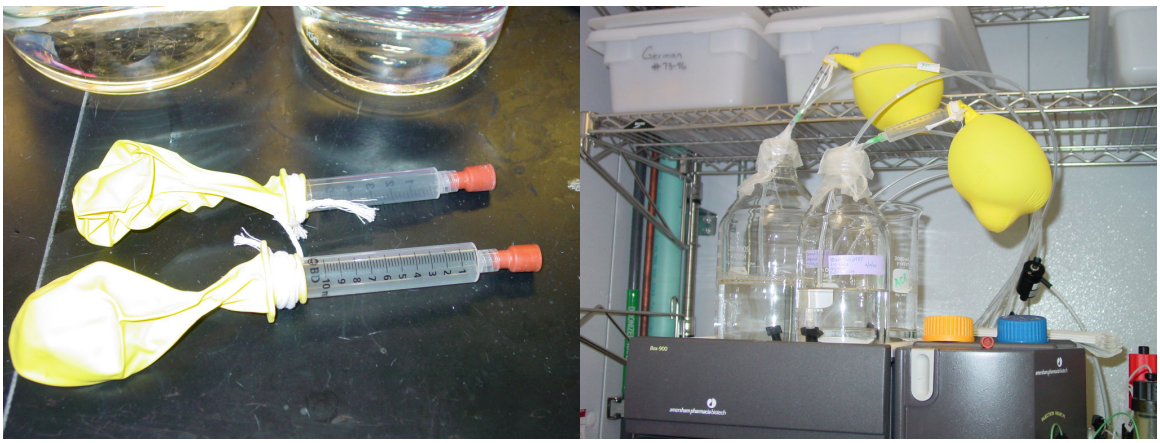

Figure 2.1. Argon-filled balloons used to keep buffers oxygen free
(left) Syringes and balloons before filling with argon gas. (right) Syringes and balloons, filled with argon gas and with needles attached, shown suspended above purification buffers.

Purified pMMO was concentrated to ~20 mg/mL for most applications, with either a Centriprep 50 for large volumes or a Microcon YM-100 for smaller volumes (Millipore Corporation, Billerica, MA). Concentrations of purified pMMO were determined by using an

extinction coefficient (253,511 $cm^{-1} \cdot M^{-1}$ per 100-kDa enzyme) determined by amino acid analysis (Protein Chemistry Laboratory, Texas A&M University, College Station).

Metal Analysis

Metal contents were determined by inductively coupled plasma-optical emission spectroscopy (ICP-OES) using a Varian Vista-MPX CCD Simultaneous ICP-OES (Analytical Services Laboratory, Northwestern University, Evanston, IL). Standards were prepared by diluting copper, zinc or iron atomic absorption standards (Sigma Aldrich, St. Louis, MO) with 2% (v/v) trace metal grade nitric acid (Fisher Scientific, Pittsburgh, PA) using acid-rinsed volumetric glassware. pMMO samples were diluted to a concentration of ~0.2 mg/mL in 2% (v/v) trace metal grade nitric acid using acid-rinsed volumetric glassware prior to analysis. All measurements were made in triplicate, and two or more independent samples were analyzed.

Activity Assays

The activity of pMMO at 30 ºC was measured by monitoring the epoxidation of propylene (*20, 61*) with duroquinol or NADH as a reductant (*61, 96*). Ethanol impurities in NADH were removed by vacuum. Duroquinol was made fresh each day by reducing duroquinone as described elsewhere (*22*). Copper-bound methanobactin was purified as described in Chapter 4.

In a typical experiment, either 49 µL protein and 1 µL 1 mg/mL NADH (aq) or 50 µL protein and a small spatula-tip full of duroquinone were mixed in a 2-mL septum sealed serum vial (Wheaton Science Products, Millville, NJ). Removing 2 mL of air from the vial and adding 2 mL propylene gas (Airgas/AGT, Palm, PA) started the reaction. After shaking at 200 rpm at 30 °C, the propylene oxide product was detected by gas chromatography using a Hewlett Packard 5890 gas chromatograph equipped with a Porapak Q column (6 ft × 1/8 in, Supelco, Bellafonte,

PA) and flame ionization detector and quantified by comparison with propylene oxide standards (Sigma Aldrich). Before the activity of purified pMMO was measured, samples were exchanged into lysis buffer containing 0.05% (w/v) Brij-58 (Anatrace). Assays of membrane-bound and solubilized pMMO were run for 3 minutes; purified pMMO was incubated 10 or 15 minutes before measuring the concentration of propylene oxide. All assays were performed in at least duplicate.

Ultraviolet-Visible-Near-Infrared (UV-Vis-NIR) Spectroscopy

Spectra were measured at room temperature with a Cary 500 UV-Vis-NIR spectrophotometer (Keck Biophysics Facility, Northwestern University, Evanston, IL) using 1-cm path length quartz cuvettes. Samples were in 50 mM Tris pH 8.5, 0.05% (w/v) DDM; the same buffer was used as the blank and to make a 100 mM dithionite stock solution. Dithionite-reduced pMMO was prepared by mixing 200 mg/mL pMMO with an equal volume of the dithionite stock solution, as previously described (*97*).

Electron Paramagnetic Resonance (EPR) Spectroscopy

Samples of purified pMMO for EPR were prepared as described above except for the inclusion of 10% (v/v) glycerol in the final samples. EPR spectra were recorded on a highly modified Bruker ESP 300 in the laboratory of Brian Hoffman (Northwestern University, Evanston, IL). Samples were kept frozen using a finger Dewar filled with liquid nitrogen. A 500 μM aqueous solution of CuEDTA was used as a standard, and EPR spectra of all samples were recorded under identical conditions as those for the standard. The spectra were background corrected by subtraction of a spectrum for buffer recorded under identical conditions. Double integration of background-corrected spectra was performed digitally using LabCalc® software.

The same field integration range was used for all samples and the spectra were baseline-corrected (linear) after the first digital integration. EPR simulations were performed using the program QPOWA, originally written by Belford and co-workers (*98, 99*), and subsequently modified by Joshua Telser (Roosevelt University, Chicago, IL and Northwestern University, Evanston, IL).

X-Ray Absorption Spectroscopy (XAS)

Two independent as-isolated pMMO samples were prepared for XAS studies in 50 mM Tris, pH 8.5, 0.5% (w/v) DDM, 250 mM NaCl and 30% (v/v) glycerol at copper concentrations between 1 and 2 mM. Samples were loaded into Lucite cells, wrapped with Kapton tape, flash frozen in liquid nitrogen and stored at –80 °C until data collection.

Additionally, several samples of reduced pMMO and one sample of oxidized pMMO were prepared for XAS analysis. Samples labeled "reduced #1", "reduced #2" and "reduced #3" were reduced as previously described (*74, 97*), and were 1.2, 1.2 and 0.7 mM in protomer, respectively. The sample labeled "oxidized #1" was reduced in the same manner, followed by addition of H_2O_2 to a concentration of ~1% and incubation on ice for 10 minutes. The concentration of the "oxidized #1" sample was 1.2 mM in protomer. The sample labeled "reduced #4" was reduced as described above, followed by removal of the dithionite via buffer exchange using an Amicon Ultra 50k MWCO (Millipore) wrapped in Parafilm (Pechiney Plastic Packaging, Chicago, IL). The final concentration of the "reduced #4" sample was not measured. Reduced and oxidized samples were also loaded into Lucite cells, wrapped with Kapton tape, flash frozen in liquid nitrogen and stored at –80 °C until data collection.

XAS data were collected at the Stanford Synchrotron Radiation Laboratory (SSRL) on

beamline 10-2, and at the National Synchrotron Light Source (NSLS) on beamline X9-b. The SSRL beamline was equipped with a Si[220] double crystal monochromator while the NSLS beamline utilized a Si[111] monochromator; both beamlines were equipped with harmonic rejection mirrors. During data collection, samples were maintained at 10 K using an Oxford Instruments continuous-flow liquid helium cryostat at SSRL and at 24 K using a He Displex Cryostat at NSLS. Protein fluorescence excitation spectra were collected using 13-element Ge solid-state detectors at both beamlines. At SSRL, a 0.6 μm nickel screen was placed between the cryostat and detector to filter background fluorescence scattering. XAS spectra at both facilities were measured in 5 eV increments in the pre-edge region (8750–8960 eV), 0.25 eV increments in the edge region (8986–9050 eV), and 0.05 $Å^{-1}$ increments in the extended X-ray absorption fine structure (EXAFS) region (to k = 13.5 $Å^{-1}$ Cu), integrating from 1 s to 20 s in a k^3 weighted manner for a total scan length of approximately 40 min. X-ray energies were individually calibrated by collecting Cu foil absorption spectra simultaneously with protein data. The first inflection point of the Cu foil spectrum was assigned to 8980.3 eV. Each fluorescence channel of each scan was examined for spectral anomalies prior to averaging and spectra were closely monitored for photoreduction. SSRL data represent the average of 6 to 7 scans while NSLS data represent the average of 9 to 10 scans.

XAS data were processed using the Macintosh OS X version of the EXAFSPAK program suite (*100*) integrated with the Feff v8 software (*101*) for theoretical model generation. Data reduction utilized a Gaussian function in the pre-edge region and a three-region cubic spline throughout the EXAFS region. Data were converted to k-space using a copper E_0 value of 9000 eV. The k cubed weighted EXAFS was truncated at 1.0 and 12.5 $Å^{-1}$ for filtering purposes. This

k range corresponds to a spectral resolution of approximately 0.14 Å for all copper-ligand interactions; therefore only independent scattering environments outside 0.14 Å were considered resolvable in the EXAFS fitting analysis (*102*). EXAFS fitting analysis was performed on raw/unfiltered data. EXAFS data were fit using both single and multiple scattering amplitude and phase functions calculated with the program Feff v8. Single scattering theoretical models were calculated for carbon, oxygen, sulfur and copper coordination to simulate copper-nearest neighbor ligand environments. A multiple scattering Cu-imidazole theoretical model was calculated to simulate the numerous scattering interactions observed from the linear ring. Scale factors (Sc) and E_0 values used during the simulations were calibrated by fitting crystallographically characterized copper models at different metal oxidation states, as described elsewhere (*74*). Criteria for judging the best-fit simulation utilized both the lowest mean square deviation between data and fit (F'), corrected for the number of degrees of freedom (*103*), and a reasonable Debye-Waller factor ($\sigma^2 < 0.006$ Å^2).

RESULTS AND DISCUSSION

Bacterial Growth, Membrane Isolation and Protein Purification

An extensive investigation was necessary to optimize the isolation of membrane-bound pMMO in order to obtain active enzyme. Variations in the growth of the cells included harvesting in mid-log phase (OD_{600} 5–8) and late log phase/stationary phase (OD_{600} 10–12) and controlling the pH during fermentation. The composition of the lysis buffer was varied by buffer type, pH and salt content. The effect of adding glycerol or Cu(II) to the lysis buffer was also checked. All buffers were degassed to ensure high oxygen levels did not inhibit or damage the enzyme. Cells were lysed either by sonication, a pressure homogenizer or French press. Finally,

the concentration of membrane-bound pMMO used for the assay was varied.

An active preparation of pMMO from *M. trichosporium* OB3b was finally obtained using the following conditions: a degassed buffer of 25 mM Pipes (pH 7.0) with 250 mM NaCl, cell lysis by sonication, and a final protein concentration over 15 mg/mL. The protein concentration appears to be particularly important for measuring enzyme activity. This may be due to stabilization of the enzyme at higher concentrations, or simply due to increased production of propylene oxide that is more readily detectable by gas chromatography. A more detailed discussion of activity assays can be found below.

Representative SDS-PAGE gels of membrane-bound and purified pMMO are shown in Figure 2.2. Membrane-bound *M. trichosporium* OB3b pMMO is shown with that from *M. capsulatus* (Bath) for comparison.

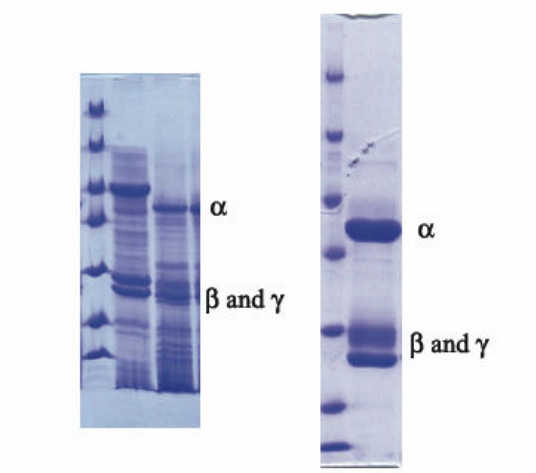

Figure 2.2. SDS-PAGE of pMMO
(left) SDS-PAGE gel of membrane-bound pMMO. Membrane bound pMMO from *M. capsulatus* (Bath) and *M. trichosporium* OB3b (center and right lanes, respectively). (right) SDS-PAGE gel of purified *M. trichosporium* OB3b pMMO (30 μg). In both gels, the left lane contains molecular mass standards: 116.0, 66.2, 45.0, 35.0, 25.0, 18.4 and 14.4 kDa.

Metal Content

The number of copper ions per protomer varies with the level of copper in the growth media. Membrane-bound pMMO isolated from cells grown at 10 μM copper contains 1.4 ± 0.2 copper ion per 100 kDa protein. The level of copper in the membrane-bound pMMO increases with increasing copper in the growth media up to approximately 50 μM copper in the growth media at which point it levels off. Therefore, a copper level of 50 μM copper in the growth media was chosen for all subsequent cell growth and protein characterization.

Table 2.1. Metal analysis of *M. trichosporium* OB3b pMMO

	Cu per 100 kDa	EPR detectable Cu (%)	Zn per 100 kDa	Fe per 100 kDa
membrane-bound	4.8 ± 1.1	97 ± 6	$2.7\ (\pm 1.8) \times 10^{-3}$	$2.1\ (\pm 0.8) \times 10^{-2}$
solubilized	4.0 ± 1.1	96 ± 24	$5.5\ (\pm 0.5) \times 10^{-3}$	$3.4\ (\pm 1.2) \times 10^{-2}$
purified	1.4 ± 0.6	86 ± 9	$1.3\ (\pm 0.6) \times 10^{-3}$	$7.6\ (\pm 6.3) \times 10^{-5}$

The membrane-bound pMMO from cells grown at 50 μM copper contains 4.8 ± 1.1 copper ions per 100 kDa protomer, and a similar stoichiometry of 4.0 ± 1.1 is obtained after solubilization (Table 2.1). By contrast, many preparations of membrane-bound and solubilized *M. capsulatus* (Bath) pMMO contain 15–20 copper ions per protomer (*10, 60, 61*). Initial reports for *M. trichosporium* OB3b membrane-bound pMMO indicated the presence of approximately 10 copper ions per 100 kDa (*96, 104*). Upon purification, the copper content is reduced to 1.4 ± 0.6 copper ions per protomer (Table 2.1). Early samples purified in the Okura laboratory contained 12.8 copper ions per 326 kDa complex (*96, 105*). This value was later revised to 2 copper ions per 94 kDa complex (*66*). The latter value is consistent with the current data as well as most reports for purified *M. capsulatus* (Bath) pMMO (*38, 61, 64*). In our experience, copper in *M. trichosporium* OB3b pMMO is more labile than that in *M. capsulatus* (Bath) pMMO. Membrane-bound, solubilized, and purified *M. trichosporium* OB3b pMMO all

contain less than 0.01 iron and zinc ions per protomer (Table 2.1). This finding is consistent with the absence of iron reported previously by the Okura laboratory; zinc was not measured in that study (*66*). Notably, all preparations of *M. capsulatus* (Bath) pMMO (*22, 38, 61, 64*) except those from the Chan laboratory contain significant amounts of iron.

Activity Assays

The average specific activity of membrane-bound *M. trichosporium* OB3b pMMO is 2.9 ± 1.7 or 3.0 ± 0.5 nmol propylene oxided (mg protein · min)$^{-1}$ with NADH or duroquinol as the reductant, respectively (Table 2.2). These results agree with values of 2–5 nmol propylene oxided (mg protein · min)$^{-1}$ reported by Okura and coworkers for membrane-bound *M. trichosporium* OB3b pMMO (*66, 96, 105*). Much higher specific activities have been reported for *M. capsulatus* (Bath) pMMO (*94*), but at this point it is unclear whether similar levels of activity are attainable with the *M. trichosporium* OB3b enzyme. The two organisms grow at different temperatures, the growth conditions and growth rates vary (*106*), and it is well documented that the specific activities of sMMO purified from *M. capsulatus* (Bath) (*107*) and *M. trichosporium* OB3b (*108*) are different despite having virtually identical active sites.

Table 2.2. Specific activity of *M. trichosporium* OB3b pMMO

	Reductant	Specific activity, nmol propylene oxided · (mg protein · min)$^{-1}$
membrane-bound	NADH	2.9 ± 1.7
	duroquinol	3.0 ± 0.5
solubilized	duroquinol	2.91 ± 0.4
purified	duroquinol	0.11 ± 0.1

The specific activity of whole cell lysate with NADH as the reductant is roughly equal to that of membrane-bound pMMO from the same protein prep. Addition of 100 μM $CuSO_4$, $Fe(NH_4)SO_4$, or $ZnSO_4$ to the assay mixture does not substantially improve the activity of

membrane-bound pMMO (Figure 2.3). The Okura laboratory has reported that copper addition up to approximately 100 μM increases activity (*96*), but those experiments utilized cells grown at 10 μM copper whereas the current cells were grown with 50 μM copper, which may be sufficient to load all the copper sites.

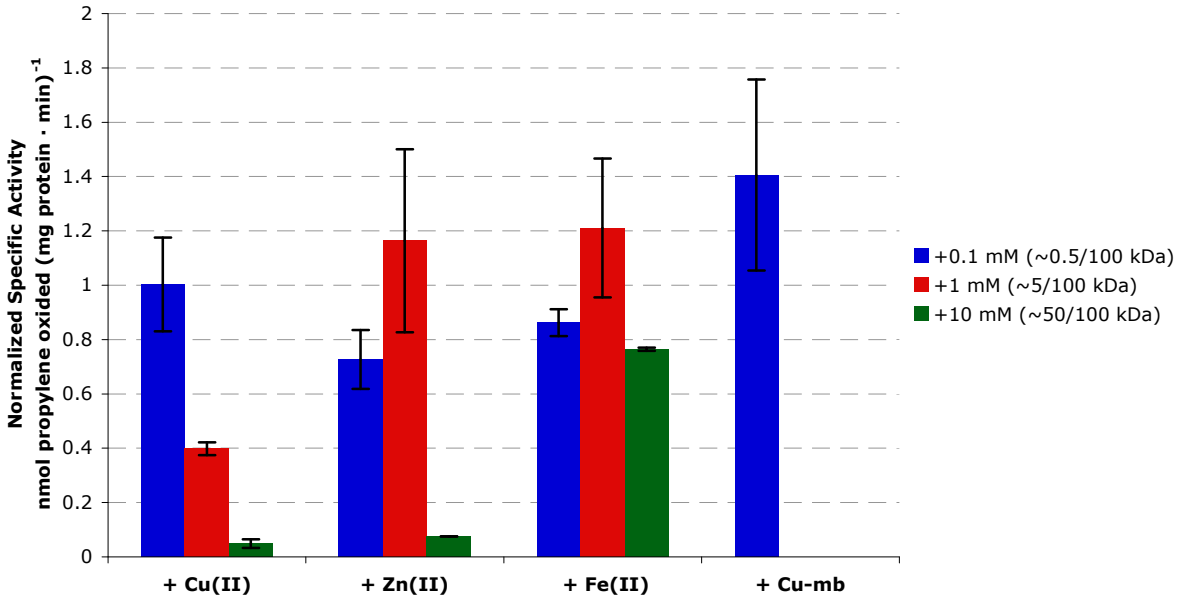

Figure 2.3. Effect of the addition of metals and methanobactin on the activity of membrane-bound pMMO
Data is shown normalized to the specific activity without the additive to account for differences in different preparations of membrane-bound pMMO. Assays were performed at 30°C with duroquinol as the reductant.

Addition of higher concentrations of metals to the assay mixture gives conflicting results (Figure 2.3). Addition of a large excess of zinc or copper causes a sharp decrease in activity. In the case of zinc, its presence in one of the metal sites of the *M. capsulatus* (Bath) crystal structure (Chapters 1 and 3) gives a reasonable explanation as to why activity may be inhibited. Addition of a large excess of iron, however, causes only a modest drop in activity. These results

need to be investigated further before any definitive conclusions can be drawn, preferably using the *M. capsulatus* (Bath) enzyme, whose higher level of specific activity will allow easier differentiation among the effects of the various assay additives.

The effect of copper-bound methanobactin (Cu-mb) from *M. trichosporium* OB3b (Chapter 4) on membrane-bound pMMO was also investigated. Addition of 0.5 Cu-mb per 100 kDa protein results in an ~40% increase in the specifc activity (Figure 2.3). A similar percent increase was seen upon addition of *M. trichosporium* OB3b Cu-mb to *M. capsulatus* (Bath) membrane-bound pMMO (*92*). In both that previous study and this work, the increase in activity was found to be higher than that from adding $CuSO_4$ (aq). Methanobactin is known to bind Cu(I), however, so a more useful control would be to measure the change in specific activity upon the addition of Cu(I) to the assay.

Unlike *M. capsulatus* (Bath) pMMO (*61*), solubilization with DDM does not appreciably decrease activity. After purification, *M. trichosporium* OB3b pMMO exhibits decreased activity of 0.11 ± 0.01 nmol propylene oxided (mg protein · min)$^{-1}$ (Table 2.2). Comparable values of 0.5–3.5 nmol propylene oxided (mg protein · min)$^{-1}$ have been reported previously (*66, 105*). Similar to results reported by Okura and coworkers, a neutral pH (*96*) and the use of Brij-58 detergent (*105*) were crucial for observing activity in purified pMMO. Attempts to improve the specific activity of purified pMMO by adding other fractions from the 15Q column used in the purification were unsuccessful. Addition of copper (100 μM $CuSO_4$ (aq)) or the synthetic lipids 1,2-dioleoyl-*sn*-glycero-3-phosphocholine (DOPC) and 1,2 dioleoyl-*sn*-glycero-3-[phospho-*rac*-(1-glycerol)] (DOPG) (Avanti Polar Lipids, Alabaster, AL) also did not improve the activity of purified pMMO.

UV-Vis-NIR Spectroscopy

The UV-Vis-NIR spectrum of *M. trichosporium* OB3b pMMO exhibits a strong peak at 280 nm with an extinction coefficient of 253,511 $cm^{-1} \cdot M^{-1}$ $protomer^{-1}$, as measured by amino acid hydrolysis (Figure 2.4).

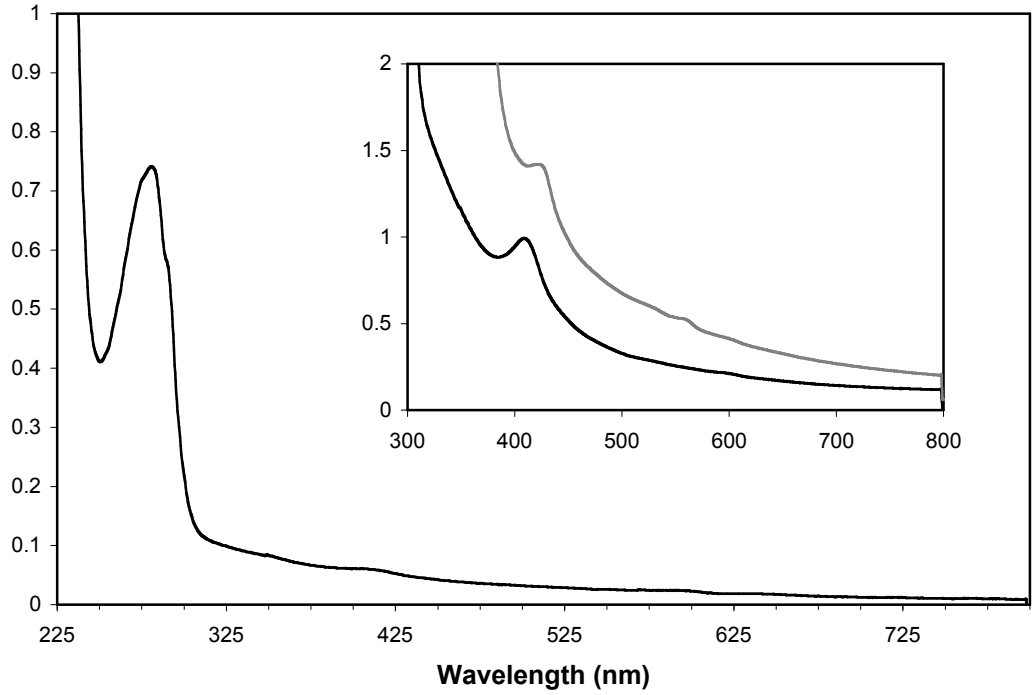

Figure 2.4. UV-Vis-NIR spectra of purified pMMO
Main figure: spectrum of 0.27 mg/mL *M. trichosporium* OB3b pMMO. Inset: spectra of ~100 mg/mL as-isolated (black line) and dithionite-reduced (grey line) *M. trichosporium* OB3b pMMO.

Additionally, a peak at 409 nm with a much lower extinction coefficient is observed in all purified samples (Figure 2.4, inset). The maximum of the peak shifts to 422 nm upon reduction with dithionite. This peak is most likely due to a small amount of a heme-containing protein that is not completely removed during purification (*109*). Assuming an extinction coefficient of 100,000 $cm^{-1} \cdot M^{-1}$ and a molecular mass of 20,000 $g \cdot mol^{-1}$ (average values for cytochromes

(*110*)), this contaminant is ~0.19% (w/w) of the purified pMMO sample. If the same calculation is done based on the amount of iron found in purified pMMO samples (Table 2.1), the estimate of cytochrome contamination is ~0.15% (w/w). Given the similarity of these estimates, it is likely that all of the iron in purified samples of *M. trichosporium* OB3b pMMO is associated with these cytochrome impurities. The distinct peaks observed in the 500-600 nm range upon reduction of *M. capsulatus* (Bath) pMMO (*97*) were not observed in samples of reduced *M. trichosporium* OB3b pMMO.

The complete genome of *M. trichosporium* OB3b is unknown; however, many heme-containing proteins were identified when the genome of *M. capsulatus* (Bath) was completed recently (*27*). In this laboratory, higher levels of cytochrome contamination (~2% w/w) were observed in purified samples of *M. capsulatus* (Bath) pMMO (*97*).

EPR Spectroscopy

The X-band EPR spectra of membrane-bound, solubilized and purified *M. trichosporium* OB3b pMMO are shown in Figure 2.5. All forms of the enzyme are heterogeneous by EPR with at least two types of closely related mononuclear type 2 Cu(II) signals. For membrane-bound and solubilized pMMO, no hyperfine coupling from nuclei other than ^{63,65}Cu is observable. However, the X-band EPR spectrum of purified pMMO exhibits resolved hyperfine coupling that can be assigned to that from ^{14}N nuclei. The two overlayed signals (Figure 2.6) in purified pMMO can be described by the following parameters: a major component with $g_{\perp}$ = 2.052, $g_{\|}$ =2.247, $A(^{63}\mathrm{Cu})_{\|}$ = 585 MHz, $A(^{63}\mathrm{Cu})_{\perp}$ = 60 MHz (this last value has significant uncertainty) and a minor component with $g_{\perp}$ = 2.060, $g_{\|}$ = 2.225, and with ^{63}Cu hyperfine coupling indistinguishable from that of the major component, but with hyperfine coupling to two

equivalent nitrogen nuclei of 40 MHz. Due to the uncertainty in the EPR parameters in the perpendicular region, which dominates the overall integrated signal intensity of the components, we cannot quantify the relative amount of the two components beyond estimating that the major component is at least 80% of the total signal. Furthermore, because of spectral overlap, it is possible that as many as three nitrogen nuclei are coupled. On the basis of the crystallographic data ((*57*) and Chapter 3), two nitrogen ligands are reasonable.

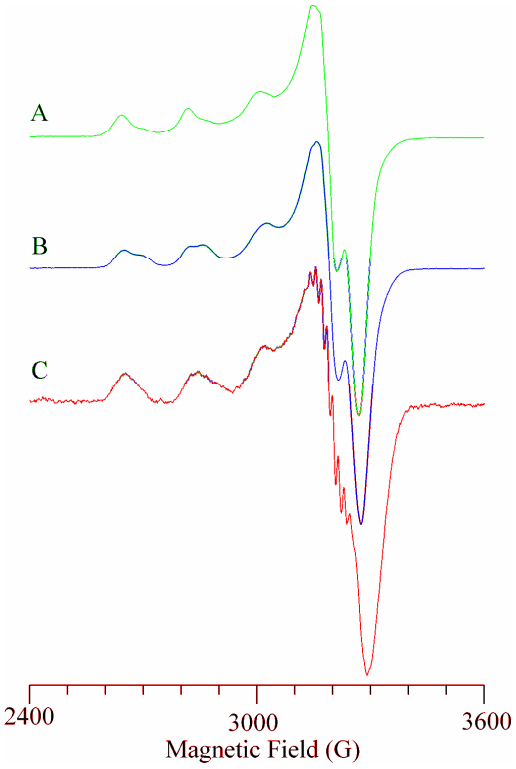

Figure 2.5. X-band EPR spectra pMMO
Spectra of membrane-bound (A), solubilized (B), and purified (C) *M. trichosporium* OB3b pMMO. The spectra have been normalized for easier comparison. Experimental conditions: temperature, 77 K; microwave frequency, 9.21 GHz; microwave power, 7 mW; 100 kHz field modulation amplitude, 5 G; time constant, 300 ms; scan time, 4 min.

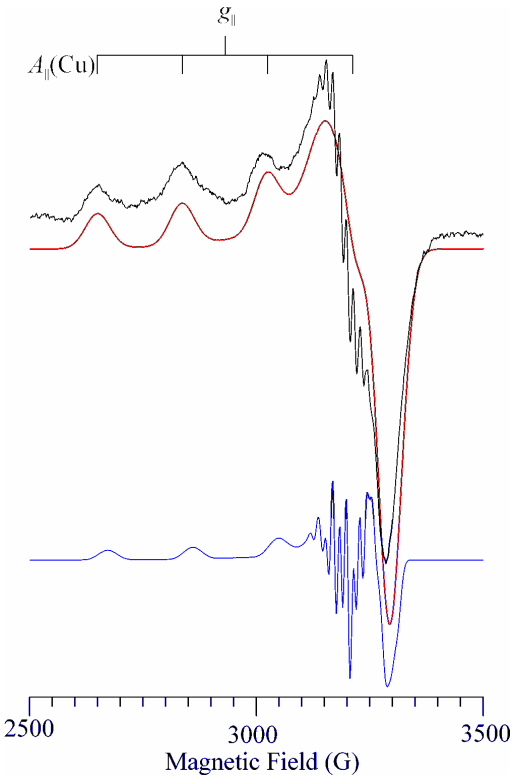

Figure 2.6. X-band EPR of purified *M. trichosporium* OB3b pMMO
The experimental spectrum is shown in black (uppermost trace). The simulation of the major component is shown in red, with parameters: $g_{\perp}$ = 2.052, $g_{\|}$ =2.247, $A(^{63}Cu)_{\|}$ = 585 MHz, $A(^{63}Cu)_{\perp}$ = 60 MHz (this last value has significant uncertainty); Gaussian lineshapes are used with single-crystal linewidths of 100 MHz (half-width at half-maximum). The simulation of the minor component is shown in blue with parameters: $g_{\perp}$ = 2.060, $g_{\|}$ = 2.225, $A(^{63}Cu)_{\|}$ = 585 MHz, $A(^{63}Cu)_{\perp}$ = 60 MHz (both ^{63}Cu hyperfine couplings are set equal to the values determined for the major component), and with hyperfine couplings to two equivalent nitrogen nuclei: $A(^{14}N)_{isotropic}$ = 40 MHz; linewidths are 18 MHz at $g_{\perp}$ and 40 MHz at $g_{\|}$. The relative intensities of the two have been scaled to approximate their relative amounts, but precise quantitation is not implied.

These spectra are similar to those reported previously for pMMOs from *M. capsulatus* (Bath), *Methylomicrobium album* BG8, and *M. trichosporium* OB3b (*22, 38, 61, 64, 71*). The $g_{\|}$ value for the minor component is smaller than the other reported parameters and could be indicative of a site slightly different from those seen in other pMMO preparations. The well

resolved hyperfine lines associated with the second, minor component are also observed in whole cell samples of *M. capsulatus* (Bath) and *M. album* BG8 (*71*). Integration relative to a Cu(II) standard indicates that ~85% of the copper in the sample is EPR active, in contrast to the 40–60% EPR active copper observed for the *M. capsulatus* (Bath) enzyme (*61, 64*). Importantly, no signal attributed to a trinuclear copper center (*69, 70*) is detected. Although initial EPR spectra from the Okura group supported the presence of a tricopper center in *M. trichosporium* OB3b pMMO (*96, 105*), the signal was not detected once the purification was optimized (*66*), consistent with the current results.

XAS Spectroscopy

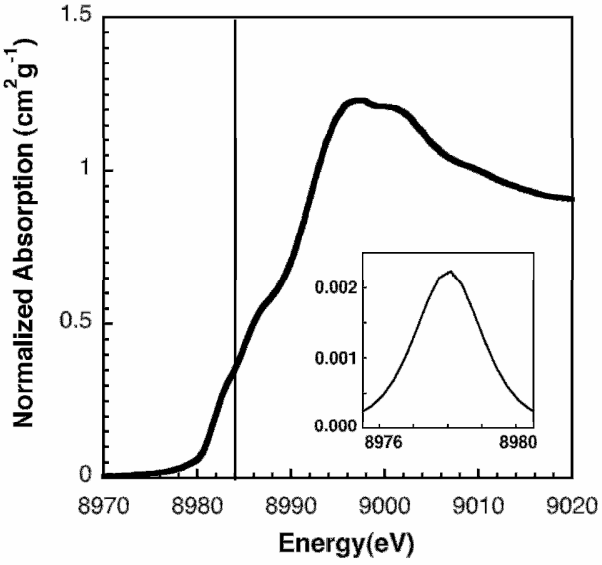

Figure 2.7. Copper XANES spectrum of purified *M. trichosporium* OB3b pMMO
The solid vertical line at 8984 eV identifies spectral features corresponding to the Cu(I) 1s→4p transition, and the inset shows an expanded view of the Cu(II) 1s→3d transition.

The copper K-edge XAS near edge spectrum of purified, as-isolated *M. trichosporium* OB3b pMMO (Figure 2.7) shows pre-edge features centered at 8980 eV and 8984 eV. The absorption

feature at 8980 eV, attributed to a 1s→3d transition for centrosymmetric Cu(II), has a low area of 0.52 (unitless) indicating that copper is partially present as Cu(I). The feature at 8984 eV, characteristic of a Cu(I) 1s→4p transition, is also observable but weak. These results indicate that the copper in this sample is a mixture of Cu(I) and Cu(II) (*111*).

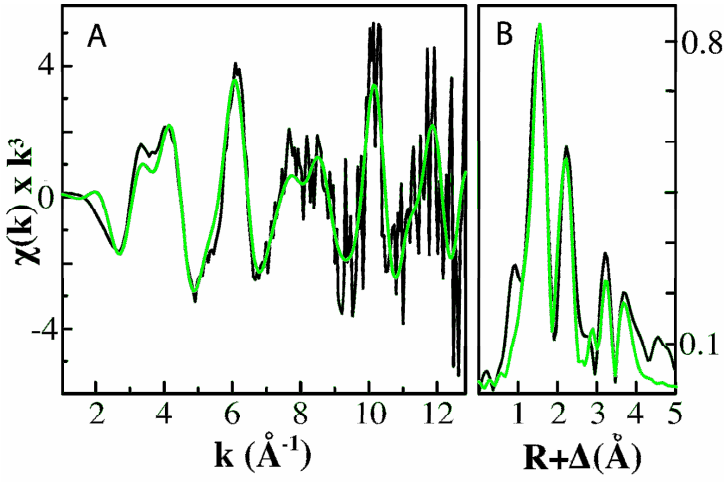

Figure 2.8. Copper EXAFS fitting analysis for purified *M. trichosporium* OB3b pMMO
(A) Raw unfiltered EXAFS data (black) and simulations (green) for copper bound to pMMO. (B) Fourier transforms of the raw EXAFS (black) and best fit simulation (green).

Copper bound to pMMO is held by an averaged nearest neighbor coordination environment constructed of nitrogen, oxygen, and copper ligands. Raw EXAFS for a representative data set shows a camel-back beat pattern at k ~ 3.8 $Å^{-1}$, characteristic of histidine imidazole multiple scattering (*112*), and a defined node in the data at k ~ 9 $Å^{-1}$ (Figure 2.8A). The Fourier transform of the Cu EXAFS (Figure 2.8B) shows two peaks below the bond length shifted value of 2.6 Å, indicative of two distinct nearest neighbor environments, as well as long range scattering at R > 3.0 Å. EXAFS simulations indicate the average Cu nearest neighbor environment is constructed of oxygen/nitrogen ligands at 1.97 Å and distinct Cu-Cu coordination at 2.52 Å (Table 2.3).

Attempts to include sulfur scattering were unsupported by these data. Long-range scattering (R > 3 Å) could be best fit with carbon scattering at 3.88 Å and 4.08 Å (Table 2.3, Fit 4). Fitting analysis using a theoretical multiple scattering imidazole model bound to Cu gave reasonable simulations (Table 2.3, Fit 5), however these simulations were not justified based on an elevated degrees of freedom weighed goodness of fit (F') parameter value relative to the best fit simulation using single scattering models only (Table 2.3, Fit 4).

Table 2.3. Summary of Cu EXAFS fitting analysis for *M. trichosporium* OB3b pMMO
Data fit over a k range of 1 to 12.5 $Å^{-1}$. Best-fit parameters are indicated in bold.

	Ligand Environment[a]				Ligand Environment[a]				Ligand Environment[a]				
Fit	**Atom[b]**	**R(Å)[c]**	**C.N.[d]**	**σ^2 [e]**	**Atom[b]**	**R(Å)[c]**	**C.N.[d]**	**σ^2 [e]**	**Atom[b]**	**R(Å)[c]**	**C.N.[d]**	**σ^2 [e]**	**F' [f]**
1[g]	O/N	1.97	2.00	3.59									1.41
2[g]	O/N	1.97	2.00	3.80	Cu	2.52	0.50	4.56					1.10
3[g]	O/N	1.97	2.00	3.85	Cu	2.52	0.50	4.22	C	3.88	3.00	3.35	1.00
4[g]	**O/N**	**1.97**	**2.00**	**3.86**	**Cu**	**2.52**	**0.50**	**4.30**	**C**	**3.88**	**3.00**	**3.47**	**0.96**
									C	**4.08**	**4.00**	**1.80**	
5[h]	N_{im}	1.99	2.50	4.12	Cu	2.50	0.50	3.83	C	3.85	2.00	1.76	1.14
									C	4.07	3.00	2.10	

[a] Independent metal-ligand scattering environment
[b] Scattering atoms: O (oxygen), N (nitrogen), C (carbon), Cu (copper)
[c] Average metal-ligand bond length for 2 independent samples
[d] Average metal-ligand coordination number for 2 independent samples
[e] Average Debye-Waller factor in $Å^2$ x 10^3 for 2 independent samples
[f] Number of degrees of freedom weighted mean square deviation between data and fit
[g] Fit using only single scattering Feff 8 theoretical models
[h] Fit using both single scattering Feff 8 model with an additional multiple scattering Cu-N(imidazole) model, generated based on crystallographic coordinates, and labeled N_{Im} in table atom designation.

These results are nearly identical to the average oxygen/nitrogen distance of 1.97 Å and Cu-Cu distance of 2.51 Å obtained for purified *M. capsulatus* (Bath) pMMO (*74*). The observation of a short Cu-Cu interaction in pMMO from a second organism strengthens the previous EXAFS results on *M. capsulatus* (Bath) pMMO (*74*) and strongly supports the presence and functional relevance of the dicopper center modeled in the *M. capsulatus* (Bath) pMMO structure (*57*).

SUMMARY

Membrane-bound *M. trichosporium* OB3b pMMO was found to have a specific activity of 3.0 ± 0.5 nmol propylene oxidized (mg protein · min)$^{-1}$ and 4.8 ± 1.1 copper ions per 100 kDa protein. After purification, the specific activity is 0.11 ± 0.1 propylene oxidized (mg protein · min)$^{-1}$ and the protein contains 1.4 ± 0.6 copper ions per 100 kDa. Both membrane-bound and purified *M. trichosporium* OB3b pMMO contain less than 0.01 iron and zinc ions per 100 kDa.

The X-band EPR spectrum of *M. trichosporium* OB3b pMMO exhibits two overlayed signals: a type 2 Cu(II) signal with no resolved ^{14}N hyperfine as well as a smaller second signal with resolved ligand hyperfine coupling indicative of nitrogen coordination. The copper XANES spectrum of as-isolated *M. trichosporium* OB3b pMMO indicates the presence of both Cu(I) and Cu(II). Copper EXAFS data indicate a copper coordination environment very similar to that in *M. capuslatus* (Bath) pMMO, including a Cu-Cu distance of ~2.5 Å.

CHAPTER 3: CRYSTAL STRUCTURE OF PARTICULATE METHANE MONOOXYGENASE FROM *METHYLOSINUS TRICHOSPORIUM* OB3B

Portions of this chapter will be published as Hakemian, A. S.; Kondapalli, K. C.; Telser, J.; Hoffman, B. M.; Stemmler, T. L.; Rosenzweig, A. C. *Biochemistry* submitted.

ABSTRACT

Methylosinus trichosporium OB3b pMMO was found to crystallize reproducibly under acidic conditions with PEG3000 as a precipitant, and the crystal structure was solved to 3.9 Å resolution. Although extensive screening was undertaken, no further improvement in resolution was attained.

Crystallographic characterization of *M. trichosporium* OB3b pMMO shows that a mononuclear copper center found in the *Methylococcus capsulatus* (Bath) pMMO X-ray structure is not present whereas a dinuclear copper center is clearly conserved. Notably, a metal center occupied by zinc in the *M. capsulatus* (Bath) pMMO structure is occupied by copper in *M. trichosporium* OB3b pMMO. These findings extend previous work on pMMO from *M. capsulatus* (Bath) and provide new insight into the functional importance of the different metal centers.

INTRODUCTION

In addition to the biophysical characterization of *Methylosinus trichosporium* pMMO presented in the previous chapter, crystallographic characterization was undertaken to address several of the questions raised by the *Methylococcus capsulatus* (Bath) pMMO crystal structure reported in 2005 (*57, 58, 97*). Of particular interest were the metal content of the zinc and mononuclear copper sites found in that structure. The zinc ion was most likely derived from the crystallization buffer, leaving the identity of the metal ion found at this location in vivo unknown. The ligands to the mononuclear copper found in the *M. capsulatus* (Bath) protein are not conserved across methanotrophs (Chapter 1 and (*94*)); therefore, it was unclear whether this site contained a metal ion in pMMO from other species.

Crystallization of a membrane protein presents a unique set of challenges. Because these proteins contain large hydrophobic areas, detergents must be used once the protein has been removed from its native lipid environment to prevent aggregation and precipitation (*113*). The large portion of the protein surface covered with these hydrophobic residues leaves relatively few polar residues available for forming crystal contacts. Thus, extensive screening in the presence of various detergents is usually required to find a successful crystallization condition (*114*). Additionally, techniques such as crystallization in lipid cubic phases or co-crystallization with antibody fragments are sometimes required (*115*).

The structure of *M. trichosporium* OB3b pMMO presented here complements previous work on *M. capsulatus* (Bath) pMMO and directly addresses questions about the metal centers raised by the *M. capsulatus* (Bath) pMMO crystal structure.

MATERIALS AND METHODS

Crystallization

For crystallization, *M. trichosporium* OB3b pMMO was purified as described in Chapter 2. The protein was then exchanged into an appropriate buffer, usually 50 mM Tris, pH 8.5, 0.03% (w/v) undecyl-ß-D-maltoside (UDM, Anatrace), by diluting and concentrating with a Microcon YM-100 three times. An initial crystallization condition was identified with the Wizard II screen (Emerald BioSystems, Bainbridge Island, WA) and optimized. Crystals were grown using sitting-drop geometry at room temperature. Incubation of crystal trays at 4 and 20 °C was attempted, but did not result in improved diffraction. Drops contained 1 μL of 18–22 mg/mL purified pMMO and 1 μL precipitant solution (100 mM cacodylate pH 6.5, 20% (v/v) PEG 3000, 250 mM magnesium formate or manganese chloride). Unlike *M. capsulatus* (Bath) pMMO (*57*), zinc is not required for crystallization. Crystals grew within two weeks, but crystals harvested after 3–6 months resulted in the best diffraction. Crystals that diffracted beyond 10 Å resolution had dimensions $1.0 \times 0.25 \times 0.25$ mm^3, but most crystals were smaller and not useful for data collection. Crystals were flash frozen using 25% (v/v) PEG 400, 75 mM cacodylate, pH 6.5, 15% (v/v) PEG 3000, and 187.5 mM magnesium formate (crystal pmmo17 in Table 3.2) or manganese chloride (crystal pmmo08 in Table 3.2) as a cryoprotectant. The crystals belong to space group $P2_12_12_1$. The unit cell dimensions varied from crystal to crystal (Table 3.2). All crystals exhibited moderate to severe anisotropy in their diffraction pattern.

Multiple methods were used in an attempt to improve diffraction of the *M. trichosporium* OB3b pMMO crystals. Addition of an ammonium sulfate precipitation to the purification protocol (*57, 97, 116*) did not result in an improvement of the purity of the protein or in the

diffraction quality of the crystals. The Wizard I screen (Emerald BioSystems) and MBClass Suite (Qiagen, Valencia, CA) were used with the detergents DDM, UDM and Cymal-5 (Anatrace) to identify other possible crystallization conditions, but no better hits were found. Crystals were serially dehydrated by soaking in progressively higher concentrations of PEG3000 (*117*). Though dehydration did not appear to damage the crystals, it also did not result in an improvement in diffraction.

Pressurization of crystals with xenon gas was attempted in the hope of identifying the methane binding site(s) in pMMO. Xenon is a small, hydrophobic species, like methane, and the identification of xenon binding site(s) would give clues as to the location of the pMMO active site (*118*). However, this treatment destroyed the diffraction of all crystals on which it was attempted.

Crystals were soaked in a cryoprotectant containing 1 mM *M. trichosporium* OB3b copper-bound methanobactin (Chapter 4) overnight and data was collected just above the copper edge, in an attempt to identify a putative methanobactin binding site on pMMO. The methanobactin did not appear to lower the diffraction quality of the crystals, but methanobactin was not visible in the anomalous maps or the electron density maps.

Finally, extensive screening was done in collaboration with the Ismagilov group at The University of Chicago (Chicago, IL). Using the microfluidic technique developed in that laboratory, it was possible to screen a large number of conditions using a very small amount of protein, as the volume of each drop was approximately 10 nL (*119*). Screening was conducted using several commercial and homemade screens, as well as with a wide range of additives. Initial screening in microfluidic plugs using the JcsG+ Suite (Qiagen) and ~12 mg/mL pMMO in

0.3% (w/v) UDM resulted in several hits (Table 3.1), with condition 87 resulting in crystals with the best diffraction. JcsG+ 87 was used to scale up the crystallization using sitting drop trays at 5 mg/mL protein concentration. At this protein concentration, the protein precipitated, although crystals did form. However, diffraction from crystals in sitting drop trays was worse that that of crystals from microfluidic plugs (Ismagilov laboratory notebook page QF8-65).

Table 3.1. Summary of JcsG+ Suite conditions from which crystals of *M. trichosporium* OB3b pMMO were obtained

All final conditions in plugs contained 0.0437 M Bis-tris pH 5.5 as a buffer and 0.1094% (w/v) PEG 3350 as a precipitant.

Condition	Salt
JcsG+ 87	none
JcsG+ 92	0.0875 M NaCl
JcsG+ 93	0.0875 M Li_2SO_4
JcsG+ 94	0.0875 M NH_4OAc
JcsG+ 95	0.0875 M $MgCl_2$

JcsG+ conditions 87 and 92 were used for further optimization in both plugs and crystallization trays. The concentration of UDM was varied, with distinct results at different detergent concentrations in the JcsG+ 92 condition. Crystals formed in 1% (w/v) UDM (final concentration) gave the best diffraction (~3.2 Å without anisotropy) (notebook page QF8-12), but the crystal quality deteriorated quickly under X-ray irradiation (after collection of ~20-30 frames of data). Many PEG molecular weights were tried as the precipitant (PEG 400, PEG MME 550, PEG 1000, PEG 3000, PEG 3350, PEG 4000, PEG 8000 and PEG 10000), and the buffer concentration was also varied (0.01M, 0.02M, 0.05M, 0.1M) (notebook page QF8-127). MES buffer gives crystals with less precipitation, but they do not diffract as well as those from the original Bis-tris condition. The synthetic lipids DOPG, DOPC, and DOPE (Avanti Polar Lipids) were used as additives in these crystallization trials, as the presence of lipids may result in more ordered protein molecules (*120*). However, the crystal quality was lower than that of

crystals that didn't contain lipids.

Additionally, co-crystallization and crystal soaks with *M. trichosporium* OB3b methanobactin and halogenated substrate and product analogs (2-iodoethanol, 2-bromoethanol, 2-chloroethanol, iodomethane, iodoethane, 1,3-diiodopropoane, 1,2-dibromoethane, 2-bromopropane, dichloromethane) were attempted. For co-crystallization, these were added to crystallization trials with a ratio of 2:1 (protein: additive) in the JcsG+ 92 condition. The crystals quality was lower than those crystals formed in the absence of additives, however (notebook page QF7-13).

Structure Determination

All data sets were collected at the GM/CA-CAT beamline at the Advanced Photon Source (Argonne National Laboratory, Argonne, IL) with a MarMosaic300 detector and processed with XDS (*121*) or MOSFLM (*122*) and SCALA (*123*) (Table 3.2). The structure was solved to 3.9 Å resolution by molecular replacement with PHASER (*124*) using the *M. capsulatus* (Bath) pMMO trimer (*57*) (accession code 1YEW) as a search model. The sequence was changed to that of *M. trichosporium* OB3b by threading the sequences (NCBI accession numbers AAA87220 (PmoA), AAF37894 (PmoB), AAF37893 (PmoC)) onto the molecular replacement model using Swiss-PdbViewer (*125*). The programs Coot (*126*) and CNS (*127*) were used for model building and refinement. Strict non-crystallographic symmetry (NCS) restraints were imposed between the three protomers throughout the refinement, and composite omit maps were used for validation. Data were additionally processed using the Diffraction Anisotropy Server (*128*), which allowed the inclusion of some data to 2.9 Å resolution (Table 3.2). Although the higher resolution shells are very incomplete, the anisotropically scaled data did reveal density for some side chains not

present in the 3.9 Å maps. The final model consists of residues 40–283, 295–317, 328–346 and 351–426 for pmoB, 12–249 for pmoA, and 18–176 for pmoC, 3 copper ions modelled on the basis of anomalous Fourier maps (*vide infra*), and 47 additional alanine residues per protomer. A Ramachandran plot generated with PROCHECK (*129*) indicates good geometry with 92.1% of the residues in the most favored and additionally allowed regions. Because native crystals were not isomorphous, molecular replacement with PHASER (*124*) and refinement were carried out independently for data sets collected from different crystals (Table 3.2).

RESULTS AND DISCUSSION

Structure Determination

The best crystals of *M. trichosporium* OB3b pMMO diffracted anisotropically to better than 4 Å resolution (Figure 3.1). The crystal structure was solved to 3.9 Å resolution, with some information also obtained from incomplete anisotropic data to 2.9 Å resolution (Table 3.2).

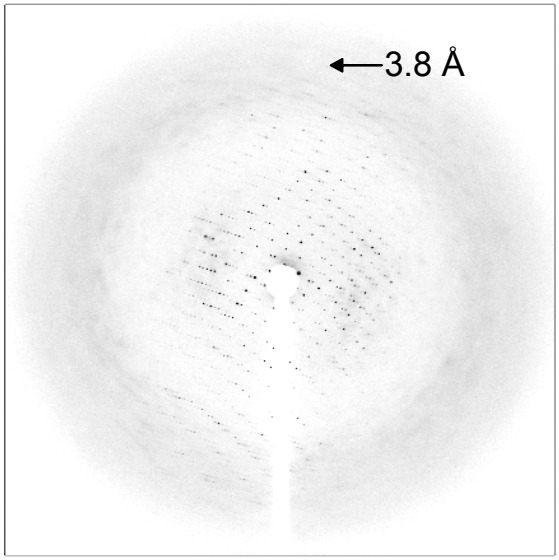

Figure 3.1. Diffraction pattern of the pmmo17 crystal used to solve the structure of *M. trichosporium* OB3b pMMO

Table 3.2. Crystallographic data collection and refinement statistics

	pmmo17	pmmo17_aniso	pmmo08_3Cu	pmmo08_3Zn
Data Collection				
Space group	$P2_12_12_1$		$P2_12_12_1$	
Cell dimensions				
a, *b*, *c* (Å)	113.8, 184.1, 203.9		117.4, 184.7, 192.3	
Wavelength (Å)	0.979	0.979	1.378	1.278
Resolution (Å)	38-3.90 (4.10-3.90)	38-2.91 (3.05-2.91)	40.0-4.30 (4.52-4.30)	40.0-5.50 (5.80-5.50)
R_{sym} [b,c]	0.086 (37.6)		0.079 (0.351)	0.067 (0.293)
$I/\sigma I$	7.5 (2.0)	8.0 (5.5)	4.1 (1.8)	4.0 (1.9)
Completeness (%)[b]	99.8 (99.8)	59.7 (4.5)	97.9 (99.2)	98.1 (99.2)
Redundancy	7.4		3.5	3.4
Refinement				
Resolution (Å)	38-3.90	38-2.91	40-4.30	
No. reflections	39693	56495	54183	
R_{work} [d] / R_{free} [e]	0.342/0.377	0.365/0.408	0.344/0.388	
No. atoms				
Protein	18945		18945	
Cu	9		9	
Average B-factor	148.8		166.6	
R.m.s deviations				
Bond lengths (Å)	0.011		0.010	
Bond angles (°)	1.864		1.679	

[a]pmmo17 and pmmo08 refer to two different crystals
[b]$R_{sym} = \Sigma| I_{obs} - I_{av}| / \Sigma F_{obs}$, where the summation is over all reflections
[c]Values in parentheses refer to the highest-resolution shell
[d]$R_{work} = \Sigma| F_{obs} - F_{calc}| / \Sigma F_{obs}$
[e]For calculation of R_{free}, 5 % of the reflections were reserved

Despite exhaustive efforts, the resolution could not be improved. A possible reason for this can be seen upon examination of the crystal packing (Figure 3.2). Though the soluble region of each pMMO trimer appears to make extensive crystal contacts with the opposite end of the adjacent trimer, there are large solvent channels between these "chains" of pMMOs. This arrangement was observed in all the crystals of *M. trichosporium* OB3b with sufficient diffraction to examine, and probably accounts for the severe anisotropy of all the data collected. In spite of these limitations, information about the overall structure and critical new insight into the metal centers of pMMO has been obtained.

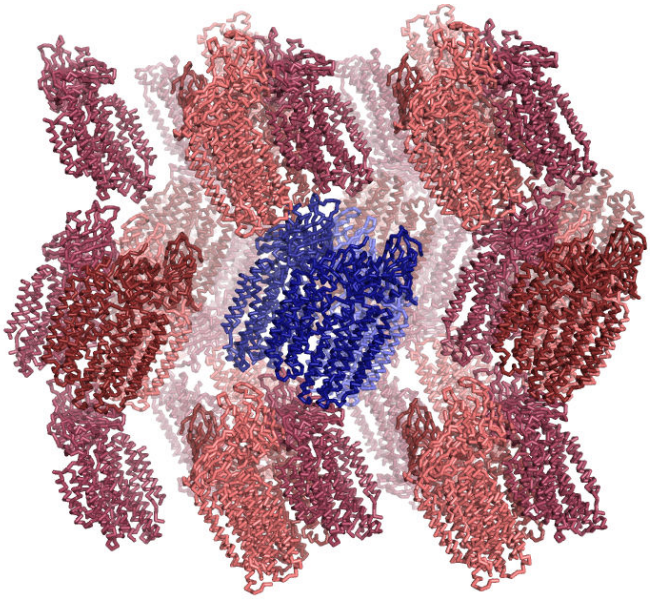

Figure 3.2. Packing of *M. trichosporium* OB3b pMMO crystals
The central pMMO trimer is shown in blue with symmetry related trimers shown in red; the top layer of symmetry related molecules has been removed for clarity. The three protomers are shown as dark, medium and light shades.

Overall Architecture

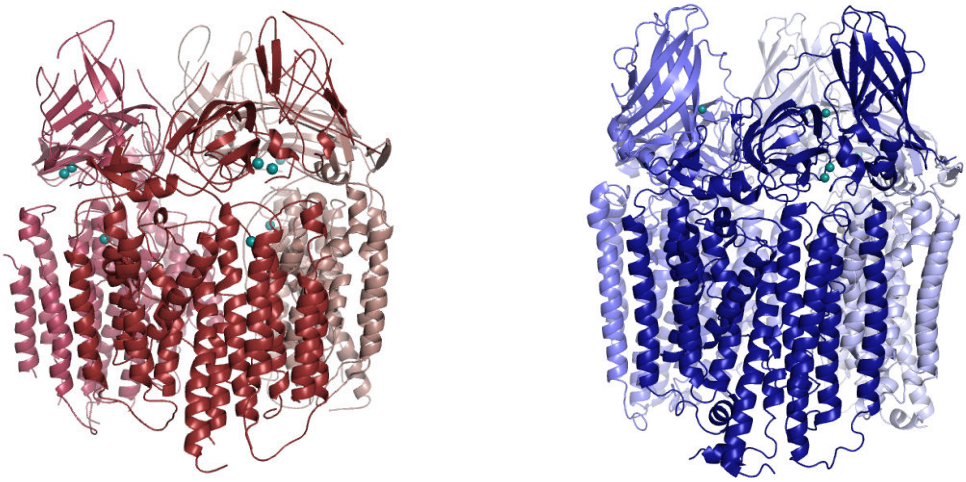

Methylosinus trichosporium OB3b pMMO

Methylococcus capsulatus (Bath) pMMO

Figure 3.3. Comparison of the overall architecture of pMMO from *M. trichosporium* OB3b and *M. capsulatus* (Bath)

The overall architecture of the enzyme is the same as *M. capsulatus* (Bath) pMMO (*57, 58*), an $\alpha_3\beta_3\gamma_3$ trimer (Figure 3.3). Each protomer has a soluble region composed of two cupredoxin-like β barrels and a transmembrane region that includes 15 α helices as compared to 14 α helices in the *M. capsulatus* (Bath) model. Clear density for an additional helix is apparent in each protomer near the first two helices of the pmoC subunit (Figure 3.4). Modeling of a polyalanine helix in this density significantly decreased the R_{free} value, although the sequence of this helix could not be determined at 3.9 Å resolution or using the anisotropically processed data (Table 3.2). One candidate for the sequence is the N-terminal 17 residues of the pmoC subunit, which are not present elsewhere in the model. However, this sequence is not predicted to be a transmembrane helix by the TMHMM server at the Center for Biological Sequence Analysis (http://www.cbs.dtu.dk/services/TMHMM/). Additional residues at the C-terminus of pmoC are also unmodeled, but if these residues are present in this helix, it is unclear how to connect the backbone to the rest of the subunit. Besides this extra helix, a helix near the C-terminal part of pmoC has been modified in the *M. trichosporium* OB3b structure. In the *M. capsulatus* (Bath) structure, residues 231–259 are modeled as a helix disconnected from the rest of pmoC (*57*). The N-terminus of this helix is on the side of pMMO opposite the soluble cupredoxin domains, and its C-terminus is in the membrane. Analysis of this sequence for both pMMOs using the TMHMM server reveals that this helix most likely runs in the opposite direction. Its orientation was therefore reversed in the current structure, although it was modeled as polyalanine due to poor density in this area, and was also shortened due to a lack of density at end furthest from the soluble region.

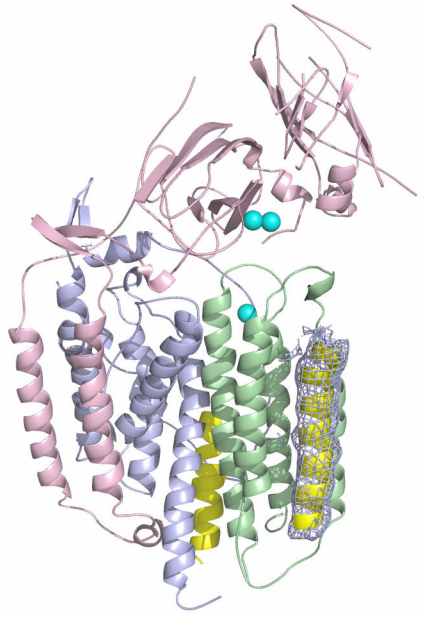

Figure 3.4. Crystal structure of *M. trichosporium* OB3b pMMO protomer
PmoB is shown in pink, pmoA in light blue, and pmoC in light green. Modeled copper ions are shown as cyan spheres. Two helices in pmoC that differ from the *M. capsulatus* (Bath) structure are shown in yellow. The helix in front, which is not present in the *M. capsulatus* (Bath) structure, is shown with the $2F_o–F_c$ electron density superimposed at 1σ. The direction of the yellow helix in back has been reversed with respect to the *M. capsulatus* (Bath) pMMO structure.

Metal Centers

Although the resolution is not sufficient to obtain details regarding metal coordination, anomalous data collected at different wavelengths provide new insight into the location and identity of the metal ions in the structure. Anomalous Fourier maps calculated using data collected just above the Cu absorption edge (Table 3.2) reveal strong, oblong density in the site modeled as a dicopper center in *M. capsulatus* (Bath) pMMO (Figure 3.5B). This density combined with the EXAFS data (Table 2.3 and Figure 2.8) strongly suggests that the dicopper center is present. Whether it is the active site remains unknown, but its existence in pMMO from two different organisms is consistent with an important functional role. By contrast, the Cu

anomalous map is devoid of density at the site occupied by the mononuclear copper center in *M. capsulatus* (Bath) pMMO (Figure 3.5A). The lack of density at this location is consistent with the replacement of one histidine with an asparagine in the *M. trichosporium* OB3b sequence, and it is therefore unlikely that this site is absolutely necessary for function. There is also no density in the Cu anomalous maps at a conserved hydrophilic site within the membrane proposed to house a trinuclear copper center (Figure 3.5D) (*68*).

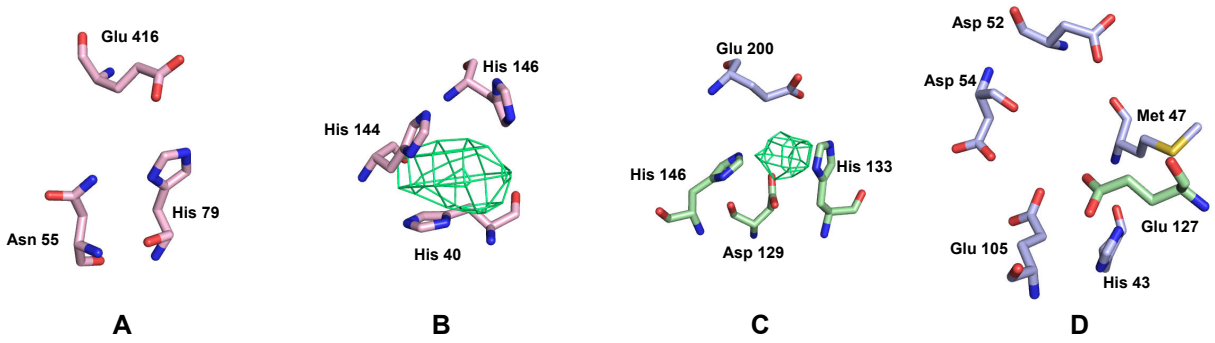

Figure 3.5. Copper anomalous difference Fourier maps of the three metal centers in *M. trichosporium* OB3b pMMO
(A) The location of the monocopper center in *M. capsulatus* (Bath) pMMO. No anomalous density is observed. (B) The location of the dicopper center in *M. capsulatus* (Bath) pMMO with the anomalous map contoured at 4σ. (C) The location of the "zinc" center in *M. capsulatus* (Bath) pMMO with the anomalous map contoured at 3σ. (D) The conserved "hydrophilic patch" within the membrane region. No anomalous density is observed. Side chain positions are not well defined at this resolution, and details of coordination cannot be acsertained. Oxygen atoms are colored red, nitrogen atoms are colored blue, and carbon atoms are colored according to subunit as in Figure 3.4.

Most striking, Cu anomalous density is also observed in the site occupied by zinc in the *M. capsulatus* (Bath) structure (Figure 3.5C), the so called "zinc site." For *M. capsulatus* (Bath) pMMO, no density was apparent at this site in Cu anomalous maps (*57*). Therefore, it seems likely that copper in this site was displaced by the high concentration of zinc used to crystallize *M. capsulatus* (Bath) pMMO. In the case of *M. trichosporium* OB3b pMMO, zinc was not

necessary for crystallization. Neither purified enzyme contains zinc ((*57*) and Table 2.1). Data were collected near the Zn absorption edge anyway, and features in the Zn anomalous map overlap with those in the Cu anomalous map as expected since the Zn edge is at higher energy. There are no features in the Zn anomalous map that are not observed in the Cu anomalous map, consistent with the absence of zinc in purified *M. trichosporium* OB3b pMMO. The "zinc site" has previously been proposed to house a diiron center (*57, 75*). Metal analysis (Table 2.1) and X-ray fluorescence scans of crystals provide no evidence for iron in *M. trichosporium* OB3b pMMO. The current data are consistent with copper occupying this site instead, but it is also possible that iron at this site could have been depleted during purification and crystallization and replaced with copper. However, even membrane-bound *M. trichosporium* OB3b pMMO has very little iron (Table 2.1) despite the presence of 40 μM iron in the growth medium.

SUMMARY

M. trichosporium OB3b pMMO has been crystallized, and the structure solved to 3.9 Å resolution. The crystallographic data and the EXAFS data presented in Chapter 2 provide strong evidence that *M. trichosporium* OB3b pMMO contains a dicopper center similar to that found in *M. capsulatus* (Bath) pMMO. The *M. capsulatus* (Bath) "zinc site" appears to house a copper ion in *M. trichosporium* OB3b pMMO, suggesting that copper may be the physiological metal ion at this conserved site. No metal ions are detected at the location of the *M. capsulatus* (Bath) monocopper center, eliminating the possibility of a functionally essential site at this position. There is no indication of a trinuclear copper cluster in *M. trichosporium* OB3b pMMO, and the copper stoichiometry is not consistent with multiple tricopper centers as proposed previously (*69*). Taken together with previous work, the characterization of *M. trichosporium* OB3b

pMMO provides new insight into the metal centers and represents a significant step toward elucidating the active site.

CHAPTER 4: THE COPPER CHELATOR METHANOBACTIN FROM *METHYLOSINUS TRICHOSPORIUM* OB3B BINDS COPPER(I)

A previous version of this chapter was published as Hakemian, A. S., Tinberg, C. E., Kondapalli, K. C., Telser, J., Hoffman, B. M., Stemmler, T. L., and Rosenzweig, A. C. (2005) *J. Am. Chem. Soc. 127*, 17142-17143.

ABSTRACT

The oxidation state of copper bound to methanobactin, a small siderophore-like molecule from the methanotroph *Methylosinus trichosporium* OB3b, was investigated. Purified methanobactin loaded with Cu(II) exhibits a weak EPR signal probably due to adventitious Cu(II). The EPR signal intensity increases significantly upon addition of the strong oxidant nitric acid. Features of the X-ray absorption near edge spectrum, including a 1s→4p transition at 8,985 eV, further indicate the presence of Cu(I). EXAFS data were best fit using a multiple scattering model generated from previously reported crystallographic parameters. These results establish definitively that *M. trichosporium* OB3b methanobactin binds Cu(I), and suggest that methanobactin itself reduces Cu(II) to Cu(I).

INTRODUCTION

Methanobactin is a small siderophore-like molecule proposed to function in copper sequestration and handling by methanotrophs, methane-oxidizing bacteria that play a key role in the global carbon cycle (*1*). Copper is critical to methanotroph metabolism, regulating expression of two methane monooxygenase (MMO) systems (*12, 13*), soluble MMO (sMMO) (*9*) and particulate MMO (pMMO) (*10*) as well as of other metabolic enzymes (*50*). In addition, copper is a pMMO cofactor (*25, 57, 58*) and stimulates the formation of intra-cytoplasmic membranes that house pMMO (*12, 38*). Methanobactin may not function solely in copper uptake, but could also play a more direct role in pMMO loading and activity. Originally referred to as a copper-binding compound (CBC), methanobactin was first detected a decade ago (*22, 88, 89*), but difficulties with degradation precluded structural characterization until recently (*37, 90*). The sequence of methanobactin from *Methylosinus trichosporium* OB3b is *N*-2-isopropylester-(4-thionyl-5-hydroxyimidazolate)-Gly^1-Ser^2-Cys^3-Tyr^4-pyrrolidine-(4-hydroxy-5-thionylimidazolate)-Ser^5-Cys^6-Met^7, and the crystal structure shows a single copper ion coordinated by an N_2S_2 donor set (Figure 4.1) (*37, 90*). On the basis of its structural similarity to iron siderophores (*130*), methanobactin may have antibacterial properties (*37*). Additional practical applications for methanobactin potentially include its use in the semiconductor industry to remove copper from wastewater (*131*). Despite its potential broad importance, key information about methanobactin, such as the oxidation state of the chelated copper ion, is lacking. Here we show by electron paramagnetic resonance (EPR) and X-ray absorption (XAS) spectroscopic methods that methanobactin binds copper in the 1+ oxidation state.

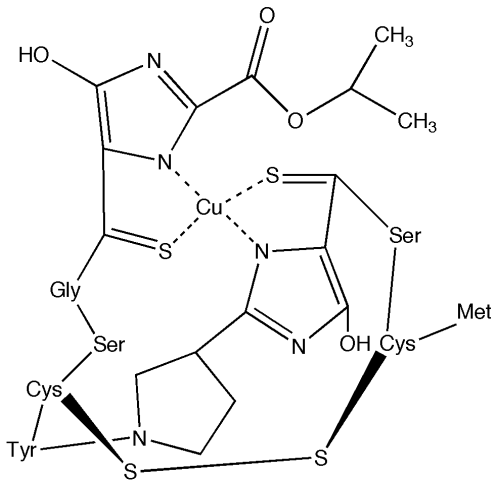

Figure 4.1. Schematic representation of the structure of methanobactin from *M. trichosporium* OB3b

MATERIALS AND METHODS

Bacterial Growth

M. trichosporium OB3b cultures were fermented in a 1.25 L BioFlo 3000 bioreactor (New Brunswick Scientific). Growth in copper-free culture media was as described previously (Chapter 2 and Reference (*95*)), except for the complete omission of copper sulfate, including from the trace elements solution. Cells were grown at 30 °C and an agitation rate of 250–300 rpm, and were purged with a 3:1 methane:air mixture at 1.2–1.6 L/min. Cells were harvested at an OD_{600} between 2 and 8, depending on the growth, and typically 200–300 mL were retained in the fermentor, and sterile media added to start another growth.

Purification of Methanobactin

The harvested media was centrifuged at 9,000 × *g* to pellet the cells, and the spent media decanted. Incubation with copper and isolation of the methanobactin were preformed as described previously (*90*). In brief, the spent media was incubated with saturating amounts (1 g/L) of $CuCl_2$ overnight while stirring at 4 °C. Precipitated $CuCl_2$ was removed by

centrifugation at 9,000 × *g* followed by filtration through a Steritop filter unit with a pore size of 0.22 µm (Millipore). The spent media was then run over a column packed with Discovery DSC-18 solid phase extraction material (Supelco). Methanobactin bound to the column, was rinsed with several column volumes of water, and eluted with 100% ethanol. The fractions containing methanobactin were divided into 1-mL aliquots, which were lyophilized and stored at –80 °C.

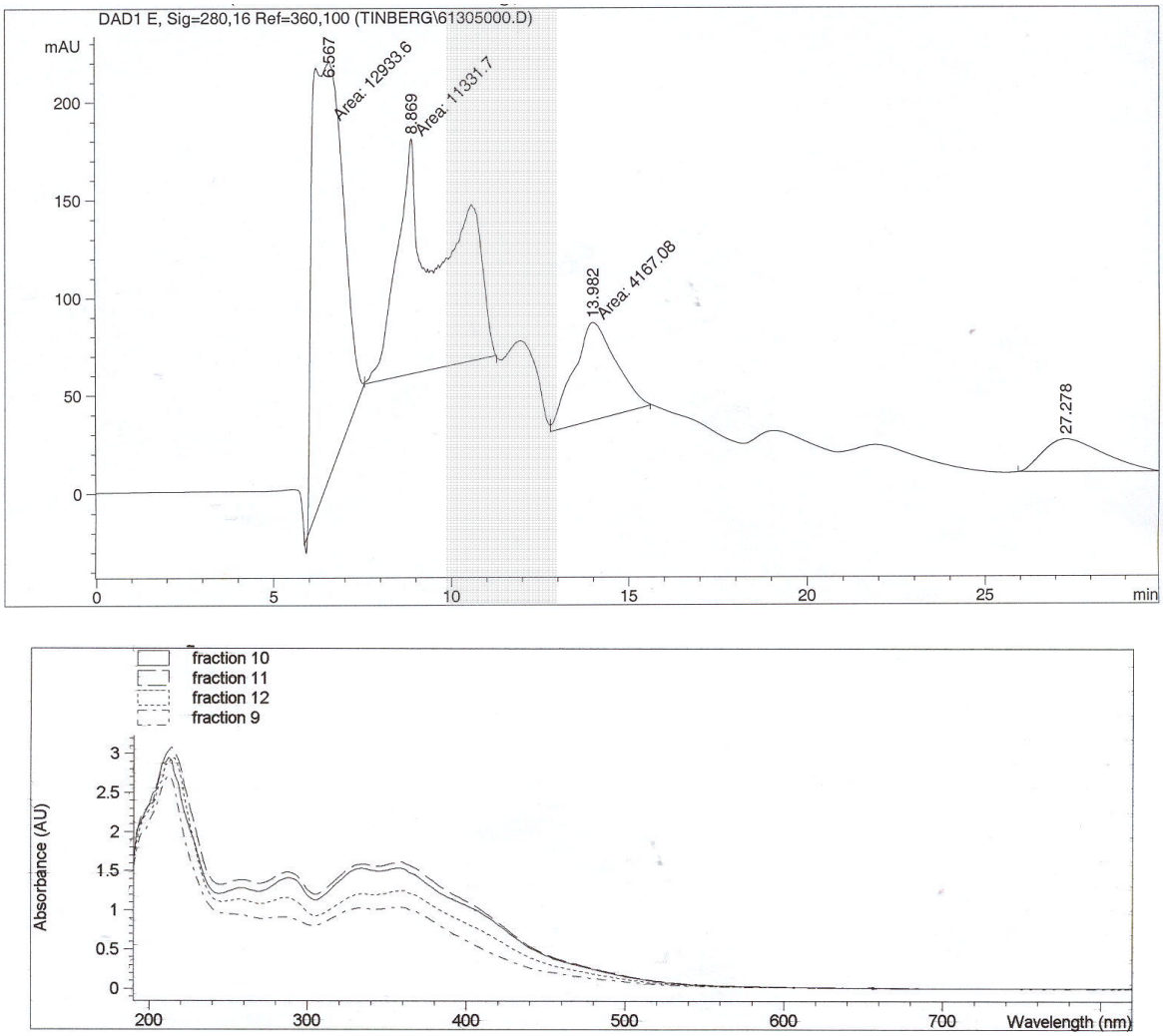

Figure 4.2. Purification of *M. trichosporium* OB3b methanobactin by size-exclusion HPLC
(top) Elution profile of SE-HPLC purification, monitored at 280 nm. Yellow colored fractions are indicated with a grey bar. (bottom) UV/Visible spectra of selected fractions from SE-HPLC column.

Methanobactin was further purified by size-exclusion HPLC. The lyophilized extract was dissolved in ddH_2O and filtered with a 0.45 μm filter. HPLC purification was performed using a Hewlett-Packard 1100 Series instrument equipped with a Bio-Sil SEC-125 SE-HPLC column, 300 × 7.8 mm, and a Bio-Sil 125 Guard column, 80 × 7.8 mm (Bio-Rad Laboratories) with a flow rate of 1 mL/min. The buffer for all experiments was 25 mM MES, 0.5 M urea, pH 6.5. Methanobactin usually eluted between 10 and 13 mL retention volume (Figure 4.2, top). UV-visible spectra of the colored fractions were recorded on a Hewlett Packard 8452A Diode Array Spectrophotometer using quartz cuvettes with a path length of 1 cm (Figure 4.2, bottom) and those with spectra matching that of methanobactin were kept. The buffer and urea were removed from these fractions with a C_{18} solid phase extraction column.

Metal Analysis

Copper concentrations were measured by graphite furnace atomic absorption spectroscopy (AAS) using a PerkinElmer AAnalyst 700 equipped with a PerkinElmer AS 800 autosampler in the laboratory of H. Godwin (Northwestern University, Evanston, IL). A 50 ppb standard was prepared by serially diluting a copper atomic absorption standard (Aldrich) with 2% (v/v) trace metal grade nitric acid (Fisher). Methanobactin samples were similarly diluted to between 5 and 200 ppb copper prior to analysis. The methanobactin concentration was measured by the absorbance at 280 nm ($\varepsilon_{280nm} = 1.65 \times 10^4$ $cm^{-1} \cdot M^{-1}$). The extinction coefficient was determined by measuring the absorbance at 280 nm of a known mass of methanobactin diluted to a known volume using volumetric glassware.

Mass Spectrometry

Methanobactin samples were prepared for MALDI-MS as described by Kim *et al.* (*90*).

Specifically, 1 μL of the methanobactin sample was mixed with 1 μL of the matrix solution (20 mM p-nitroanaline in a 4:1 water:ethanol solution) on the MALDI plate. The sample was allowed to dry in air for approximately 30 min. MALDI spectra were recorded on a Perseptive Biosystems Voyager DE-Pro MALDI-TOF mass spectrometer (Analytical Services Laboratory, Northwestern University, Evanston, IL) in negative-ion mode. Typical instrument parameters were 20,000 V accelerating voltage, 95% grid voltage, 0.2% guide wire voltage, 150 nsec delay time, 150 shots/spectrum and a laser intensity of ~4000 (this last value was highly dependant on the age of the laser).

Samples for ESI-MS were submitted to the Analytical Services Laboratory at Northwestern University. Spectra were recorded on a Finnigan LCQ Advantage mass spectrometer in negative ion mode.

EPR Spectroscopy

EPR spectra were recorded on a highly modified Bruker ESP 300 in the laboratory of B. Hoffman (Northwestern University). Samples were kept frozen using a finger Dewar filled with liquid nitrogen. A 1 mM aqueous solution of CuEDTA was used as a standard, and EPR spectra of all samples were recorded under identical conditions (9.31 GHz microwave frequency, 10 mW microwave power, 5 G field modulation amplitude, 160 ms time constant, 2 min scan time) as those for the standard. The spectra were background corrected by subtraction of a spectrum for buffer recorded under identical conditions. Double integration of background-corrected spectra was performed digitally using LabCalc® software. The same field integration range was used for all samples and the spectra were baseline-corrected (linear) after the first digital integration.

XAS Spectroscopy

Samples were dissolved in a 50% glycerol, 50% ddH_2O solution, and loaded into Lucite cells wrapped with Kapton tape. Samples were flash frozen in liquid nitrogen and stored at –80 °C or below until data collection. XAS measurements were acquired on reproducible independent samples. Data sets for independent samples were collected at beamline 10-2 at the Stanford Synchrotron Radiation Laboratory (SSRL) (Menlo Park, CA) and at beamline X9-B at the National Synchrotron Light Source (NSLS), Brookhaven National Laboratory (Upton, NY). SSRL beamline 10-2 was equipped with Si(220) double crystal monochromators detuned 50% for harmonic rejection, and NSLS beamline X9-B was equipped with a Si(111) monochromator with a harmonic rejection mirror. Samples were maintained at 10 K using an Oxford Instruments continuous-flow liquid helium cryostat at SSRL and at 24 K using a He Displex Cryostat at NSLS. Fluorescence excitation spectra were collected using 30-element Ge solid-state array detectors at SSRL and a 13-element Ge solid-state detector at NSLS. XAS spectra were measured using 5 eV steps in the pre-edge region (8750–8960 eV), 0.25 eV steps in the edge region (8986–9050 eV) and 0.05 $Å^{-1}$ increments in the extended X-ray absorption fine structure (EXAFS) region (to k = 13.1 $Å^{-1}$), integrating from 1 s to 20 s in a k^3 weighted manner for a total scan length of approximately 40 min. X-ray energies were calibrated from simultaneous collection of a copper foil absorption spectrum using a first inflection point energy of 8980.3 eV. Fluorescence data from each scan were examined for spectral anomalies prior to averaging, and spectra were closely monitored for photoreduction. SSRL data represent the average of 6 to 7 scans, whereas NSLS data represent the average of 9 to 10 scans. Data presented in Figure 4.6 represent the experimental results from only the SSRL data, but data collected on a duplicate

independent sample at NSLS gave identical results. Data presented in Table 4.1 are the average fit values from both data sets.

XAS data were processed using the Macintosh OS X version of the EXAFSPak program suite (*100*) integrated with the Feff v7.0 software (*101*) for theoretical model generation. Data reduction utilized a Gaussian function in the pre-edge region and a three-region cubic spline through the EXAFS region. Data were converted to *k*-space using E_0 values of 9000 eV for Cu. The k^3 weighted EXAFS was truncated at 1.0 and 13.14 $Å^{-1}$ for filtering purposes and Fourier transformed. Data were then Fourier-filtered to isolate the EXAFS for each peak in the Fourier transform. EXAFS data fitting analysis performed on both Fourier filtered and raw/unfiltered data gave equivalent structural results. Model and methanobactin EXAFS data were fit using both single and multiple scattering amplitude and phase functions calculated using Feff v7.0. Single scattering Feff v7.0 models were calculated for carbon, oxygen, sulfur and copper coordination to simulate copper-ligand environments. Multiple scattering Feff v7.0 models were generated for copper-imidazole interactions and for the complete methanobactin copper coordination environment (< 5 Å) using crystallographic coordinates for zinc-imidazole systems (*132*) and for the full methanobactin structure (*37*). For copper-ligand interactions, a scale factor of 0.85 and E_0 values of –12, –14 and –16 eV for Cu-O/N/C, Cu-S and Cu-Cu single scattering interactions (–8.28 eV for multiple scattering interactions) were calibrated by fitting crystallographically characterized models. When simulating empirical data, metal-ligand coordination numbers were fixed at half-integer values while the absorber-scatterer bond length (R) and Debye-Waller factor (σ^2) were allowed to vary freely.

RESULTS AND DISCUSSION

Methanobactin Isolation and Mass Spectrometry

Spent media from *M. trichosporium* OB3b was incubated with $CuCl_2$, and methanobactin was isolated and purified by protocols similar to those described by Graham and co-workers (*89, 90*). Analysis of the final product by MALDI-MS (Figure 4.3) or ESI-MS gave a single peak at 1215 Da, corresponding to an 1153 Da methanobactin molecule that has lost one or two hydrogen atoms and bound one copper atom. Anaerobic incubation of spent media with CuCl also gave a peak at 1215 Da (Figure 4.4), indicating that apo methanobactin can be fully loaded with one copper ion by treatment with either Cu(II) or Cu(I).

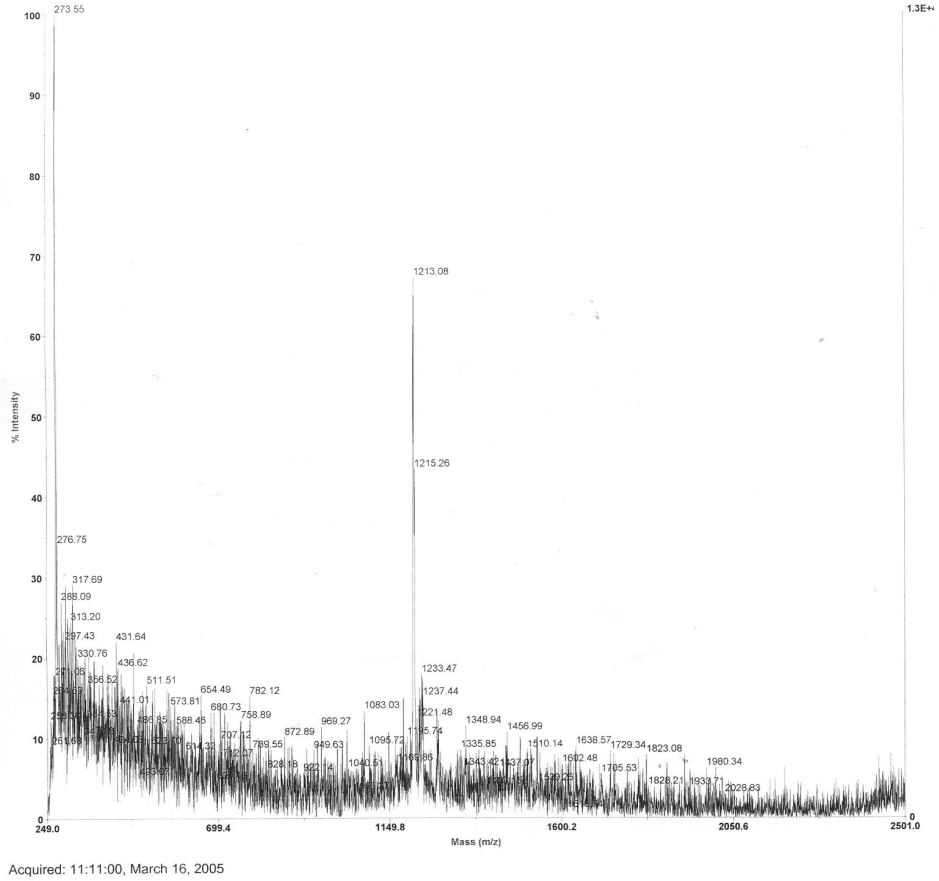

Figure 4.3. MALDI-MS spectrum of *M. trichosporium* OB3b pMMO

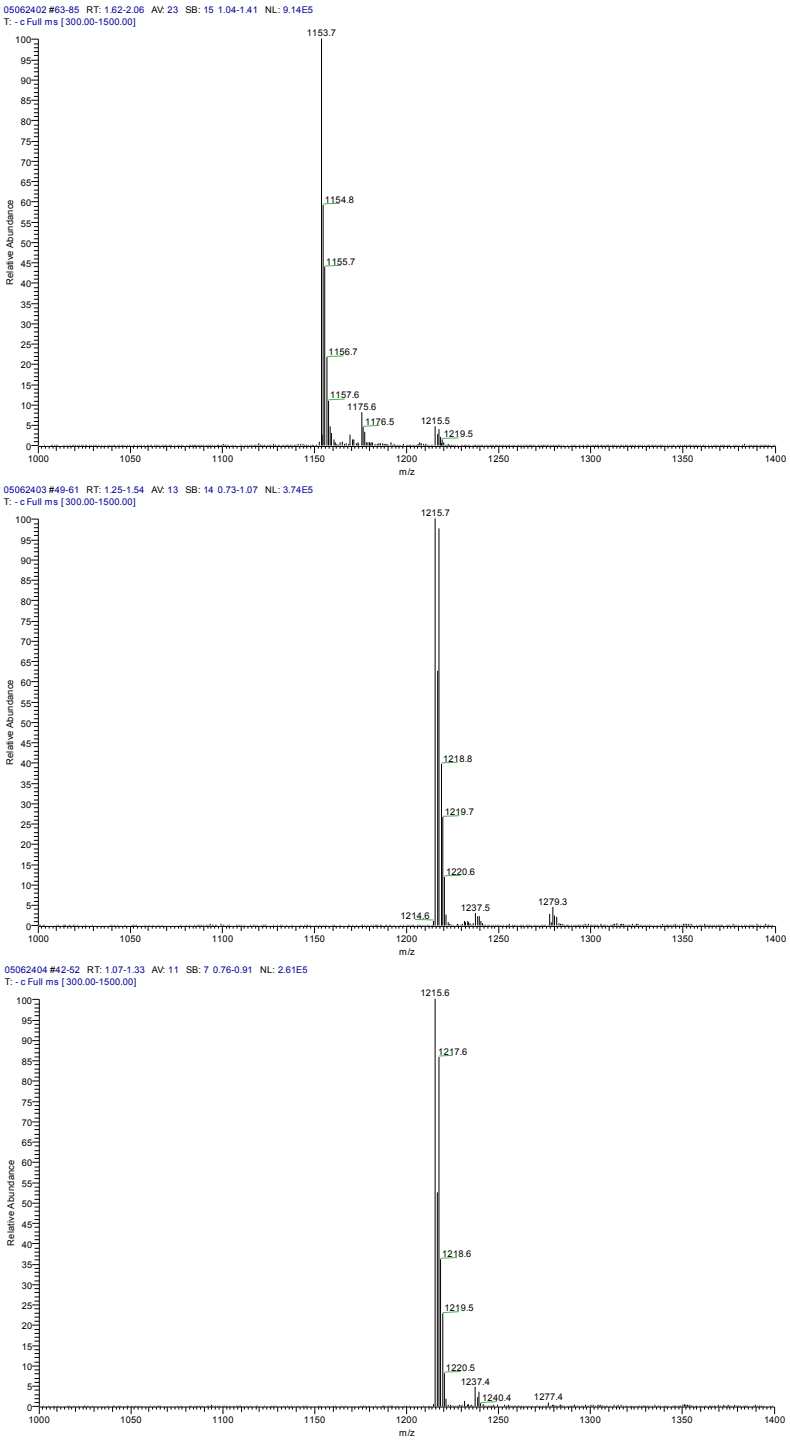

Figure 4.4. ESI-MS spectra of methanobactin
Shown before incubation with copper (top), after incubation with Cu(I) (middle) and after incubation with Cu(II) (bottom).

EPR Spectroscopy

The X-band EPR spectrum of Cu(II)-loaded methanobactin (Figure 4.5, blue trace) shows a weak, poorly resolved signal with $g_{\|}$ = 2.32(2), $g_{\perp}$ = 2.07(1), and $A_{\|}$ = 420(20) MHz (130 G) (all parameters determined by spectral simulation). A similar sized peptide from *M. trichosporium* OB3b denoted CBC-L_1 gave EPR parameters of $g_{\|}$ = 2.42, $g_{\perp}$ = 2.087, and $A_{\|}$ = 128 G (*88*), and together with EPR data on a less pure preparation from *Methylococcus capsulatus* (Bath) (*22*) suggested the presence of Cu(II). These $g_{\|}$ and $A_{\|}$ values are more characteristic of Cu(II) with N_xO_{4-x} (x = 0, 1, 2) coordination than of Cu(II) with sulfur ligation, which typically exhibits much smaller $g_{\|}$ values (*133*). No EPR quantitation was reported for the *M. trichosporium* OB3b CBC-L_1. The spin Hamiltonian parameters and low intensity of the EPR signal in all of these cases suggest that the signal arises from adventitious Cu(II), however. To determine if our methanobactin samples contained EPR-silent Cu(I), we added the strong oxidant nitric acid, which generated an intense Cu(II) signal. The EPR parameters for this signal (Figure 4.5, red trace) are $g_{\|}$ = 2.40(1), $g_{\perp}$ = 2.07(1), and $A_{\|}$ = 430(10) MHz (130 G). These $g_{\|}$ and $A_{\|}$ values are characteristic of Cu(II) with an O_4 donor set (*133*) as expected for methanobactin-bound Cu(I) that is released and oxidized by nitric acid. Methanobactin is known to degrade and lose copper at low pH (*90*). The quantity of Cu(II) present after nitric acid treatment, as measured by double integration of the EPR signal using $[CuEDTA]^{2-}$ as a standard, increased significantly, by a factor of 6.7 ± 0.7 (measurement repeated on triplicate samples) as compared to as-isolated samples. Metal analysis by atomic absorption spectroscopy indicates the presence of 1.09 ± 0.21 copper ions per methanobactin molecule. These data indicate that copper is bound to methanobactin as Cu(I) with the presence of a small amount of adventitious Cu(II). This finding

is consistent with previously reported X-ray photoelectron spectroscopic (XPS) data interpreted as evidence for Cu(I). In that study, however, appropriate standards containing Cu(I) or Cu(II) bound to N,S ligands were not examined by XPS (*37*).

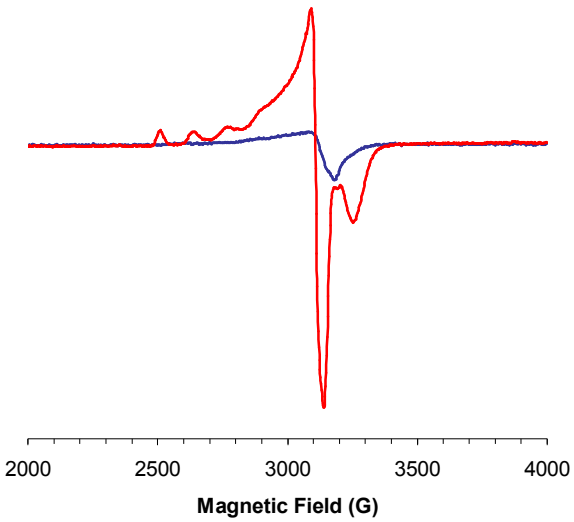

Figure 4.5. EPR spectra of Cu(II)-loaded methanobactin
Representative EPR spectra of Cu(II)-loaded methanobactin (2.2 mM) from *Methylosinus trichosporium* OB3b before (blue, 0.39 mM Cu(II)) and after (red, 3.0 mM Cu(II)) the addition of 2.5% nitric acid. Experimental conditions: temperature, 77 K, microwave frequency, 9.31 GHz; microwave power, 10 mW; field modulation amplitude, 5 G; time constant, 160 ms; scan time, 2 min.

XAS Spectroscopy

To further investigate the copper oxidation state in methanobactin, we collected Cu K edge XAS data on Cu(II)-loaded methanobactin samples. The XANES spectrum (Figure 4.6, top) clearly indicates the presence of Cu(I), as shown by the presence of a 1s→4p transition at 8,985 eV and edge features resembling four coordinate cuprous models (*111*). The lack of a 1s→3d transition at 8,980 eV, characteristic of Cu(II), further shows there is no appreciable Cu(II) (*111*).

Copper EXAFS data (Figure 4.6, bottom) were best fit using a multiple scattering model generated from the crystallographic parameters (*37*). Long-range scattering, reminiscent of imidazole scattering patterns from coordinated histidines (*134*), includes an additional carbon scattering environment at 4.16 Å. The data can also be reasonably fit with single scattering models, however (Table 4.1). The excellent agreement between the simulations with two Cu-N interactions (2.03 and 2.05 Å) and two Cu-S interactions (2.34 and 2.40 Å) in a combined multiple scattering model system reflects a copper coordination environment nearly identical to that observed in the crystal structure.

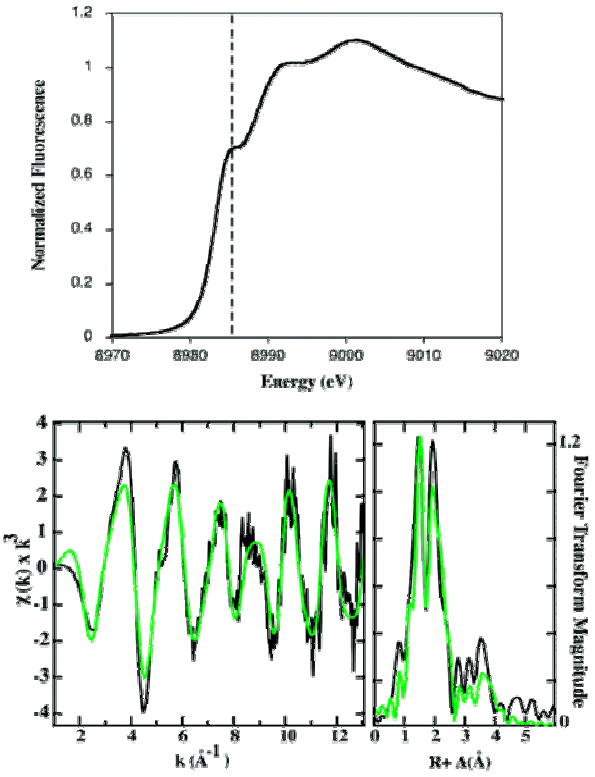

Figure 4.6. XAS analysis of Cu(II)-loaded methanobactin
Top: Cu XANES spectrum. Dashed line identifies the 1s→4p transition at 8,985 eV. Bottom: EXAFS (left) and its Fourier transform (right). Raw data are shown in black with the best fit superimposed in green.

Table 4.1. Summary of copper EXAFS fitting analysis for methanobactin samples
Data were fit over a *k* range of 1 to 13.1 $Å^{-1}$. Values in bold represent the overall best-fit parameters.

	Ligand Environment[a]				**Ligand Environment**[a]				**Ligand Environment**[a]				
Fit	**Atom**[b]	**R(Å)**[c]	**C.N.**[d]	**σ^2**[e]	**Atom**[b]	**R(Å)**[c]	**C.N.**[d]	**σ^2**[e]	**Atom**[b]	**R(Å)**[c]	**C.N.**[d]	**σ^2**[e]	**F'**[f]
1[g]	S	2.37	1.5	4.26									1.20
2[g]	S	2.38	1.5	3.56	O/N	2.02	1.5	4.64					0.60
3[g]	S	2.38	1.5	3.58	O/N	2.02	1.5	4.60	O/N	2.84	1.0	5.27	0.55
4[g]	S	2.38	1.5	3.72	O/N	2.02	1.5	4.78	C	2.81	1.0	1.38	0.52
	C	2.97	1.0	3.13									
5[g]	S	2.38	1.5	3.73	O/N	2.02	1.5	4.79	C	2.81	1.0	1.53	0.51
	C	2.97	1.0	3.49	C	3.51	0.5	3.36					
6[g]	S	2.37	1.5	3.69	O/N	2.02	1.5	4.75	C	2.83	1.5	3.29	0.39
	C	3.00	1.0	2.44	C	3.49	0.5	1.93	C	4.14	4.0	4.67	
7[h]	S	2.36	2.0	4.36	N_{Im}	2.04	2.0	4.38	C	2.84	1.0	3.33	0.51
8[i]	**xtal**	**2.03**	**1.0**	**3.08**					**C**	**4.16**	**7.0**	**4.63**	**0.37**
	N_2S_2	***2.05***	***1.0***	***3.12***									
		2.34	***1.0***	***3.54***									
		2.40	***1.0***	***3.64***									

[a] Independent metal-ligand scattering environment
[b] Scattering atoms: O (oxygen), N (nitrogen), C (carbon), Cu (copper)
[c] Average metal-ligand bond length for 2 independent samples
[d] Average metal-ligand coordination number for 2 independent samples
[e] Average Debye-Waller factor in $Å^2 \times 10^3$ for 2 independent samples
[f] Number of degrees of freedom weighted mean square deviation between data and fit
[g] Fit using only single scattering Feff 7 theoretical models
[h] Fit using both single scattering Feff 7 model with an additional multiple scattering Cu-N(imidazole) model, labeled N_{Im} in table atom designation.
[i] Fit using both multiple scattering Feff 7 model generated from all atoms within 5 Å in the crystal structure and single scattering Feff 7 model for additional Cu•••C interaction.

SUMMARY

M. trichosporium OB3b methanobactin has been isolated and purifed. Copper-bound methanobactin has a molecular mass of 1215 Da, as determined by mass spectrometry. Cu-EXAFS fitting analysis indicates a copper N_2S_2 coordination environment virtually identical to

that observed in the crystal structure (*37*).

The spectroscopic data presented here establish definitively that *M. trichosporium* OB3b methanobactin binds Cu(I) despite the fact that loading can be accomplished by the addition of Cu(II). The XANES spectrum of *M. trichosporium* OB3b copper-bound mb (Cu-mb) exhibits a 1s→4p transition at 8985 eV indicative of Cu(I) and lacks features attributable to Cu(II). The EPR spectrum of Cu-mb only shows weak signals with $g_{\|}$ and $A_{\|}$ values that are characteristic of copper with N_xO_{4-x} ligands, as would be expected from adventitiously bound Cu(II).

In subsequent work reported by DiSpirito and coworkers, it has been shown that EPR signals attributable to Cu(II) with sulfur ligation typically disappear < 10 min after Cu(II) addition to mb (*92*). Thus, mb itself is capable of reducing Cu(II) to Cu(I). The optical spectrum of Cu-mb also lacks features characteristic of Cu(II) (*90*). Spectral and kinetic data suggest that mb initially binds Cu(II) as a dimer with coordination by 4-hydroxy-5-thionylimidazolate and possibly tyrosine, followed by reduction to Cu(I) and coordination by 4-thionyl-5-hydroxyimidazolate (*93*).

REFERENCES

1. Hanson, R. S., and Hanson, T. E. (1996) Methanotrophic Bacteria. *Microbiol. Rev. 60*, 439-471.

2. Trotsenko, Y. A., and Khmelenina, V. N. (2002) Biology of extremophilic and extremotolerant methanotrophs. *Arch. Microbiol. 177*, 123-131.

3. Dumont, M. G., and Murrell, J. C. (2005) Community-level analysis: Key genes of aerobic methane oxidation. *Methods Enzymol. 397*, 413-427.

4. Park, S., Brown, K. W., and Thomas, J. C. (2002) The effect of various environmental and design parameters on methane oxidation in a model biofilter. *Waste Manag. Res. 20*, 434-444.

5. Tol, R. S. J., Heintz, R. J., and Lammers, P. E. M. (2003) Methane emission reduction: An application of *FUND*. *Clim. Change 57*, 71-98.

6. Periana, R. A., Bhalla, G., Tenn, W. J., Young, K. J. H., Liu, X. Y., Mironov, O., Jones, C. J., and Ziatdinov, V. R. (2004) Perspectives on some challenges and approaches for developing the next generation of selective, low temperature, oxidation catalysts for alkane hydroxylation based on the CH activation reaction. *J. Mol. Catal. A 220*, 7-25.

7. Lontoh, S., and Semrau, J. D. (1998) Methane and trichloroethylene degradation by *Methylosinus trichosporium* OB3b expressing particulate methane monooxygenase. *Appl. Environ. Microbiol. 64*, 1106-1114.

8. Sullivan, J. P., Dickinson, D., and Chase, H. A. (1998) Methanotophs, *Methylosinus tricosporium* OB3b, sMMO, and their application to bioremediation. *Crit. Rev. Microbiol. 24*, 335-373.

9. Merkx, M., Kopp, D. A., Sazinsky, M. H., Blazyk, J. L., Müller, J., and Lippard, S. J. (2001) Dioxygen activation and methane hydroxylation by soluble methane monooxygenase: A tale of two irons and three proteins. *Angew. Chem. Int. Ed. Engl. 40*, 2782-2807.

10. Lieberman, R. L., and Rosenzweig, A. C. (2004) Biological methane oxidation: Regulation, biochemistry, and active site structure of particulate methane monooxygenase. *Crit. Rev. Biochem. Mol. Biol. 39*, 147-164.

11. Murrell, J. C., McDonald, I. R., and Gilbert, B. (2000) Regulation of expression of methane monooxygenases by copper ions. *Trends Microbiol. 8*, 221-225.

12. Prior, S. D., and Dalton, H. (1985) The effect of copper ions on membrane content and methane monooxygenase activity in methanol-grown cells of *Methylococcus capsulatus* (Bath). *J. Gen. Microbiol. 131*, 155-163.

13. Stanley, S. H., Prior, S. D., Leak, D. J., and Dalton, H. (1983) Copper stress underlies the fundamental change in intracellular location of methane mono-oxygenase in methane-oxidizing organisms: Studies in batch and continuous culture. *Biotechnol. Lett. 5*, 487-492.

14. Rosenzweig, A. C., Frederick, C. A., Lippard, S. J., and Nordlund, P. (1993) Crystal structure of a bacterial non-haem iron hydroxylase that catalyses the biological oxidation of methane. *Nature 366*, 537-543.

15. Nordlund, P., and Reichard, P. (2006) Ribonucleotide reductases. *Annu. Rev. Biochem. 75*, 681-706.

16. Fox, B. G., Lyle, K. S., and Rogge, C. E. (2004) Reactions of the diiron enzyme stearoyl-acyl carrier protein desaturase. *Acc. Chem. Res. 37*, 421-429.

17. Notomista, E., Lahm, A., DiDonato, A., and Tramontano, A. (2003) Evolution of bacterial and archaeal multicomponent monooxygenases. *J. Mol. Evol. 56*, 435-445.

18. Sazinsky, M. H., and Lippard, S. J. (2006) Correlating structure with function in bacterial multicomponent monooxygenases and related diiron proteins. *Acc. Chem. Res. 39*, 558-566.

19. Baik, M. H., Newcomb, M., Friesner, R. A., and Lippard, S. J. (2003) Mechanistic studies on the hydroxylation of methane by methane monooxygenase. *Chem. Rev. 103*, 2385-2419.

20. Colby, J., Stirling, D. I., and Dalton, H. (1977) The soluble methane monooxygenase of *Methylococcus capsulatus* (Bath). *Biochem. J. 165*, 395-402.

21. Phelps, P. A., Agarwal, S. K., Speitel, G. E., Jr., and Georgiou, G. (1992) *Methylosinus trichosporium* OB3b mutants having constitutive expression of soluble methane monooxygenase in the presence of high levels of copper. *Appl. Environ. Microbiol. 58*, 3701-3708.

22. Zahn, J. A., and DiSpirito, A. A. (1996) Membrane-associated methane monooxygenase from *Methylococcus capsulatus* (Bath). *J. Bacteriol. 178*, 1018-1029.

23. Arp, D. J., Sayavedra-Soto, L. A., and Hommes, N. G. (2002) Molecular biology and biochemistry of ammonia oxidation. *Arch. Microbiol. 178*, 250-255.

24. Holmes, A. J., Costello, A., Lidstrom, M. E., and Murrell, J. C. (1995) Evidence that particulate methane monooxygenase and ammonia monooxygenase may be evolutinarily related. *FEMS Microbiol. Lett. 132*, 203-208.

25. Chan, S. I., Chen, K. H.-C., Yu, S. S.-F., Chen, C.-L., and Kuo, S. S.-J. (2004) Toward delineating the structure and function of the particulate methane monooxygenase from methanotrophic bacteria. *Biochemistry 43*, 4421-4430.

26. Burrows, K. J., Cornish, A., Scott, D., and Higgins, I. J. (1984) Substrate specificities of the soluble and particulate methane mono-oxygenases of *Methylosinus trichosporium* OB3b. *J. Gen. Microbiol. 130*, 327-333.

27. Ward, N., Larsen, Ø., Sakwa, J., Bruseth, L., Khouri, H., Durkin, A. S., Dimitrov, G., Jiang, L., Scanlan, D., Kang, K. H., Lewis, M., Nelson, K. E., Methé, B., Wu, M., Heidelberg, J. F., Paulsen, I. T., Fouts, D., Ravel, J., Tettelin, H., Ren, Q., Read, T., DeBoy, R. T., Seshadri, R., Salzberg, S. L., Jensen, H. B., Birkeland, N. K., Nelson, W. C., Dodson, R. J., Grindhaug, S. H., Holt, I., Eidhammer, I., Jonasen, I., Vanaken, S., Utterback, T., Feldblyum, T. V., Fraser, C. M., Lillehaug, J. R., and Eisen, J. A. (2004) Genomic insights into methanotrophy: The complete genome sequence of *Methylococcus capsulatus* (Bath). *PLoS Biol. 2*, e303.

28. Semrau, J. D., Chistoserdov, A., Lebron, J., Costello, A., Davagnino, J., Kenna, E., Holmes, A. J., Finch, R., Murrell, J. C., and Lidstrom, M. E. (1995) Particulate methane monooxygenase genes in methanotrophs. *J. Bacteriol. 177*, 3071-3079.

29. Stoylar, S., Costello, A. M., Peeples, T. L., and Lidstrom, M. E. (1999) Role of multiple gene copies in particulate methane monooxygenase activity in the methane-oxidizing bacterium *Methylococcus capsulatus* Bath. *Microbiology 145*, 1235-1244.

30. Stainthorpe, A. C., Lees, V., Salmond, G. P. C., Dalton, H., and Murrell, J. C. (1990) The methane monooxygenase gene-cluster of *Methylococcus capsulatus* (Bath). *Gene 91*, 27-34.

31. Kelly, D. P., Anthony, C., and Murrell, J. C. (2005) Insights into the obligate methanotroph *Methylococcus capsulatus*. *Trends Microbiol. 13*, 195-198.

32. Arguello, J. M. (2003) Identification of ion-selectivity determinants in heavy-metal transport P-1B-type ATPases. *J. Membr. Biol. 195*, 93-108.

33. Banci, L., and Rosato, A. (2003) Structural genomics of proteins involved in copper homeostasis. *Acc. Chem. Res. 36*, 215-221.

34. Rosenzweig, A. C. (2002) Metallochaperones: Bind and deliver. *Chem. Biol. 9*, 673-677.

35. Wernimont, A. K., Huffman, D. L., Finney, L. A., Demeler, B., O'Halloran, T. V., and Rosenzweig, A. C. (2003) Crystal structure and dimerization equilibria of PcoC, a methionine-rich copper resistance protein from *Escherichia coli*. *J. Biol. Inorg. Chem. 8*, 185-194.

36. Zhang, L., Koay, M., Mahert, M. J., Xiao, Z., and Wedd, A. G. (2006) Intermolecular transfer of copper ions from the CopC protein of *Pseudomonas syringae*. Crystal structures of fully loaded (CuCuII)-Cu-I forms. *J. Am. Chem. Soc. 128*, 5834-5850.

37. Kim, H. J., Graham, D. W., DiSpirito, A. A., Alterman, M. A., Galeva, N., Larive, C. K., Asunskis, D., and Sherwood, P. M. A. (2004) Methanobactin, a copper-acquisition compound from methane-oxidizing bacteria. *Science 305*, 1612-1615.

38. Choi, D.-W., Kunz, R. C., Boyd, E. S., Semrau, J. D., Antholine, W. E., Han, J.-I., Zahn, J. A., Boyd, J. M., de la Mora, A. M., and DiSpirito, A. A. (2003) The membrane-associated

methane monooxygenase (pMMO) and pMMO-NADH:quinone oxidoreductase complex from *Methylococcus capsulatus* Bath. *J. Bacteriol. 185*, 5755-5764.

39. Nielsen, A. K., Gerdes, K., Degn, H., and Murrell, J. C. (1996) Regulation of bacterial methane oxidation: Transcription of the soluble methane mono-oxygenase operon of *Methylococcus capsulatus* (Bath) is repressed by copper ions. *Microbiology 142*, 1289-1296.

40. Nielsen, A. K., Gerdes, K., and Murrell, J. C. (1997) Copper-dependent reciprocal transcriptional regulation of methane monooxygenase genes in *Methylococcus capsulatus* and *Methylosinus trichosporium*. *Mol. Microbiol. 25*, 399-409.

41. Murrell, J. C., Gilbert, B., and McDonald, I. R. (2000) Molecular biology and regulation of methane monooxygenase. *Arch. Microbiol. 173*, 325-332.

42. Csáki, R., Bodrossy, L., Klem, J., Murrell, J. C., and Kovács, K. L. (2003) Genes involved in the copper-dependent regulation of soluble methane monooxygenase of *Methylococcus capsulatus* (Bath): Cloning, sequencing and mutational analysis. *Microbiology 149*, 1785-1795.

43. Stafford, G. P., Scanlan, J., McDonald, I. R., and Murrell, J. C. (2003) *rpoN*, *mmoR* and *mmoG*, genes involved in regulating the expression of soluble methane monooxygenase in *Methylosinus trichosporium* OB3b. *Microbiology 149*, 1771-1784.

44. Stock, A. M., Robinson, V. L., and Goudreau, P. N. (2000) Two-component signal transduction. *Annu. Rev. Biochem. 69*, 183-215.

45. West, A. H., and Stock, A. M. (2001) Histidine kinases and response regulator proteins in two-component signaling systems. *Trends Biochem. Sci. 26*, 369-376.

46. Hefti, M. H., Françoijs, K.-J., de Vries, S. C., Dixon, R., and Vervoort, J. (2004) The PAS fold. A redefinition of the PAS domain based upon structural prediction. *Eur. J. Biochem. 271*, 1198-1208.

47. Taylor, B. L., Rebbapragada, A., and Johnson, M. S. (2001) The FAD-PAS domain as a sensor for behavioral responses in *Escherichia coli*. *Antiox. Redox Signal. 3*, 867-879.

48. Ukaegbu, U. E., Henery, S., and Rosenzweig, A. C. (2006) Biochemical characterization of MmoS, a sensor protein involved in copper-dependent regulation of soluble methane monooxygenase. *Biochemistry 45*, 10191-10198.

49. Martinez-Argudo, I., Little, R., Shearer, N., Johnson, P., and Dixon, R. (2004) The NifL-NifA system: A multidomain transcriptional regulatory complex that integrates environmental signals. *J. Bacteriol. 186*, 601-610.

50. Zahn, J. A., Bergmann, D. J., Boyd, J. M., Kunz, R. C., and DiSpirito, A. A. (2001) Membrane-associated quinoprotein formaldehyde dehydrogenase from *Methylococcus capsulatus* (Bath). *J. Bacteriol. 183*, 6832-6840.

51. Berson, O., and Lidstrom, M. E. (1997) Cloning and characterization of *corA*, a gene encoding a copper-repressible polypeptide in the type I methanotroph, *Methylomicrobium albus* BG8. *FEMS Microbiol. Lett. 148*, 169-174.

52. Fjellbirkeland, A., Kruger, P. G., Bemanian, V., Høgh, B. T., Murrell, J. C., and Jensen, H. B. (2001) The C-terminal part of the surface-associated protein MopE of the methanotroph *Methylococcus capsulatus* (Bath) is secreted into the growth medium. *Arch. Microbiol. 176*, 197-203.

53. Karlsen, O. A., Berven, F. S., Stafford, G. P., Larsen, Ø., Murrell, J. C., Jensen, H. B., and Fjellbirkeland, A. (2003) The surface-associated and secreted MopE protein of *Methylococcus capsulatus* (Bath) responds to changes in the concentration of copper in the growth medium. *Appl. Environ. Microbiol. 69*, 2386-2388.

54. Karlsen, O. A., Kindingstad, L., Angelskår, S. M., Bruseth, L. J., Straume, D., Puntervoll, P., Fjellbirkeland, A., Lillehaug, J. R., and Jensen, H. B. (2005) Identification of a copper-repressible C-type heme protein of *Methylococcus capsulatus* (Bath). A member of a novel group of the bacterial di-heme cytochrome *c* peroxidase family of proteins. *FEBS J. 272*, 6324-6335.

55. Kao, W.-C., Chen, Y.-R., Yi, E. C., Lee, H., Tian, Q., Wu, K.-M., Tsai, S.-F., Yu, S. S.-F., Chen, Y.-J., Aebersold, R., and Chan, S. I. (2004) Quantitative proteomic analysis of metabolic regulation by copper ions in *Methylococcus capsulatus* (Bath). *J. Biol. Chem. 279*, 51554-51560.

56. Karlsen, O. A., Ramsevik, L., Bruseth, L. J., Larsen, Ø., Brenner, A., Berven, F. S., Jensen, H. B., and Lillehaug, J. R. (2005) Characterization of a prokaryotic haemerythrin from the methanotrophic bacterium *Methylococcus capsulatus* (Bath). *FEBS J. 272*, 2428-2440.

57. Lieberman, R. L., and Rosenzweig, A. C. (2005) Crystal structure of a membrane-bound metalloenzyme that catalyses the biological oxidation of methane. *Nature 434*, 177-182.

58. Lieberman, R. L., and Rosenzweig, A. C. (2005) The quest for the particulate methane monooxygenase active site. *Dalton Trans. 21*, 3390-3396.

59. Sommerhalter, M., Lieberman, R. L., and Rosenzweig, A. C. (2005) X-ray crystallography and biological metal centers: Is seeing believing?, *Inorg. Chem. 44*, 770-778.

60. Yu, S. S.-F., Chen, K. H.-C., Tseng, M. Y.-H., Wang, Y.-S., Tseng, C.-F., Chen, Y.-J., Huang, D.-S., and Chan, S. I. (2003) Production of high-quality particulate methane monooxygenase in high yields from *Methylococcus capsulatus* (Bath) with a hollow-fiber membrane bioreactor. *J. Bacteriol. 185*, 5915-5924.

61. Lieberman, R. L., Shrestha, D. B., Doan, P. E., Hoffman, B. M., Stemmler, T. L., and Rosenzweig, A. C. (2003) Purified particulate methane monooxygenase from *Methylococcus capsulatus* (Bath) is a dimer with both mononuclear copper and a copper-containing cluster. *Proc. Natl. Acad. Sci. USA 100*, 3820-3825.

62. Tsuprun, V. L., Akent'eva, N. P., Tagunova, I. V., Orlova, E. V., Grigoryan, A. N., Gvozdev, R. I., and Kiselev, N. A. (1987) Electron-microscopy of methanemonooxygenase from the methane-oxidizing bacteria *Methylococcus-capsulatus*. *Dokl. Akad. Nauk SSSR 292*, 490-493.

63. Kitmitto, A., Myronova, N., Basu, P., and Dalton, H. (2005) Characterization and structural analysis of an active particulate methane monooxygenase trimer from *Methylococcus capsulatus* (Bath). *Biochemistry 44*, 10954-10965.

64. Basu, P., Katterle, B., Andersson, K. K., and Dalton, H. (2003) The membrane-associated form of methane mono-oxygenase from *Methylococcus capsulatus* (Bath) is a copper/iron protein. *Biochem. J. 369*, 417-427.

65. Nguyen, H.-H. T., Elliott, S. J., Yip, J. H.-K., and Chan, S. I. (1998) The particulate methane monooxygenase from *Methylococcus capsulatus* (Bath) is a novel copper-containing three-subunit enzyme. *J. Biol. Chem. 273*, 7957-7966.

66. Miyaji, A., Kamachi, T., and Okura, I. (2002) Improvement of the purification method for retaining the activity of the particulate methane monooxygenase from *Methylosinus trichosporium* OB3b. *Biotechnol. Lett. 24*, 1883-1887.

67. Yu, S. S.-F., Ji, C.-Z., Wu, Y. P., Lee, T.-L., Lai, C.-H., Lin, S.-C., Yang, Z.-L., Wang, V. C.-C., Chen, K. H.-C., and Chan, S. I. (2007) The C-terminal aqueous-exposed domain of the 45 kDa subunit of the particulate methane monooxygenase in *Methylococcus capsulatus* (Bath) is a Cu(I) sponge. *Biochemistry 46*, 13762-13774.

68. Chan, S. I., Wang, V. C.-C., Lai, J. C.-H., Yu, S. S.-F., Chen, P. P.-Y., Chen, K. H.-C., Chen, C.-L., and Chan, M. K. (2007) Redox potentiometry studies of particulate methane monooxygenase: Support for a trinuclear copper cluster active site. *Angew. Chem. Int. Ed. Engl. 46*, 1992-1994.

69. Hung, S. C., Chen, C.-L., Chen, K. H.-C., Yu, S. S.-F., and Chan, S. I. (2004) The catalytic copper clusters of the particulate methane monooxygenase from methanotrophic bacteria: Electron paramagnetic resonace spectral simulations. *J. Chin. Chem. Soc. 51*, 1229-1244.

70. Chen, K. H.-C., Chen, C.-L., Tseng, C.-F., Yu, S. S.-F., Ke, S.-C., Lee, J.-F., Nguyen, H. T., Elliott, S. J., Alben, J. O., and Chan, S. I. (2004) The copper clusters in the particulate methane monooxygenase (pMMO) from *Methylococcus capsulatus* (Bath). *J. Chin. Chem. Soc. 51*, 1081-1098.

71. Lemos, S. S., Collins, M. L. P., Eaton, S. S., Eaton, G. R., and Antholine, W. E. (2000) Comparison of EPR-visible Cu2+ sites in pMMO from *Methylococcus capsulatus* (Bath) and *Methylomicrobium album* BG8. *Biophys. J. 79*, 1085-1094.

72. Yuan, H., Collins, M. L. P., and Antholine, W. E. (1997) Low-frequency EPR of the copper in particulate methane monooxygenase from *Methylomicrobium albus* BG8. *J. Am. Chem. Soc. 119*, 5073-5074.

73. Yuan, H., Collins, M. L. P., and Antholine, W. E. (1998) Concentration of Cu, EPR-detectable Cu, and formation of cupric-ferrocyanide in membranes with pMMO. *J. Inorg. Biochem. 72*, 179-185.

74. Lieberman, R. L., Kondapalli, K. C., Shrestha, D. B., Hakemian, A. S., Smith, S. M., Telser, J., Kuzelka, J., Gupta, R., Borovik, A. S., Lippard, S. J., Hoffman, B. M., Rosenzweig, A. C., and Stemmler, T. L. (2006) Characterization of the partiulate methane monooxygenase metal centers in multiple redox states by X-ray absorption spectroscopy. *Inorg. Chem. 45*, 8372-8381.

75. Martinho, M., Choi, D. W., DiSpirito, A. A., Antholine, W. E., Semrau, J. D., and Munck, E. (2007) Mössbauer studies of the membrane-associated methane monooxygenase from *Methylococcus capsulatus* Bath: Evidence for a diiron center. *J. Am. Chem. Soc. 129*, 15783-15785.

76. Matoba, Y., Kumagai, T., Yamamoto, A., Yoshitsu, H., and Sugiyama, M. (2006) Crystallographic evidence that the dinuclear copper center of tyrosinase is flexible during catalysis. *J. Biol. Chem. 281*, 8981-8990.

77. Rosenzweig, A. C., and Sazinsky, M. H. (2006) Structural insights into dioxygen-activating copper enzymes. *Curr. Opin. Struct. Biol. 16*, 729-735.

78. Shiemke, A. K., Cook, S. A., Miley, T., and Singleton, P. (1995) Detergent solubilization of membrane-bound methane monooxygenase requres plastoquinol analogs as electron donors. *Arch. Biochem. Biophys. 321*, 421-428.

79. Katterle, B., Gvozdev, R. I., Abudu, N., Ljones, T., and Andersson, K. K. (2002) A continuous-wave electron-nuclear double resonance (X-band) study of the Cu+2 sites of particulate methane mono-oxygenase of *Methylococcus capsulatus* (strain M) in membrane and pure dopamine β-mono-oxygenase of the adrenal medulla. *Biochem. J. 363*, 677-686.

80. Yu, S. S.-F., Wu, L.-Y., Chen, K. H.-C., Luo, W.-I., Huang, D.-S., and Chan, S. I. (2003) The stereospecific hydroxylation of [2,2-2H2]butane and chiral dideuteriobutanes by the particulate methane monooxygenase from *Methylococcus capsulatus* (Bath). *J. Biol. Chem. 278*, 40658-40669.

81. Shiemke, A. K., Arp, D. J., and Sayavedra-Soto, L. A. (2004) Inhibition of membrane-bound methane monooxygenase and ammonia monooxygenase by diphenyliodonium: Implications for electron transfer. *J. Bacteriol. 186*, 928-937.

82. Wilkinson, B., Zhu, M., Priestley, N. D., Nguyen, H.-H. T., Morimoto, H., Williams, P. G., Chan, S. I., and Floss, H. G. (1996) A concerted mechanism for ethane hydroxylation by the particulate methane monooxygenase from *Methylococcus capsulatus* (Bath). *J. Am. Chem. Soc. 118*, 921-922.

83. Huang, D.-S., Wu, S.-H., Wang, Y.-S., Yu, S. S.-F., and Chan, S. I. (2002) Determination of the carbon kinetic isotope effects on propane hydroxylation mediated by the methane monooxygenase from *Methylococcus capsulatus* (Bath) by using stable carbon isotopic analysis. *ChemBioChem 3*, 760-765.

84. Elliott, S. J., Zhu, M., Tso, L., Nguyen, H.-H. T., Yip, J. H.-K., and Chan, S. I. (1997) Regio- and stereoselectivity of particulate methane monooxygenase from *Methylococcus capsulatus* (Bath). *J. Am. Chem. Soc. 119*, 9949-9955.

85. Chen, P. P. Y., and Chan, S. I. (2006) Theoretical modeling of the hydroxylation of methane as mediated by the particulate methane monooxygenase. *J. Inorg. Biochem. 100*, 801-809.

86. Balasubramanian, R., and Rosenzweig, A. C. (2007) Structural and mechanistic insights into methane oxidation by particulate methane monooxygenase. *Acc. Chem. Res. 40*, 573-580.

87. Fitch, M. W., Graham, D. W., Arnold, R. G., Agarwal, S. K., Phelps, P., Speitel, G. E., Jr., and Georgiou, G. (1993) Phenotypic characterization of copper-resistant mutants of *Methylosinus trichosporium* OB3b. *Appl. Environ. Microbiol. 59*, 2771-2776.

88. DiSpirito, A. A., Zahn, J. A., Graham, D. W., Kim, H. J., Larive, C. K., Derrick, T. S., Cox, C. D., and Taylor, A. (1998) Copper-binding compounds from *Methylosinus trichosporium* OB3b. *J. Bacteriol. 180*, 3606-3613.

89. Téllez, C. M., Gaus, K. P., Graham, D. W., Arnold, R. G., and Guzman, R. Z. (1998) Isolation of copper biochelates from *Methylosinus trichosporium* OB3b and soluble methane monooxygenase mutants. *Appl. Environ. Microbiol. 64*, 1115-1122.

90. Kim, H. J., Galeva, N., Larive, C. K., Alterman, M., and Graham, D. W. (2005) Purification and physical-chemical properties of methanobactin: A chalkophore from *Methylosinus trichosporium* OB3b. *Biochemistry 44*, 5140-5148.

91. Hakemian, A. S., Tinberg, C. E., Kondapalli, K. C., Telser, J., Hoffman, B. M., Stemmler, T. L., and Rosenzweig, A. C. (2005) The copper chelator methanobactin from *Methylosinus trichosporium* OB3b binds copper(I). *J. Am. Chem. Soc. 127*, 17142-17143.

92. Choi, D. W., Antholine, W. E., Do, Y. S., Semrau, J. D., Kisting, C. J., Kunz, R. C., Campbell, D., Rao, V., Hartsel, S. C., and DiSpirito, A. A. (2005) Effect of methanobactin on the activity and electron paramagnetic resonance spectra of the membrane-associated methane monooxygenase in *Methylococcus capsulatus* Bath. *Microbiology 151*, 3417-3426.

93. Choi, D. W., Zea, C. J., Do, Y. S., Semrau, J. D., Antholine, W. E., Hargrove, M. S., Pohl, N. L., Boyd, E. S., Geesey, G. G., Hartsel, S. C., Shafe, P. H., McEllistrem, M. T., Kisting, C. J., Campbell, D., Rao, V., de la Mora, A. M., and DiSpirito, A. A. (2006) Spectral, kinetic, and thermodynamic properties of Cu(I) and Cu(II) binding by methanobactin from *Methylosinus trichosporium* OB3b. *Biochemistry 45*, 1442-1453.

94. Hakemian, A. S., and Rosenzweig, A. C. (2007) The biochemistry of methane oxidation. *Annu. Rev. Biochem. 76*, 223-241.

95. Fox, B. G., Froland, W. A., Jollie, D. R., and Lipscomb, J. D. (1990) Methane monooxygenase from *Methylosinus trichosporium* OB3b. *Methods Enzymol. 188*, 191-202.

96. Takeguchi, M., and Okura, I. (2000) Role of iron and copper in particulate methane monooxygenase in *Methylosinus trichosporium* OB3b. *Catal. Surv. Jpn. 4*, 51-63.

97. Lieberman, R. L. (2005) Biophysical and structural characterization of particulate methane monooxygenase from *Methylococcus capsulatus* (Bath). Ph.D. thesis, Northwestern University, Evanston, Illinois.

98. Belford, R. L., and Belford, G. G. (1973) Eigenfield expansion technique for efficient computation of field-swept fixed-frequency spectra from relaxation master equations. *J. Chem. Phys. 59*, 853-854.

99. Belford, R. L., and Nilges, M. J. (1979) in *EPR Symposium, 21st Rocky Mountain Conference*, Denver, CO.

100. George, G., George, S. J., and Pickering, I. J. (2001) EXAFSPAK: A suite of computer programs for analysis of X-ray absorption spectra, Menlo Park, CA.

101. Ankudinov, A. L., and Rehr, J. J. (1997) Relativistic calculations of spin-dependent x-ray-absorption spectra. *Phys. Rev. B 56*, R1712-R1715.

102. Lee, P. A., Citrin, P. H., Eisenberger, P., and Kincaid, B. M. (1981) Extended x-ray absorption fine structure - its strengths and limitations as a structural tool. *Rev. Mod. Phys. 53*, 769-806.

103. Bencze, K. Z., Kondapalli, K. C., and Stemmler, T. L. (2007) X-ray absorption spectroscopy, in *Applications of Physical Methods to Inorganic and Bioinorganic Chemistry: Handbook, Encyclopedia of Inorganic Chemistry* (Scott, R. A., and Lukehart, C. M., Eds.), pp 513-528, John Wiley & Sons, Ltd, Chichester, UK.

104. Takeguchi, M., Miyakawa, K., and Okura, I. (1999) The role of copper in particulate methane monooxygenase from *Methylosinus trichosporium* OB3b. *J. Mol. Catal. A 137*, 161-168.

105. Takeguchi, M., Miyakawa, K., and Okura, I. (1998) Purification and properties of particulate methane monooxygenase from *Methylosinus trichosporium* OB3b. *J. Mol. Catal. A 132*, 145-153.

106. Whittenbury, R., Phillips, K. C., and Wilkinson, J. F. (1970) Enrichment, isolation and some properties of methane-utilizing bacteria. *J. Gen. Microbiol. 61*, 205-218.

107. DeWitt, J. G., Bentsen, J. G., Rosenzweig, A. C., Hedman, B., Green, J., Pilkington, S., Papaefthymiou, G. C., Dalton, H., Hodgson, K. O., and Lippard, S. J. (1991) X-ray absorption, mössbauer, and EPR studies of the dinuclear iron center in the hydroxylase component of methane monooxygenase. *J. Am. Chem. Soc. 113*, 9219-9235.

108. Fox, B. G., Froland, W. A., Dege, J. E., and Lipscomb, J. D. (1989) Methane monooxygenase from *Methylosinus trichosporium* OB3b. *J. Biol. Chem. 264*, 10023-10033.

109. Hellwig, P., Soulimane, T., Buse, G., and Mantele, W. (1999) Electrochemical, FTIR, and UV/VIS spectroscopic properties of the *ba*3 oxidase from *Thermus thermophilus*. *Biochemistry 38*, 9648-4658.

110. Bartsch, R. G. (1971) Cytochromes: bacterial. *Methods Enzymol. 23*, 344-363.

111. Kau, L.-S., Spira-Solomon, D. J., Penner-Hahn, J. E., Hodgson, K. O., and Solomon, E. I. (1987) X-ray absorption edge determination of the oxidation state and coordination number of copper: application to the type 3 site in *Rhus vernicifera* laccase and its reaction with oxygen. *J. Am. Chem. Soc. 109*, 6433-6442.

112. Wang, S., Lee, M. H., Hausinger, R. P., Clark, P. A., Wilcox, D. E., and Scott, R. A. (1994) Structure of the dinuclear active side of urease. X-ray absorption spectroscopic study of native and 2-mercaptoethanol-inhibited bacterial and plant enzymes. *Inorg. Chem. 33*, 1589-1593.

113. Hjelmeland, L. M., and Chrambach, A. (1984) Solubilization of functional membrane proteins. *Methods Enzymol. 104*, 305-318.

114. Ostermeier, C., and Michel, H. (1997) Crystallization of membrane proteins. *Curr. Opin. Struct. Biol. 7*, 697-701.

115. Byrne, B., and Iwata, S. (2002) Membrane protein complexes. *Curr. Opin. Struct. Biol. 12*, 239-243.

116. Englard, S., and Seifter, S. (1990) Precipitation techniques. *Methods Enzymol. 182*, 285-300.

117. Heras, B., and Martin, J. L. (2005) Post-crystallization treatments for improving diffraction quality of protein crystals. *Acta Crystallogr., Sect D: Biol. Crystallogr. 61*, 1173-1180.

118. Whittington, D. A., Rosenzweig, A. C., Frederick, C. A., and Lippard, S. J. (2001) Xenon and halogenated alkanes track putative substrate binding cavities in the soluble methane monooxygenase hydroxylase. *Biochemistry 40*, 3476-3482.

119. Li, L., Mustafi, D., Fu, Q., Tereshko, V., Chen, D. L., Tice, J. D., and Ismagilov, R. F. (2006) Nanoliter microfluidic hybrid method for simultaneous screening and optimization validated with crystallization of membrane proteins. *Proc. Natl. Acad. Sci. USA 103*, 19243-19248.

120. Zhang, H., Kurisu, G., Smith, J. L., and Cramer, W. A. (2003) A defined protein-detergent-lipid complex for crystallization of integral membrane proteins: The cytochrome b_6f complex of oxygenic photosynthesis. *Proc. Natl. Acad. Sci. USA 100*, 5160-5163.

121. Kabsch, W. (1993) Automatic processing of rotation diffraction data from crystals of initially unknown symmetry and cell constants. *J. Appl. Crystallogr. 26*, 795-800.

122. Leslie, A. G. W. (1992) Recent chaanges to the MOSFLM package for processing film and image plate data. *Joint CCP4 + ESF-EAMCB Newsletter on Protein Crystallography 26*.

123. 4, C. C. P. N. (1994) The CCP4 Suite: Programs for Protein Crystallography. *Acta Crystallogr., Sect D: Biol. Crystallogr. 50*, 760-763.

124. McCoy, A. J., Grosse-Kunstleve, R. W., Storoni, L. C., and Read, R. J. (2005) Likelihood-enhanced fast translation functions. *Acta Crystallogr., Sect D: Biol. Crystallogr. 61*, 458-464.

125. Guex, N., and Peitsch, M. C. (1997) SWISS-MODEL and the Swiss-PdbViewer: An environment for comparitive protein modeling. *Electrophoresis 18*, 2714-2723.

126. Emsley, P., and Cowtan, K. (2004) Coot: Model-Building Tools for Molecular Graphics. *Acta Crystallogr., Sect D: Biol. Crystallogr. 60*, 2126-2132.

127. Brünger, A., Adams, P., Clore, G., DeLano, W., Gros, P., Grosse-Kunstleve, R., Jiang, J., Kuszewski, J., Nilges, M., Pannu, N., Read, R., Rice, L., Simonson, T., and Warren, G. (1998) Crystallography & NMR system: A new software suite for macromolecular structure determination. *Acta Crystallogr., Sect D: Biol. Crystallogr. 54*, 905-921.

128. Strong, M., Sawaya, M. R., Wang, S., Phillips, M., Cascio, D., and Eisenberg, D. (2006) Toward the structural genomics of complexes: Crystal structure of a PE/PPE protein complex from Mycobacterium tuberculosis. *PNAS 103*, 8060-8065.

129. Laskowski, R. A. (1993) PROCHECK: a program to check the stereochemical quality of protein structures. *J. Appl. Crystallogr. 26*, 283-291.

130. Demange, P., Bateman, A., Mertz, C., Dell, A., Piémont, Y., and Abdallah, M. A. (1990) Bacterial siderophores: Structure of pyoverdins Pt, siderophores of *Pseudomonas tolaasii* NCPPB 2192, and pyoverdins Pf, siderophores of *Pseudomonas fluorescens* CCM 2798. Identification of an unusual natural amino acid., *Biochemistry 29*, 11041-11051.

131. Ruiz, A., and Ogden, K. L. (2004) Biotreatment of copper and isopropyl alcohol in waste from semiconductor manufacturing. *IEEE Trans. Semicond. Manufacturing 17*, 538-543.

132. Garrett, T. P. J., Guss, J. M., and Freeman, H. C. (1983) Hexakis(imidazole)manganese(II) dichloride tetrahydrate, $[Mn(C_3H_4N_2)_6]Cl_2 \oplus 4H_2O$, and hexakis(imidazole)zinc(II) dichloride tetrahydrate, $[Zn(C_3H_4N_2)_6\backslash]Cl_2 \oplus 4H_2O$. *Acta Crystallogr., Sect. C: Cryst. Struct. Commun. 39*, 1027-2031.

133. Peisach, J., and Blumberg, W. E. (1974) Structural implications derived from the analysis of EPR spectra of natural and artificial copper proteins. *Arch. Biochem. Biophys. 165*, 691-708.

134. Stemmler, T. L., Sossong, T. M., Jr., Goldstein, J. I., Ash, D. E., Elgren, T. E., Kurtz, D. M., Jr., and Penner-Hahn, J. E. (1997) EXAFS comparison of the dimanganese core structures of manganses catalase, arginase, and manganese-substituted ribonucleotide reductase and hemerythrin. *Biochemistry 36*, 9847-9858.

APPENDIX A: MULTIPLE SEQUENCE ALIGNMENTS OF THE *PMO* AND *AMO* SUBUNITS

Alignments made using ClustalW (http://www.ebi.ac.uk/clustalw; Higgins D, Thompson J, Gibson T, Thompson JD, Higgins DG, Gibson TJ (1994). CLUSTAL W: improving the sensitivity of progressive multiple sequence alignment through sequence weighting, position-specific gap penalties and weight matrix choice. *Nucleic Acids Res*. *22*, 4673-4680.)

For simplicity, only subunits for which the entire sequence is known are included.

Key:
X – Ligand to the dinuclear copper center in 1YEW
X – Ligand to the mononuclear copper center in 1YEW
X – Ligand to the zinc center in 1YEW
X – Part of the "Hydrophilic patch" identified in 1YEW

Sequence Information

	Organism	*GenBank Accession Number(s)*		
MCB	*Methylococcus capsulatus* (Bath)	PmoA1: AAB49821.1 PmoA2: AAB51065.1	PmoB1: YP_114234 PmoB2: AAB51066.1	PmoC1: AAB49820.1 PmoC2: AAB51064.1 PmoC3: AAD43965.2
MNI	*Methylomicrobium* sp. NI	PmoA: BAE86885.1	PmoB: BAE86886.1	PmoC: BAE86884.1
MTR	*Methylosinus trichosporium* OB3b	PmoA: AAA87220.2	PmoB: AAF37894.1	PmoC: AAF37893.1
MCYS	*Methylocystis* sp. M	PmoA: AAC45295.2	PmoB: AAF37897.1	PmoC: AAF37896.1
SC2	*Methylocystis* sp. SC2	PmoA1: CAE47800.1 PmoA2: CAE48352.1	PmoB1: CAE47801.1 PmoB2: CAE48353.1	PmoC1: CAE47799.1 PmoC2: CAE48351.1
GSC	*Methylocystis* sp. GSC357	PmoA: ABD57885.1		PmoC: ABD57884.1
MAC	*Methylocapsa acidiphila*	PmoA: CAJ01617.1	PmoB: CAJ01618.1	PmoC: CAJ01616.1
UNC	uncultured methanotroph	PmoA: CAJ01563.1	PmoB: CAJ01562.1	PmoC: CAJ01564.1
NEU	*Nitrosomonas europaea*	AmoA1: AAC38651.1 AmoA2: AAC38653.1	AmoB: AAA66195.1	AmoC2: NP_842074.1 AmoC3: NP_841452.1
NET	*Nitrosomonas eutropha*	AmoA1: AAB08985.1 AmoA2: AAB16816.1		AmoC: ZP_00670795.1
GH22	*Nitrosomonas* sp. GH22	AmoA: AAL86636.1		
JL21	*Nitrosomonas* sp. JL21	AmoA: AAL86638.1		
AL212	*Nitrosomonas* sp. AL212	AmoA: AAL86637.1		
NCR	*Nitrosomonas cryotolerans* ATCC 49181	AmoA: AAG60667.1	AmoB: AAG60668.1	
ENI11	*Nitrosomonas* sp. ENI-11		AmoB: BAB84332.1	AmoC2: BAB84330.1
TK794	*Nitrosomonas* sp. TK794			AmoC: BAA92238.1
NAV	*Nitrosospira* sp. NpAV	AmoA1: AAB86881.1 AmoA2: AAB87792.1 AmoA3: AAB53437.1		AmoC2: AAB87791.1 AmoC3: AAB53436.1 AmoC4: AAC69319.1
N39	*Nitrosospira* sp. Np39-19	AmoA1: AAC25055.1 AmoA2: AAB70814.1 AmoA3: AAB65662.1		
NMU	*Nitrosospira multiformis* ATCC 25196	AmoA1: AAB51760.1 AmoA2: AAB48015.1 AmoA3: AAB48534.1	AmoB: YP_413443.1	AmoC1: YP_413148.1 AmoC2: YP_413445.1
N24	*Nitrosospira multiformis* 24C	AmoA: AAC25057.1		
NBR	*Nitrosospira briensis* C-128	AmoA: AAB38709.1		
C113	*Nitrosococcus* sp. C-113	AmoA: AAF03938.1	AmoB: AAF03939.1	
NVT	*Nitrosovibrio tenuis* NV-12	AmoA: AAB38710.1		
NOC	*Nitrosococcus oceani*		AmoB: ABA58954.1	AmoC: ABA58956.1

PmoA/AmoA

```
MCB PmoA1       --------------------MSAAQSA----------------------- 7
MCB PmoA2       --------------------MSAAQSA----------------------- 7
MNI PmoA        --------------------MSASQSA----------------------- 7
MTR PmoA        --------------------MFTS-KSGGAIG------------------ 11
MCYS PmoA       --------------------MSQS-KSGGAVG------------------ 11
SC2 PmoA1       --------------------MSQS-KSGGAVG------------------ 11
SC2 PmoA2       --------------------MSASIETGSPTG------------------ 12
GSC PmoA        --------------------MSSSSKSGGAVG------------------ 12
MAC PmoA        MLMFKRKPNLAAGGPVTEAIEASPGLEGGAGANAPTLAADAGVLSAGARA 50
UNC PmoA        --MLRDKSMKTGAAPAAESILASPGIEGGAGANAPVAAAN-----VGAVA 43
NEU AmoA1       ------------------MSIFRTEEILKAAK------------------ 14
NEU AmoA2       ------------------MSIFRTEEILKAAK------------------ 14
NET AmoA1       ------------------MSIFRTEEILKAAK------------------ 14
NET AmoA2       ------------------MSIFRTEEILKAAK------------------ 14
GH22 AmoA       ------------------MSIFRTEEILKAAK------------------ 14
JL21 AmoA       --------------------MTRTDEIIAAAK------------------ 12
AL212 AmoA      --------------------MSRTDEIIAAAK------------------ 12
NCR AmoA        --------------------MSRTDEILKAAK------------------ 12
NAV AmoA1       --------------------MSRTDEILKAAK------------------ 12
NAV AmoA2       --------------------MSRTDEILKAAK------------------ 12
NAV AmoA3       --------------------MSRTDEILKAAK------------------ 12
N39 AmoA1       ----------------------------------------------------
N39 AmoA2       --------------------MSRTDEILKAAK------------------ 12
N39 AmoA3       --------------------MSRTDEILKAAK------------------ 12
NMU AmoA1       --------------------MSRTDEILKAAK------------------ 12
NMU AmoA2       --------------------MSRTDEILKAAK------------------ 12
NMU AmoA3       --------------------MSRTDEILKAAK------------------ 12
N24 AmoA        --------------------MSRTDEIIRAAK------------------ 12
NBR AmoA        --------------------MSRTDEILKAAK------------------ 12
C113 AmoA       --------------------MSALTSA----------------------- 7
NVT AmoA        --------------------MSRTDEILKAAK------------------ 12

MCB PmoA1       -----VRSHAEAVQVSRTIDWMALFVVFFVIVGSYHIHAMLTMGDWDFWS 52
MCB PmoA2       -----VRSHAEAVQVSRTIDWMALFVVFFVIVGSYHIHAMLTMGDWDFWS 52
MNI PmoA        -----VRSRAEAVKVSRTIDYMILFTAFFVVLGGYHIHYMLTGGDWDFWT 52
MTR PmoA        ----PFHSVAEAAGCVKTTDWMFLTLLFLAVLGGYHIHFMLTAGDWDFWV 57
MCYS PmoA       ----PFNSVAEAAGCVATTDWMLLVLLFFAVLGGYHVHFMLTAGDWDFWV 57
SC2 PmoA1       ----PFNSVAEAAGCVQTVDWMLLVLLFFAVLGGYHVHFMLTAGDWDFWV 57
SC2 PmoA2       ---KTWKSKEEFLGCVILTDWILLVILFAVLLGSFHIHYMLLAGDWDFWI 59
GSC PmoA        ----PFHSVAEAAGCVQTVDWLLLTLLFFAVLGGYHVHFMLTAGDWDFWV 58
MAC PmoA        AAGSPFNSKAEAAGLVKTADILLLASLFLITLGGYHIHAMLTMGDWDFWI 100
UNC PmoA        AAASPFHSRAEAAGAVRTADLLILTFLFLIMIGGYHVHAMLTMGDWDFWV 93
NEU AmoA1       -------MPPEAVHTSRLIDAVYFPILIILLVGTYHMHFMLLAGDWDFWM 57
NEU AmoA2       -------MPPEAVHMSRLIDAVYFPILIILLVGTYHMHFMLLAGDWDFWM 57
NET AmoA1       -------MPPEAVHMSRLIDAVYFPILVVLLVGTYHMHFMLLAGDWDFWM 57
NET AmoA2       -------MPPEAVHMSRLIDAVYFPILVVLLVGTYHMHFMLLAGDWDFWM 57
GH22 AmoA       -------MPPEAVHMSRLIDAVYFPILVVLLVGTYHMHFMLLAGDWDFWM 57
JL21 AmoA       -------MPPEAVRMSRYIDAVYFPILCILLVGTYHMHFMLLAGDWDFWL 55
AL212 AmoA      -------MPPEAVKMSRYIDAVYFPILCILLVGTFHMHFMLLAGDWDFWL 55
NCR AmoA        -------MPPEAIKMSRMIDAVYFPILCILLVGTYHMHFMLLAGDWDFWL 55
NAV AmoA1       -------MPPESVKMSRMIDAIYFPILCILLVGTYHMHFMLLAGDWDFWL 55
NAV AmoA2       -------MPPESVKMSRMIDAIYFPILCILLVGTYHMHFMLLAGDWDFWL 55
NAV AmoA1       -------MPPESVKMSRMIDAIYFPILCILLVGTYHMHFMLLAGDWDFWL 55
N39 AmoA1       --------------MSRMIDAVYFPILCILLVGTYHMHFMLLAGDWDFWL 36
N39 AmoA2       -------MPPEAVKMSRMIDAVYFPILCILLVGTYHMHFMLLAGDWDFWL 55
N39 AmoA3       -------MPPEAVKMSRMIDAVYFPILCILLIGTYHMHFMLLAGDWDFWL 55
NMU AmoA1       -------MPPEAVKMSRMIDVIYFPILCILLVGTYHMHFMLLAGDWDFWL 55
NMU AmoA2       -------MPPEAVKMSRMIDVIYFPILCILLVGTYHMHFMLLAGDWDFWL 55
NMU AmoA3       -------MPPEAVKMSRMIDVIYFPILCILLVGAYHMHFMLLAGDWDFWL 55
N24 AmoA        -------MPPEAVKMSRMIDVIYFPILCILLVGTYHMHFMLLAGDWDFWL 55
NBR AmoA        -------MPPEAVKMSRMIDAVYFPILCILLVGTYHMHFMLLAGDWDFWL 55
C113 AmoA       -----VRTPEEAAKVSRTLDFLALGAFFGILLASHHVHVMLLMGDWDFWV 52
NVT AmoA        -------MPPEAVKMSRMIDAVYFPILCILLVGTYHMHFMLLAGDWDFWL 55
                                  * : :       :. .*:* **  ******
```

```
MCB PmoA1       DWKDRRLWVTVTPIVLVTFPAAVQSYLWERYRLPWGATVCVLGLLLGEWI 102
MCB PmoA2       DWKDRRLWVTVTPIVLVTFPAAVQSYLWERYRLPWGATVCVLGLLLGEWI 102
MNI PmoA        DWKDRRLWVTVAPIVSITFPAAVQAVLWWRYRIAWGATLCVLGLLLGEWI 102
MTR PmoA        DWKDRRMWPTVVPILGVTFAAAAQAFFWENFKLPFGATFAVSGLLIGEWI 107
MCYS PmoA       DWKDRRMWPTVLPILGVTFCAASQAFWWVNFRLPFGAVFAVLGLMIGEWI 107
SC2 PmoA1       DWKDRRMWPTVVPILGVTFCAAAQAFWWVNFRLPFGAVFAALGLLIGEWI 107
SC2 PmoA2       DFKDRRMWPTVTPIVAMCFAAAAQSFFWTRFRLPIGATTVVLALLIGEWI 109
GSC PmoA        DWKDRRMWPTVIPILGVTFCAAAQAFFWVNFRLPFGAVFAALGLLIGEWI 108
MAC PmoA        DWKDRRFWPTVLPIVLVTFPAAAQAYFWESFRLPFGATFLVLGLLFGEWV 150
UNC PmoA        DWKDRRMWPTVLPIMLVTFPAAAQYFFWEHFRLPFGATFLCVALLFGEWL 143
NEU AmoA1       DWKDRQWWPVVTPIVGITYCSAIMYYLWVNYRQPFGATLCVVCLLIGEWL 107
NEU AmoA2       DWKDRQWWPVVTPIVGITYCSAIMYYLWVNYRQPFGATLCVVCLLIGEWL 107
NET AmoA1       DWKDRQWWPVVTPIVGITYCSAIMYYLWVNYRQPFGATLCVVCLLIGEWL 107
NET AmoA2       DWKDRQWWPVVTPIVGITYCSAIMYYLWVNYRQPFGATLCVVCLLIGEWL 107
GH22 AmoA       DWKDRQWWPVVTPIVGITYCSAIMYYLWVNYRQPFGATLCVVCLLIGEWL 107
JL21 AmoA       DWKDRQWWPVVTPIVGIMYCAALMYYLWVNYRLPFGATLCIVCLLVGEWL 105
AL212 AmoA      DWKDRQWWPVVTPIAGIMYCAALMYYLWVNYRLPFGATLCIVCLLVGEWL 105
NCR AmoA        DWKDRQYWPVVTPIVGIMYCAAIMYYLWVNYRLPFGATLCIVCLLVGEWL 105
NAV AmoA1       DWKDRQWWPVVTPIVGITYCATIMYYLWVNYRLPFGATLCIVCLLVGEWL 105
NAV AmoA2       DWKDRQWWPVVTPIVGITYCATIMYYLWVNYRLPFGATLCIVCLLVGEWL 105
NAV AmoA3       DWKDRQWWPVVTPIVGITYCATIMYYLWVNYRLPFGATLCIVCLLVGEWL 105
N39 AmoA1       DWKDRQWWPVVTPIVGITYCAAIMYYLWVNYRLPFGATLCIVCLLSGEWL 86
N39 AmoA2       DWKDRQWWPVVTPIVGITYCAAIMYYLWVNYRLPFGATLCIVCLLSGEWL 105
N39 AmoA3       DWKDRQWWPVVTPIVGITYCAAIMYYLWVNYRLPLGAILCIVCLLSGEWL 105
NMU AmoA1       DWKDRQWWPVVTPIVGITYCAAIMYYLWVNYRLPFGATLCIVCLLVGEWL 105
NMU AmoA2       DWKDRQWWPVVTPIVGITYCAAIMYYLWVNYRLPFGATLCIVCLLVGEWL 105
NMU AmoA3       DWKDRQWWPVVTPIVGITYCAAIMYYLWVNYRLPFGATLCIVCLLVGEWL 105
N24 AmoA        DWKDRQWWPVVTPIVGITCYAAIMYYLWVNYRLPYGATLCIVCLLVGEWL 105
NBR AmoA        DWKDRQWWPVVTPIVGITYCAAIMYYLWVNYRLPFGATLCVVCLLTGEWL 105
C113 AmoA       DWKDRRFWVTVVPIVSVAYPAAAQAFFWEKFRLPFGATLVTLGLLAGEWA 102
NVT AmoA        DWKDRQWWPVVTPIVGITYCAAIMYYLWVNYRLPFGATLCIVCLLAGEWL 105
                *:***: * .* **  :   ::     *  :: . **      *: **

MCB PmoA1       NRYFNFWGWTYFPINFVFPASLVPGAIILDTVLMLSGSYLFTAIVGAMGW 152
MCB PmoA2       NRYFNFWGWTYFPINFVFPASLVPGAIILDTVLMLSGSYLFTAIVGAMGW 152
MNI PmoA        NRYFNFWGWTYFPVNFVFPSNLMPGAIVLDVILMLSNSMTLTAVVGGLAW 152
MTR PmoA        NRYCNFWGWTYFPISLVFPSALVVPALWLDIIMLLSGSYVITAVVGSLGW 157
MCYS PmoA       NRYVNFWGWTYFPISLVFPSAMIVPAIWLDVILLLSGSYVITAVVGSLGW 157
SC2 PmoA1       NRYVNFWGWTYFPISLVFPSALIVPAIWLDVILLLSGSYVITAIVGSLGW 157
SC2 PmoA2       NRYDNFWGWTFFPINLVFPSALIPMGFWLDIVLMISGSWLVTALLGGLGW 159
GSC PmoA        NRYVNFWGWTYFPISLVFPSALIVPAIWLDVILLLSGSYVITAVVGSLGW 158
MAC PmoA        NRYTNFWGWTYFPISLVWPTSLVPAALFLDIVLLLSRSFIVTAIVGAMGW 200
UNC PmoA        DRYISFWGWTYP----------------------------------------- 155
NEU AmoA1       TRYWGFYWWSHYPINFVTPGIMLPGALMLDFTLYLTRNWLVTALVGGGFF 157
NEU AmoA2       TRYWGFYWWSHYPINFVTPGIMLPGALMLDFTLYLTRNWLVTALVGGGFF 157
NET AmoA1       TRYWGFYWWSHYPLNFVTPGIMLPGALMLDFTMYLTRNWLVTALVGGGFF 157
NET AmoA2       TRYWGFYWWSHYPLNFVTPGIMLPGAFMLDFTMYLTRNWLVTALVGGGFF 157
GH22 AmoA       TRYWGFYWWSHYPLNFVTPGIMLPGALMLDFTMYLTRNWLVTALVGGGFF 157
JL21 AmoA       TRYWGFYWWSHYPLNFVLPSTMIPGALMMDTIMLLTGNWLVTALLGGGFF 155
AL212 AmoA      TRYWGFYWWSHYPINFVLPSTMIPGALMLDTIMLLTGDWLITALLGGAFW 155
NCR AmoA        TRYWGFYWWSHYPMNFVLPSTMIPGALMLDTVMLLTRSWLVTALVGGGFF 155
NAV AmoA1       TRFWGFYWWSHYPINFVLPSTMIPGALIMDTVMLLTRNWMITALVGGGAF 155
NAV AmoA2       TRFWGFYWWSHYPINFVLPSTMIPGALIMDTVMLLTRNWMITALVGGGAF 155
NAV AmoA3       TRFWGFYWWSHYPINFVLPSTMIPGALIMDTVMLLTRNWMITALVGGGAF 155
N39 AmoA1       TRYWGFYWWSHYPISFVFPSTMIPGALVMDTVMLLTRNWMITALVGGGAF 136
N39 AmoA2       TRYWGFYWWSHYPISFVFPSTMIPGALVMDTVMLLTRNWMITALVGGGAF 155
N39 AmoA3       TRYWGFYWWSHNPISFVFPSTMIPGALVMDTVMLLTRNWMITALVGGGAF 155
NMU AmoA1       TRFWGFYWWSHYPMNFVFPSTMIPGALVMDTVLLLTRNWMITALVGGGAF 155
NMU AmoA2       TRFWGFYWWSHYPMNFVFPSTMIPGALVMDTVLLLTRNWMITALVGGGAF 155
NMU AmoA3       TRFWGFYWWSHYPMNFVFPSTMIPGALGMDTVLLLTRNWMITALVGGGAF 155
N24 AmoA        TRFWGFYWWSHYPINFVFPSTMIPGALIMDTVMLLTRNWMITALIGGGAF 155
NBR AmoA        TRYWGFYWWSHYPINFVFPSTMIPGALVMDTVMLLTRNWMITALVGGGAF 155
C113 AmoA       NRYFNFVGFTYFPINFVWPTILLPMALFLDAMLAISKSYGLTAVVGGLMY 152
NVT AmoA        TRFWGFYWWSHYPMSFVFPSTMIPGALVMDTVMLLTRNWMITALVGGGAF 155
                 *: .*  ::.
```

```
MCB PmoA1       GLIFYPGNWPIIAPLHVPVENNGMLMSIADIQGYNYVRTGTPEYIRMVEK 202
MCB PmoA2       GLIFYPGNWPIIAPLHVPVEYNGMLMSIADIQGYNYVRTGTPEYIRMVEK 202
MNI PmoA        GLLFYPGNWPIIAPLHVPVEYNGMMMTLADLQGYHYVRTGTPEYIRMVEK 202
MTR PmoA        GLLFYPNNWPAIAALHQATEQHGQLMSLADLVGFHFVRTSMPEYIRMVER 207
MCYS PmoA       GLLFYPNNWPAIAAFHQATEQHGQLMTLADLIGLHFVRTSMPEYIRMVER 207
SC2 PmoA1       GLLFYPNNWPAIAAFHQATEQHGQLMTLADLIGFHFVRTSMPEYIRMVER 207
SC2 PmoA2       GLLFYPINWPVLAQYHQAAEIDGVLLTLADLIGFNYVRTGTPEYIRMVER 209
GSC PmoA        GLLFYPNNWPAIAAFHQATEQHGQLMSLADLIGLHFVRTSMPEYIRMVER 208
MAC PmoA        GLLLYPSNWPILAPYHQATEQYGLLMSLADLIGFEYVRTSMPEYLRIVER 250
UNC PmoA        ------------------TEQYGTLMSLADVIGFHNVRTSMPEYIRIIER 187
NEU AmoA1       GLLFYPGNWPIFGPTHLPIVVEGTLLSMADYMGHLYVRTGTPEYVRHIEQ 207
NEU AmoA2       GLLFYPGNWPIFGPTHLPIVVEGTLLSMADYMGHLYVRTGTPEYVRHIEQ 207
NET AmoA1       GLMFYPGNWPIFGPTHLPIVVEGTLLSMVDYMGHLYVRTGTPEYVRHIEQ 207
NET AmoA2       GLMFYPGNWPIFGPTHLPIVVEGTLLSMADYMGHLYVRTGTPEYVRHIEQ 207
GH22 AmoA       GLMFYPGNWPIFGPTHLPIVVEGTLLSMADYMGHLYVRTGTPEYVRHIEQ 207
JL21 AmoA       GLFFYPGNWPIFGPTHLPVVVEGVLLSIADYTGFLYVRTGTPEYVRLIEQ 205
AL212 AmoA      GLFFYPGNWPIFGPTHLPLVVEGVLLSVADYTGFLYVRTGTPEYVRLIEQ 205
NCR AmoA        GLFFYPGNWPIFGPTHLPVVVEGVLLSLADYTGFLYVRTGTPEYVRLIEQ 205
NAV AmoA1       GLLFYPGNWPIFGPTHLPLVAEGVLLSLADYTGFLYVRTGTPEYVRLIEQ 205
NAV AmoA2       GLLFYPGNWPIFGPTHLPLVAEGVLLSLADYTGFLYVRTGTPEYVRLIEQ 205
NAV AmoA3       GLLFYPGNWPIFGPTHLPLVAEGVLLSLADYTGFLYVRTGTPEYVRLIEQ 205
N39 AmoA1       GLLFYPGNWPIFGPTHLPLVVEGVLLSVADYTGFLYVRTGTPEYVRNIEQ 186
N39 AmoA2       GFLFYPGNWPIFGPTHLPLVVEGVLLSVADYTGFLYVRTGTPEYVRNIEQ 205
N39 AmoA3       GLLFYPGNWPIFGPTHLPLVVEGVLLSVADYTGFLYVRTGTPEYVRNIEQ 205
NMU AmoA1       GLLFYPGNWTIFGPTHLPLVAEGVLLSVADYTGFLYVRTGTPEYVRLIEQ 205
NMU AmoA2       GLLFYPGNWTIFGPTHLPLVAEGVLLSVADYTGFLYVRTGTPEYVRLIEQ 205
NMU AmoA3       GLLFYPGNWTIFGPTHLLLVAEGVLLSVADYTGFLYVRTGTPEYVRLIEQ 205
N24 AmoA        GLLFYPGNWPIFGPTHLPLVAEGVLLSVADYTGFLYVRTGTPEYVRLIEQ 205
NBR AmoA        GLLFYPGNWPIFGPTHLPLAAEGVLLSVADYTGFLYVRTGTPEYVRNIEQ 205
C113 AmoA       GLLMYPANWPLLSAFHVPAEYNGVVMSLADVAGYQYVRTGTPEYIRMVEK 202
NVT AmoA        GLLFYPGNWPIFGLTHLPLVVEGVLLSVADYTGFLYVRTGTPEYVRNIEQ 205
                                  * ::::.*  *   ***. **:* :*:

MCB PmoA1       GTLRTFGKDVAPVSAFFSAFMSILIYFMWHFIGRWFSNERFLQST----- 247
MCB PmoA2       GTLRTFGKDVAPVSAFFSAFMSILIYFMWHFIGRWFSNERFLQST----- 247
MNI PmoA        GTLRTFGKDVAPVSAFFSGFVSILIYFLWHFFGSWFGSEKFVQGS----- 247
MTR PmoA        GTLRTFGKEVVPVAAFFSGFVSMMVYFLWWFVGKWYSTTKVIQKI----- 252
MCYS PmoA       GTLRTFGKDVVPVAAFFSGFVSMMVYFLWWFMGRWYSTTKRIEQI----- 252
SC2 PmoA1       GTLRTFGKDVVPVAAFFSGFVSMMVYFLWWFMGRWYSTTKIIDTI----- 252
SC2 PmoA2       GTLRTFGKDVVPVAAFFSGFISMLVYFLWWNMGKWFSTTKYLEIEEV--- 256
GSC PmoA        GTLRTFGKDVVPVAAFFSGFVSMMVYFLWWFMGRWYSTTKVIDKI----- 253
MAC PmoA        GTMRTFGKDVVAVAAFFSGFVSILVYFWWWYVGKLFSTVAYTKEV----- 295
UNC PmoA        GTMRTFGKDVVGVAAFFSGFVSIIVYFVWWYVGKMFSTTKYMKSIYPINL 237
NEU AmoA1       GSLRTFGGHTTVIAAFFSAFVSMLMFTVWWYLGKVYCTAFFYVKGKRGRI 257
NEU AmoA2       GSLRTFGGHTTVIAAFFSAFVSMLMFTVWWYLGKVYCTAFFYVKGKRGRI 257
NET AmoA1       DSLRTFGGHTTVIAAFFAAFVSMLMFAVWWYLGKVYCTAFFYVKGKRGRI 257
NET AmoA2       GSLRTFGGHTTVIAAFFAAFVSMLMFAVWWYLGKVYCTAFFYVKGKRGRI 257
GH22 AmoA       GSLRTFGGHTTVIAAFFAAFVSMLMFAVWWYLGKVYCTAFFYVKGKRGRI 257
JL21 AmoA       GSLRTFGGHTTVIAAFFSAFVSMLMFCVWWYFGKLYCTAFYYVKGERGRI 255
AL212 AmoA      GSLRTFGGHTTVIAAFFSAFVSMLMFCVWWYFGKLYCTAFFYVKGERGRI 255
NCR AmoA        GSLRTFGGHTTVIAAFFAAFVSMLMFCVWWYFGKLYCTAFTMLRCKR-QV 254
NAV AmoA1       GSLRTFGGHTTVIAAFFSAFVSMLMFCVWWYFGKLYCTAFYYVKGPRGRV 255
NAV AmoA2       GSLRTFGGHTTVIAAFFSAFVSMLMFCVWWYFGKLYCTAFYYVKGPRGRV 255
NAV AmoA3       GSLRTFGGHTTVIAAFFSAFVSMLMFCVWWYFGKLYCTAFYYVKGPRGRV 255
N39 AmoA1       GSLRTFGGHTTVIAAFFAAFISMLMFCIWWYFGKLYCTAFFYVKGHRGRV 236
N39 AmoA2       GSLRTFGGHTTVIAAFFAAFISMLMFCIWWYFGKLYCTAFFYVKGHRGRV 255
N39 AmoA3       GSLRTFGGHTTVIAAFFAAFISMLMFCIWWYFGKLYCTAFFYVKGHRGRV 255
NMU AmoA1       GSLRTFGGHTTVIASFFSAFVSMLMFTVWWYFGKVYCTAFYYVKGARGRV 255
NMU AmoA2       GSLRTFGGHTTVIASFFSAFVSMLMFTVWWYFGKVYCTAFYYVKGARGRV 255
NMU AmoA3       GSLRTFGGHTTVIASFFSAFVSMLMFTVWWYFGKVYCTAFYYVKGARGRV 255
N24 AmoA        GSLRTFGGHTTVIAAFFSAFVSMLMFTVWWYFGKVYCTAFFYVKGPRGRI 255
NBR AmoA        GSLRTFGGHTTVIASFFAAFVSMLMFCLWWYFGKLYCTAFFYVKGTRGRV 255
C113 AmoA       GTLRTFGKDVVPVSAFFAGFVAMVMYFVWHFVGRWFSKDYSVDQC----- 247
NVT AmoA        GSLRTFGGHTTVIAAFFAAFISMLMFTIWWYFGKLYCTAFFYVKGHRGRV 255
                .::**** ... :::**:.*:::::::  *  .*  : .
```

```
MCB PmoA1       --------------------------------------------------
MCB PmoA2       --------------------------------------------------
MNI PmoA        --------------------------------------------------
MTR PmoA        --------------------------------------------------
MCYS PmoA       --------------------------------------------------
SC2 PmoA1       --------------------------------------------------
SC2 PmoA2       --------------------------------------------------
GSC PmoA        --------------------------------------------------
MAC PmoA        --------------------------------------------------
UNC PmoA        VWPTSLVPQALFLDIVLLLSKSFIVTAIVGSMGFSLLLYPNNWVILAQFHQ 288
NEU AmoA1       VHRNDVTAFGEEGFPEGIK-------------------------------- 276
NEU AmoA2       VHRNDVTAFGEEGFPEGIK-------------------------------- 276
NET AmoA1       VQRNDVTAFGEEGFPEGIK-------------------------------- 276
NET AmoA2       VQRNDVSAFGEEGFPEGIK-------------------------------- 276
GH22 AmoA       VQRNDVTAFGEEGFPEGIK-------------------------------- 276
JL21 AmoA       SMKNDVTAFGEKGFAQGIK-------------------------------- 274
AL212 AmoA      SMKNDVTAFGEKGFAQGIK-------------------------------- 274
NCR AmoA        SMKHDVTAFGEEGFAEGIK-------------------------------- 273
NAV AmoA1       TMKNDVTAYGEEGFPEGIK-------------------------------- 274
NAV AmoA2       TMKNDVTAYGEEGFPEGIK-------------------------------- 274
NAV AmoA3       TMKNDVTAYGEEGFPEGIK-------------------------------- 274
N39 AmoA1       TMKNDVTAFGEEGFPEGIK-------------------------------- 255
N39 AmoA2       TMKDDVTAFGEEGFPEGIK-------------------------------- 274
N39 AmoA3       TMKNDVTAFGEEGFPEGIK-------------------------------- 274
NMU AmoA1       SMKNDVTAFGEEGFAEGIK-------------------------------- 274
NMU AmoA2       SMKNDVTAFGEEGFAEGIK-------------------------------- 274
NMU AmoA3       SMKNDVTAFGEEGFAEGIK-------------------------------- 274
N24 AmoA        SMKNDVTAYGEEGFPEGIK-------------------------------- 274
NBR AmoA        TMKNDVTAFGEEGFPEGIK-------------------------------- 274
C113 AmoA       --------------------------------------------------
NVT AmoA        TMKNDVTAFGEEGFPEGIK-------------------------------- 274
```

PmoB/AmoB

```
MCB PmoB1       ---MK--TIKDRIAKWS--------AIGLLSAVAATAFYAPSASAHGEKS 37
MCB PmoB2       ---MK--TIKDRIAKWS--------AIGLLSAVAATAFYAPSASAHGEKS 37
MNI PmoB        ---MK--IIKDKVAKLS--------FVALLVSVTAAMFYTPTASAHGEKS 37
MTR PmoB        ---MK--ALERMAELATGRVGKLLGL-SVAAAVAATAASVAPAEAHGEKS 44
MCYS PmoB       ---MK--KLVKLAAFG----------AAAAVAATLGAIAPASAHGEKS 33
SC2 PmoB1       ---MK--KFVKLAAIG----------AAAAVAATLGAVAPASAHGEKS 33
SC2 PmoB2       ---MKSLNLHSMAKCATARVVRLWILGLAVAGALTTLPAATPAAAHGERS 47
MAC PmoB        ---MFSTLAGHAKRQAG-----RLWALGLAVGLAASMAGSGPADAHGEKS 42
UNC PmoB        ---MTTTMFSSLARQTG-----RLWALVLAAALAVTMAAIGPADAHGEKS 42
NEU AmoB        ---MGIKNLYKRGVMGLYG-----VAYAVAALAMTVTLDVSTVAAHGERS 42
NCR AmoB        ---MSIKNIFKLGIIGLYG-----VAYGVATLALTVVLDVSPVAAHGERS 42
ENI11 AmoB      ---MGIKNLYKRGVMGLYG-----IAYAVAALAMTVTLDVSTVAAHGERS 42
NAV AmoB1       ---MNAKNLFKLGVIGLY---------GMATLALS-TLDISPAAAHGERS 37
NAV AmoB2       ---MNAKNLFKLGVIGLY---------GMATLALS-TLDISPAAAHGERS 37
NAV AmoB3       ---MNAKNLFKLGVIGLY---------GMATLALS-TLDISPAAAHGERS 37
NMU AmoB        -----MKNLFKKSIAGVC---------SLAALGLALTLDIQPAAAHGERS 36
C113 AmoB       MENMKGTHITNRAKKWL--------AIGFTAVIASSVFYIPTVAAHGEKA 42
NOC AmoB        ------------------------------MIASSVFYIPTVAAHGEKA 19
                   :                                  .. ****::
```

```
MCB PmoB1       QAAFMRMRTIHWYDLSWSKEKVKINETVEIKGKFHVFEGWPETVDEPDVA 87
MCB PmoB2       QAAFMRMRTIHWYDLSWSKEKVKINETVEIKGKFHVFEGWPETVDEPDVA 87
MNI PmoB        QAAFMRMRTIHWFDLNWSKDMVSVNETMSISGKFHVFAGWPETVDKPEVA 87
MTR PmoB        QQAFLRMRTLNWYDVKWSKTSLNVNESMVLSGKVHVFSAWPQAVANPKSS 94
MCYS PmoB       QQAFLRMRTLNWYDVQWSKTTVNVNEEMILSGKVHVFSAWPQAVANPRVS 83
SC2 PmoB1       QQAFLRMRTLNWYDVQWSKTTVNVNEEMVLSGKIHVFSAWPQAVANPRVS 83
SC2 PmoB2       QQAFLRMRTLNWYDVKWSKTELNVNDEMELTGKVHVFSGWPQAVARPGES 97
MAC PmoB        QAAFLRMRTLNWYDVKWSKTSLNVNEEMEITGKLHIMDAWPVAVAKPEVA 92
UNC PmoB        QAAFLRMRTLNWYDVVWSKTNVAVNEEYEITGKLHIMNSWPAAIKVPDQC 92
NEU AmoB        QEPFLRMRTVQWYDIKWGPEVTKVNENAKITGKFHLAEDWPRAAAQPDFS 92
NCR AmoB        QEPFLRMRTIQWYDLKWGPQTTKVNDIATMTGKFHLAEDWPRAVGKPERA 92
ENI11 AmoB      QEPFLRMRTVQWYDIKWGPEVTKVNENAKITGKFHLAEDWPRAAASPDFS 92
NAV AmoB1       QEPFLRMRTIQWYDMKWGPDTTKVNDFATMTGKFHLAEDWPRAVGKPGRA 87
NAV AmoB2       QEPFLRMRTIQWYDMKWGPDTTKVNDFATMTGKFHLAEDWPRAVGKPGRA 87
NAV AmoB3       QEPFLRMRTIQWYDMKWGPDTTKVNDFATMTGKFHLAENWPRAVGKPGRA 87
NMU AmoB        QEPFLRMRTIQWYDMKWGPETTKVNDIATMTGKFHLAEDWPRAVGKPGRA 86
C113 AmoB       QAAFLRMRTIHWYDMVWSKDTIAVNETYTISGKFRVFEDWPEAVEVPHVS 92
NOC AmoB        QAAFLRMRTIHWYDMVWSKDTIAVNETYTISGKFRVFEDWPEAVEKPHVS 69
                * .*:****:.*:*: *.     :*:   :.**.::   ** :   *  .

MCB PmoB1       FLNVGMPGPVFIRKESYIGG----QLVPRSVRLEIGKTYDFRVVLKARRP 133
MCB PmoB2       FLNVGMPGPVFIRKESYIGG----QLVPRSVRLEIGKTYDFRVVLKARRP 133
MNI PmoB        FLNIGIPGPVFIRAGSWIGG----QLVPRSVSLELGETYEFKVLLKARRP 133
MTR PmoB        FLNAGEPGPVLVRTAQFIGE----QFAPRSVSLEVGKDYAFSIDLKARRA 140
MCYS PmoB       FLNAGEPGPVLVRTAQFIGE----QFAPRSVSLEIGKDYAFSINLRGRRA 129
SC2 PmoB1       FLNAGEPGPVLVRTAQFIGE----QFAPRSVSLVPGNDYAFSINLRGRRA 129
SC2 PmoB2       FLNVGEPGPVLIRKSAFVGE----VPVPRTFSMDVGNDYEYKIVLKARRQ 143
MAC PmoB        FLNVGMPGPVLVREGSFLGG----KFVPRSTSLELGKTYEFRVLLKARRQ 138
UNC PmoB        FLNTGQPGAMAARLGVWVGAPGQMQFTPRSMRLDVGKTYAFRILLKGRRP 142
NEU AmoB        FFNVGSPSPVFVRLSTKING----HPWFISGPLQIGRDYEFEVNLRARIP 138
NCR AmoB        FFNVGSPSPVFVRLSTKLNG----EPTFIAGPLVIGRDYEFEVKLKARIP 138
ENI11 AmoB      FFNVGSPSPVFVRLSTKING----HPWFISGPLQIGRDYEFEVNLRARIP 138
NAV AmoB1       FFNVGSPSPVFVRLSTKLNG----EPTYISGPLEIGRDYAFEVKLKARIP 133
NAV AmoB2       FFNVGSPSPVFVRLSTKLNG----EPTYISGPLEIGRDYAFEVKLKARIP 133
NAV AmoB3       FFNVGSPSPVFVRLSTKLNG----EPTYISGPLEIGRDYAFEVKLKAPIP 133
NMU AmoB        FFNVGSPSPVFVRLSTKLNG----EPTYISGPMEIGRDYAFEVRLKARIP 132
C113 AmoB       FLNAGQPGPVTTRLTSYING----MFVPRSIGLELGGDYEFEMTMQGRRP 138
NOC AmoB        FLNAGQPGPVTARLTSYVNG----MFVPRSIGLELGGDYEFEMTMQGRRP 115
                *:* * *..:  *    :.          :  :  *  * : : ::.

MCB PmoB1       GDWHVHTMMNVQGGGPIIGPGKWITVEGSMSEFRNPVTTLTGQTVDLENY 183
MCB PmoB2       GDWHVHTMMNVQGGGPIIGPGKWITVEGSMSEFRNPVTTLTGQTVDLENY 183
MNI PmoB        GDWHVHTMMNVEGGGPIIGPGKWVTITGSMGDFKNPITTLTGETIDLETY 183
MTR PmoB        GRWHVHAQINVEGGGPIIGPGQWIEIKGDMADFKDPVTLLDGTTVDLETY 190
MCYS PmoB       GRWHVHAQINVEGGGPIIGPGQWIEIKGDMKDFTDPVTLLDGSTVDLENY 179
SC2 PmoB1       GRWHVHAQINVEGGGPIIGPGQWIEIKGDMKDFTDPVTLLDGSTVDLETY 179
SC2 PmoB2       GRYHVHVQINVKDGGPIVGPGQWITIKGDMKDFTNPVTLLEGSTIDLETY 193
MAC PmoB        GRWHVHTQLSVQTGGPIIGPGQWVEIKGDMADFKNPVTLLNGEVIDLEQY 188
UNC PmoB        GHWHTHVQLSVMTGGPIPGPGQYIDIKGNFSDFVDDVKLLNGTTVDIETY 192
NEU AmoB        GRHHMHAMLNVKDAGPIAGPGAWMNITGSWDDFTNPLKLLTGETIDSETF 188
NCR AmoB        GRHHMHAMVNVKDAGPIAGPASWMNITGSWDDFTNPIKTLTGKTIDTETF 188
ENI11 AmoB      GRHHMHAMLNVKDAGPIAGPGAWMNITGSWDDFTNPLKLLTGETVDSETF 188
NAV AmoB1       GRHHMHAMVNIKDAGPIAGPAAWMNITGSWDDFTNPVKLLTGETIDTETF 183
NAV AmoB2       GRHHMHAMVNIKDAGPIAGPAAWMNITGSWDDFTNPVKLLTGETIDTETF 183
NAV AmoB3       GSHHMHTMVNIKDAGPIAGPAAWMNITGSWDDFTNPVKLLTGETIDTETF 183
NMU AmoB        GRHHMHAMVNIKDAGPIAGPAAWMNISGSWDDFTNPVKLLTGETIDTETF 182
C113 AmoB       GTWHVHTLLNVQGGGPLIGPGKYITITGDMADFENKVTDLTGNTVNLETM 188
NOC AmoB        GTWHVHTLLNVQGGGPLIGPGKYITITGDMADFESKITDLTGNTVNLETM 165
                *  * *. :.:  .**: **. :: : *.  :* . :. * * .:: *
```

```
MCB PmoB1       NEGNTYFWHAFWFAIGVAWIGYWSRRPIFIPRLLMVDAGRADELVSATDR 233
MCB PmoB2       NEGNTYFWHAFWFAIGVAWIGYWSRRPIFIPRLLMVDAGRADELVSATDR 233
MNI PmoB        ALDGVYGWHLFWYVLGVAWMVYWCRKPVFIPRRIAVDAGKADSLITPTDK 233
MTR PmoB        GIDRIYAWHFPWMIAAAAWILYWFFKKGIIASYLRISEGKDEEQIGDDDR 240
MCYS PmoB       GISRIYAWHLPWLAVGAAWILFWFIRKGIIASYVRVAEGRPDDVIGDDDR 229
SC2 PmoB1       GISRVYAWHLPWLAVGAAWILFWFVRKGIIASYLRVATGKVDEQVTDDDK 229
SC2 PmoB2       GITWTYIYHFFWMAAAAAWILYWFMTKGIIVRYWQVKAGKGRELIGQDEK 243
MAC PmoB        KIGNIYFWHTVWFIAGVAWVFYWFRKRGFVGRYISVASGKGGELITPLER 238
UNC PmoB        GIGKIYMWHLFWIVVGGWWILYWFGKRGFIGRFAWVASGKAEEVITPQER 242
NEU AmoB        NLSNGIFWHVVWMSIGIFWIGVFTARPMFLPRSRVLLAYGDDLLMDPMDK 238
NCR AmoB        NHGNGVFWHALWMGLGVFWIGYFVARPMFLPRSRVLLAYGDELLLDPMDR 238
ENI11 AmoB      NLSNGIFWHVVWMSIGIFWIGVFTIRPMFLPRSRVLLAYGDDLLMDPMDK 238
NAV AmoB1       NFNNGIFWHLLWLGLGCFWIGYYVARPMFLPRSRVLLAYGDDLLLDPMDK 233
NAV AmoB2       NFNNGIFWHLLWLGLGCFWIGYYVARPMFLPRSRVLLAYGDDLLLDPMDK 233
NAV AmoB3       NFNNGIFWHLLWLGLGCFWIGYYVARPMFLPRSRVLLAYGDDLLLDPMDK 233
NMU AmoB        NFSNGIFWHILWLSLGIFWIGYYVARPMFLPRSRVLLAYGDELLLDPMDR 232
C113 AmoB       ATGTVIGWHLFWYVLGIAWIVWWARRPMFLPRYMRVEAGEANDLVTAQDK 238
NOC AmoB        ATGTVIGWHLFWYVLGIAWIWWWARRPMFLPRYMRIEAGEANDLVTAQDK 215
                       :*  *   .  *:  :     ::     :        :   ::

MCB PmoB1       KVAMGFLAATILIVVMAMSSANSKYPITIPLQAGTMRGMKPLELP----- 278
MCB PmoB2       KVAMGFLAATILIVVMAMSSANSKYPITIPLQAGTMRGMKPLELP----- 278
MNI PmoB        KVGMAFAAGTMAIVAISMGQANEKYPVTTPLQAGLMRGIKSLELP----- 278
MTR PmoB        RVGAIVLAVTILATIIGYAVTNSTFPRTIPLQAGLQKPLTPIIEEGTAGV 290
MCYS PmoB       RIGAIVLALTILATIVGYAVTNSTFPRTIPLQAGLQKPLTPIETEGTVGV 279
SC2 PmoB1       RIGAIVLALTILATIVGYAVTNSTFPRTIPLQAGLQKPLTPLVTDGTAGV 279
SC2 PmoB2       RIGAVTLAAVLLAVLVFYASANREFPRTLPMQAGLLTGISPIDEP----- 288
MAC PmoB        QIGAGALAATLLVVIISYALTASEFPRTIPLQAGNIRAIDALN------I 282
UNC PmoB        VVGAITLLAVLLVVIIFYAITVSGNPNTIPLQAGDFRNITALENE----V 288
NEU AmoB        KITWVLAILTLALVWGGYRYTENKHPYTVPIQAGQSK-VAALPVA----- 282
NCR AmoB        KVGLAVAILTCAIVWGGYRYTETVHPYTVPIQAGESK-VAPLPIA----- 282
ENI11 AmoB      KITWVLAILTLALVWGGYRYTENKHPYTVPIQAGQSK-VAALPVA----- 282
NAV AmoB1       KVAWIVLIATFGIVWGGYRYTETKHPYTVPIQAGESK-VQPMPVK----- 277
NAV AmoB2       KVAWIVLIATFGIVWGGYRYTETKHPYTVPIQAGESK-VQPMPVK----- 277
NAV AmoB3       KVAWIVLIATLALVWGGYRYTETKHPYTVPIQAGESK-VQPMPVK----- 277
NMU AmoB        KVAWVVLILTFGIVWGGYRYTETKHPYTVPIQAGESK-VEPLPVK----- 276
C113 AmoB       KVTIGVLVGVLLIVLFGYKSAEEKFPVTIPLQAGLLGTIEPLPVDY---- 284
NOC AmoB        KLTIGVLVGVLLIILFGFKSAEDKFPVTIPLQAGLLGTIDSLPVDY---- 261
                 :       .          :    * * *:***    : .:

MCB PmoB1       -APTVSVKVEDATYRVPGRAMRMKLTITNHGNSPIRLGEFYTASVRFLDS 327
MCB PmoB2       -APTVSVKVEDATYRVPGRAMRMKLTITNHGNSPIRLGEFYTASVRFLDS 327
MNI PmoB        -QPTVSVKVVDASYRVPGRAMQMTLEITNNGDSAVRLAEFNTASVRFLDA 327
MTR PmoB        GPHVVTAELKGGVYKVPGRELTIQVKVTNKTDEPLKLGEYTAAGLRFLNP 340
MCYS PmoB       GKEQVTTELNGGVYKVPGRELTINVKVKNGTSQPVRLGEYTAAGLRFLNP 329
SC2 PmoB1       GKERVTSELNGGVYKVPGRELTINVKVTNSTSEPLRLGEYTAAGLRFLNP 329
SC2 PmoB2       -RSTVAVQFKGGSYTVPGRELRIRAKVTNNGKEPIRLGEFTSAGLRFLNP 337
MAC PmoB        PESPIKVEYLRGTYKVPGRELVATYKITNTGKEPVRVGEFATATLRFLNP 332
UNC PmoB        DSGPITIKYLNGTYKVPGRELVANFKITNNGKEPLRIGEFNTAGLRFLNP 338
NEU AmoB        -PNPVSIVITDANYDVPGRALRVTMEVTNNGDIPVTFGEFTTAGIRFINS 331
NCR AmoB        -PNPVAIKVTHANYDVPGRALRVTMSITNNGDTGINIGEFTTAGVRFVNA 331
ENI11 AmoB      -PNPVSIVITDANYDVPGRALRVTMEVTNNGDIPVTFGEFTTAGIRFINS 331
NAV AmoB1       -PNPIAIKVTHANYDVPGRALRVTMSVTNSGDTAYRIGEFTTAGVRFINK 326
NAV AmoB2       -PNPIAIKVTHANYDVPGRALRVTMSVTNSGDTAYRIGEFTTAGVRFINK 326
NAV AmoB3       -PNPIAIKVTHANYDVPGRALRVTMSVTNSGDTAYRIGEFTTAGVRFINK 326
NMU AmoB        -PNPIAIKVTHANYDVPGRALRVTMSVTNSGDKPYRIGEFTTAGVRFINK 325
C113 AmoB       -NSMVSAKVLKANYRVPGRTITMTVELTNHTDQVLSIGEFNTGGIRFMNA 333
NOC AmoB        -NSMVSANVLKANYRVPGRTISMTVEITNHTDQVISIGEFNTGGIRFMNA 310
                    :      . * **** :     :.*  .    ..*: :. :**::
```

```
MCB PmoB1       D-VYKDTTGYPEDLLAEDGLSVSDNSPLAPGETRTVDVTASDAAWEVYRL 376
MCB PmoB2       D-VYKDTTGYPEDLLAEDGLSVSDNSPLAPGETRTVDVTASDAAWEVYRL 376
MNI PmoB        D-VYEDDTNYPDDLLAEEGLSVSDNSPLAPGETRTVDVTASDAAWEVYRL 376
MTR PmoB        D-VFTTKPEFPDYLLADRGL-STDPTPLAPGETKTIEVKVQDARWDIERL 388
MCYS PmoB       T-VFTQKPDFPDYLLADRGL-SND-DVIAPGESKEIVVKIQDARWDIERL 376
SC2 PmoB1       D-VFTTKPDFPDYLLADRGL-STDPTPIAPGETKEIAVKVQDARWDIERL 377
SC2 PmoB2       D-VFTTRPDFPDYLLADRGLSVSDPNPIAPGETRDLEVIVQDARFDIERL 386
MAC PmoB        D-VYTQKVDYPEYILAERGLSLSDNAPIAPGETKELTVKVQDARWDTERL 381
UNC PmoB        D-VYTAKVVYPDYLLAERGLSLNDNSPIAPGETRDVAVTVQDARWDTERL 387
NEU AmoB        TGRKYLDPQYPRELIA-VGLNFDDESAIQPGQTKELKMEAKDALWEIQRL 380
NCR AmoB        LGQEHLDPAYPRELVA-TGLSMDDDTAIEPGETREVKMEAKDALWEVQRL 380
ENI11 AmoB      TGRKYLDPQYPRELIA-VGLNFDDESAIQPGQTKELKMEAKDALWEIQRL 380
NAV AmoB1       VGLKHLDRNYPKELVA-TGLSFDNDAPIQPGETREVKMVAKDALWEVQRL 375
NAV AmoB2       VGLKHLDRNYPKELVA-TGLSFDNDALIQPGETREVKMEAKDALWEVQRL 375
NAV AmoB3       VGLKHLDRNYPKELVA-TGLSFDNDAPIQPGETREVKMEAKDALWEVQRL 375
NMU AmoB        VGLKHLDRGYPKELVA-TGLSFDNETPIQPGETREVKMEAKDALWEVQRL 374
C113 AmoB       N-VRSDDTGYPEELLAPEGLEMSQQD-IAPGETVVVDISATDAAWEVQRM 381
NOC AmoB        N-VRVDETDYPEELLAPEGLEVSQQD-IAPGETVVVDISATDAAWEVQRM 358
                          :*  ::*  **   :   : **::  : :   ** ::  *:

MCB PmoB1       SDIIYDPDSRFAGLLFFFDATGNRQVVQIDAPLIPSFM----- 414
MCB PmoB2       SDIIYDPDRRFAGLLFFFDATGNRQVVQIDAPLIPSFM----- 414
MNI PmoB        ADLIYDPDSRFAGLLFFIDEDGNRQMTMVDAPLIPTFI----- 414
MTR PmoB        SDLAYDTDSQIGGLLMFFSPSGKRYATEIGGPVIPKFVAGDMP 431
MCYS PmoB       SDLAYDTDSQVGGLLFFFTPDGKRFAAEIGGPVIPKFVAGDMP 419
SC2 PmoB1       SDLAYDTDSQIGGLLMFFSPTGRRFAAEIGGPVIPKFVAGDMP 420
SC2 PmoB2       SDLAYDTDSQFGGLLFFFSPSGERQRAEIGGPVIPKFQAGATL 429
MAC PmoB        ADLAYDVDSSFAGLMFFFTPSGARYEVETGGPVIPEFLP---- 420
UNC PmoB        SGLAYDVDSSFAGVLFFFSPSGARYPMEVGGPVIPTFMPV--- 427
NEU AmoB        MALLGDPESRFGGLLMSWDAEGNRHINSIAGPVIPVFTKL--- 420
NCR AmoB        MALLGDPESRFGGLLMTWDEEGNRYINSIAGAVIPVFS----- 418
ENI11 AmoB      MALLGDPESRFGGLLMSWDAEGNRHINSIAGPVIPVFTKL--- 420
NAV AmoB1       MALLGDPESRFGGLLMTWSDSGDRNINSIAGAVIPVFTKL--- 415
NAV AmoB2       MALLGDPESRFGGLLTTWSDSGDRNINSIAGAVIPVFTKL--- 415
NAV AmoB3       MALLGDPESRFGGLLMTWSDSGDRNINSIAGAVIPVFTKL--- 415
NMU AmoB        MALLGDPESRFGGLLMTWSEDGDRNINSIAGAVIPVFTKL--- 414
C113 AmoB       ADVIYDPDSRFAGLIFFIDPEGNEIPIPVGGPLVPTFV----- 419
NOC AmoB        ADVIYDPDSRFAGLIFFVDPEGNEIPIPIGGPLVPTFV----- 396
                  :  * :* ..*::                ::  :
```

PmoC/AmoC

```
MCB PmoC1       -------------------------------------MAATTIGG------ 8
MCB PmoC2       -------MHETKQGGEKRFTGAICRCSHRYNSMEVKMAATTIGG------ 37
MCB PmoC3       -------------------------------------MATTTAGG------ 8
MNI PmoC        -------------------------------------MAATTESV--K--- 9
MTR PmoC        -------------------------------------MSVTTET------- 7
MCYS PmoC       -------------------------------------MSSTTST------- 7
SC2 PmoC1       -------------------------------------MSSTTDT------- 7
SC2 PmoC2       -------------------------------------MNQTTEK-----AV 9
GSC PmoC        -------------------------------------MSSTTET------- 7
MAC PmoC        -------------------------------------MSLITETS--PSRA 12
UNC PmoC        MAPSISLAPTPRWAAPRVSTAKPGLNPQQHSKEASDMSLVTGT----AHT 46
NEU AmoC2       -------------------------------------MATTLGTS-SASSV 13
NEU AmoC3       -------------------------------------MATSILKDKTAQQV 14
NET AmoC        -------------------------------------MATNILKDKAAQQV 14
ENI11 AmoC2     -------------------------------------MATTLGTS-SASSV 13
TK794 AmoC      -------------------------------------MATTLGTS-SASSV 13
NAV AmoC2       -------------------------------------MATTLGTSGSHAGS 14
NAV AmoC3       -------------------------------------MATTLGTSGSHAGS 14
NAV AmoC4       -------------------------------------MATTVETSGSHAGS 14
NMU AmoC1       ----------------------------------MSAITPETIAVGHKRESS 18
NMU AmoC2       -------------------------------------MATTMGTS-SPAKT 13
NAC AmoC        -------------------------------------MAATSRA-----VA 9
```

```
MCB PmoC1       ---AAAAEAPLLDKKWLTFALAIYTVFYLWVRWYEGVYGWSAGLDSFAPE 55
MCB PmoC2       ---AAAAEAPLLDKKWLTFALAIYTVFYLWVRWYEGVYGWSAGLDSFAPE 84
MCB PmoC3       ---IAAIDRLLLDKKWLVFAIGIYTVFYLWVRWYEGVYGWSAGLDSFAPE 55
MNI PmoC        ---ADAAEAPLLNQKNIIAGASLYLVFYAWVRWYEGVYGWSAGLDSFAPE 56
MTR PmoC        TAGAAAGSDAIVDLRGMWVGVAGLNIFYLIVRIYEQIYGWRAGLDSFAPE 57
MCYS PmoC       AAGAAAEVESVVDLRGMWIGLAVLNVFYLIVRIYEQVFGWRAGLDSFAPE 57
SC2 PmoC1       AARAAAGTEAVVDLKGMWIGLAVLNGFYLVVRIYEQIYGWRAGLDSFAPE 57
SC2 PmoC2       SAAQAGETDTIVNYKPAYITMGVMLVFYVGIRVYEQYFGWKAGLDSFAPE 59
GSC PmoC        AAGAAAGTDTVVDLRGMWIGLVVLDIFYLIVRIYEQVFGWRAGLDSFAPE 57
MAC PmoC        DAAALSAATPVWDPKPFIIGTVALTVFYIGVRIYEQVFGWYAGLDSFSPE 62
UNC PmoC        GEAAAVAEAPLFNGMPLILGTIAINAFYIGVRIYEQVFGQFAGLDSFAPE 96
NEU AmoC2       SSR-GYDMSLWYDSKFYKFGMITMLLVAIFWVWYQRYFAYSHGMDSMEPE 62
NEU AmoC3       TDKPAYDKSEWFDAKYYKYGLLPILGIAVFWVWYQRTFAYSHGMDSMEPD 64
NET AmoC        ADKPTYDKSEWFDAKYYKFGLLPILAVAVMWVYFQRTYAYSHGMDSMEPE 64
ENI11AmoC2      SSR-GYDMSLWYDSKFYKFGMITMLLVAIFWVWYQRYFAYSHGMDSMEPE 62
TK794 AmoC      SSR-GYDMSLWYDSKFYKFGLITMLLVAIFWVWYQRYFAYSHGMDSMEPE 62
NAV AmoC2       SGR-DYDMSLWYDSRWYKFGLITMLGVAIFWIWFQRTFAYSHGMDSMEPE 63
NAV AmoC3       SGR-DYDMSLWYDSRWYKFGLITMLGVAIFWIWFQRTFAYSHGMDSMEPE 63
NAV AmoC4       SGR-DYDMSLWYDSRWYKFGLITMLGVAIFWIWFQRTFAYSHGMDSKEPE 63
NMU AmoC1       ASSAAYDMSEWYDSRFYKLGLLPILGMAVFWVWFQRTYAYSHGMDSMEPE 68
NMU AmoC2       SGR-DYDMSLWYDSKWYKFGLITMLAVAIFWIWYQRTFAYSHGMDSMEPE 62
NOC AmoC        QGVAEKETADLFAWRGMWLAVAAFFAFYICVRWYEGVYGWKYGLDAFSPE 59
                                       .      ::  :.   *:*:  *:

MCB PmoC1       FETYWMNFLYTEIVLEIVTASILWGYLWKTRDR--NLAALTPREELRRNF 103
MCB PmoC2       FETYWMNFLYTEIVLEIVTASILWGYLWKTRDR--NLAALTPREELRRNF 132
MCB PmoC3       FETYWMNFLYTEIVLEIVTASILWGYLWKTRDR--NLAALTPREELRRNF 103
MNI PmoC        FETYWMNFLYIEMVLEVLTASILWGYIWKSRDR--KVMSITPREELRRHL 104
MTR PmoC        FQTYWLSILWTEIPLELVSGLALAGWLWKTRDR--NVDAVAPREELRRHV 105
MCYS PmoC       FQTYWMSILWTEIPLELVSGLGLAGYLWKTRDR--NVDAVAPREEMRRLV 105
SC2 PmoC1       FQTYWMSILWTEIPLELISGIGLAGFLWKTRTR--DFSTLTAREEMRRLV 105
SC2 PmoC2       FQTYWMNLMWTELPLEFVAFCGIGGYLWKTRDR--NIDAVAPREEMRRIL 107
GSC PmoC        FQTYWLSILWTEIPLELVSGIGLAGYLWKTRDR--NVDAVAPREEMRRLV 105
MAC PmoC        FQKYWMTILYIEEPTELIAFLGLIGYLWKTRPN--DLDTVAPREELRRIF 110
UNC PmoC        FTTYWMTILYIEEPVELISFLALVGWMWKTRDM--DVANVAPREEMRRVF 144
NEU AmoC2       FDRVWMGLWRVHMAIMPLFALVTWGWILKTRDTKEQLDNLDPKLEIKRYF 112
NEU AmoC3       FDRIWMGLWRVQMVVIALAAFSIWGWLLKTRNTAEQLASLTPKQEIKRYF 114
NET AmoC        FDRIWMGLWRVQMAVLPLIALFTWGWLYKTRNTAEQLANLTPKQEIKRYF 114
ENI11 AmoC2     FDRVWMGLWRVHMAIMPLFALVTWGWIMKTRDTKEQLDNLDPKLEVKRYF 112
TK794 AmoC      FDRVWMGLWRVHMAIMPLFALVTWGWIWKTRDTEEQLNNLXPKLEIKRYF 112
NAV AmoC2       FEKVWMGLWRVHMIVMPIFALVTWGWIWKTRDT--NLDNLDPKLEIKRYF 111
NAV AmoC3       FEKVWMGLWRVHMIVMPIFALVTWGWIWKTRDT--NLDNLDPKLEIKRYF 111
NAV AmoC4       FEKVWMGLWRVHMIVMPIFALVTWGWIWKTRDT--NLDNLDPKLEIKRYF 111
NMU AmoC1       FEQIWMGLWRFQMMLWPTLALIVWGWIWKTRDTQEQLASLAVKKEIKRYF 118
NMU AmoC2       FEKVWMGLWRVHMIVMPLFALITWGWIWKTRDTKEQLDNLDPKLEVKRYF 112
NOC AmoC        FQTYWMNLLYIELVVEALATAALVSYLIKTRDR--NMEAMTPREELRRYC 107
                *   *: :   .            .:: *:*    ..  :  : *::*
```

```
MCB PmoC1       THLVWLVAYAWAIYWGASYFTEQDGTWHQTIVRDTDFTPSHIIEFYLSYP 153
MCB PmoC2       THLVWLVAYAWAIYWGASYFTEQDGTWHQTIVRDTDFTPSHIIEFYLSYP 182
MCB PmoC3       THLVWLVAYAWAIYWGASYFTEQDGTWHQTIVRDTDFTPSHIIEFYLSYP 153
MNI PmoC        THWTWLMMYGIAIYFGASYFTEQDGTWHQTIVRDTDFTPSHIIEFYLSYP 154
MTR PmoC        VLVEWLVVYAVAIYWGASFFTEQDGTWHMTVIRDTDFTPSHIIEFYMSYP 155
MCYS PmoC       VLVQWLVVYGIAIYWGASFFTEQDGAWHMTVIRDTDFTPSHIIEFYMSYP 155
SC2 PmoC1       VEVQWLVVYAAAIYWGASFFTEQDGTWHMTVIRDTDFTPSHIIEFYMSYP 155
SC2 PmoC2       TLIGWLAVYAFSVYWGASYFTEQDGTWHQTVIRDTDFTPSHILEFYLSYP 157
GSC PmoC        NLVQWLTVYGIAIYWGASFFTEQDGTWHMTVIRDTDFTPSHIIEFYMSYP 155
MAC PmoC        YLFNWIFVYGVAIYWGASYFTEQDGTWHQTVIRDTDFTPSHIIEFYMSYP 160
UNC PmoC        NLISWIMMYGIAIYWGASYFTEQDGTWHMTVIRDTDFTPSHIIEFYMSYP 194
NEU AmoC2       YYMMWLGVYIFGVYWGGSFFTEQDASWHQVIIRDTSFTPSHVVVFYGSFP 162
NEU AmoC3       YFMMWLGVYIFAVYWGSSFFTEQDASWHQVIIRDTSFTPSHIPLFYGSFP 164
NET AmoC        YFLMWLGVYIFAVYWGSSFFTEQDASWHQVIIRDTSFTPSHIPLFYGSFP 164
ENI11 AmoC2     YYMMWLGVYIFGVYWGGSFFTEQDASWHQVIIRDTSFTPSHVVVFYGSFP 162
TK794 AmoC      YYMMWLGVYIXGVYWGGSFFTGQDASWHQVIIRDTSFTPSHVVVFYGSFP 162
NAV AmoC2       YWMMWLGVYLFGVYWGGSFFTGQDASWHQVIIRDTSFTPSHVVVFYGSFP 161
NAV AmoC3       YWMMWLGVYLFGVYWGGSFFTEQDASWHQVIIRDTSFTPSHVVVFYGSFP 161
NAV AmoC4       YWMMWLGVYLFGVYWGGSFFTEQDASWHQVIIRDTSFTPSHVVVFYGSFP 161
NMU AmoC1       YFLMWLGVYMFAVYWGSSFFTEQDASWHQVIIRDTSFTPSHIPLFYGAFP 168
NMU AmoC2       YWMMWLGVYLFGVYWGGSFFTEQDASWHQVIIRDTSFTPSHVVVFYGSFP 162
NOC AmoC        TLYMWWVVYGVGLFWGASFFTEQDGAWHQTVVRDTDFTPSHIIEFYMSYP 157
                    *   *  .::::*.*:** **.:** .::***.*****:  ** ::*

MCB PmoC1       IYIITGFAAFIYAKTRLPFFA-KGISLPYLVLVVGPFMILPNVGLNEWGH 202
MCB PmoC2       IYIITGFAAFIYAKTRLPFFA-KGISLPYLVLVVGPFMILPNVGLNEWGH 231
MCB PmoC3       IYIITGFAAFIYAKTRLPFFA-KGISLPYLVLVVGPFMILPNVGLNEWGH 202
MNI PmoC        IYIITGGASFLYAKTRLPTYQ-QGLSLQYLVVVVGPFMILPNVGLNEWGH 203
MTR PmoC        IYSIMAVGAFFYAKTRIPYFA-HGFSLAFLIVAIGPFMIIPNVGLNEWGH 204
MCYS PmoC       IYSVIAVGAFFYAKTRIPYFA-HGYSLAFLIVAIGPFMIIPNVGLNEWGH 204
SC2 PmoC1       IYSVIAVGGFFYAKTRLPYFA-KGYSVAYLIVAIGPFMIIPNVGLNEWGH 204
SC2 PmoC2       IYIICGWGAFMYAHTRIPQFA-KRISLAFLMFFAGPFMIFPNIGLNEWGH 206
GSC PmoC        IYSVIAVGAFFYAKTRIPFFA-HGYSLAFLIVAIGPFMIIPNVGLNEWGH 204
MAC PmoC        IYIIMGVGGFVYARTRLPTFGSKGYSVAYLLLFVGPFMIFPNVALNEWGH 210
UNC PmoC        MYIVIGVGGFMYARTRLPTYACKGWSIAYVLLFVGPFMIFPNVGLNEWGH 244
NEU AmoC2       MYIVCGVATYLYAMTRLPLFS-RGISFPLVMAIAGPLMILPNVGLNEWGH 211
NEU AmoC3       VYIIMGIAMIIYAKTRLPLYN-KGWSFPLIMVVAGPLMSLPNVGLNEWGH 213
NET AmoC        VYIIMGVSMIIYANTRLPLYN-KGWSFPLIMTVAGPLMSLPNVGLNEWGH 213
ENI11 AmoC2     MYIVCGVATYLYAMTRLPLFS-RGISFPLVMAIAGPLMILPNVGLNEWGH 211
TK794 AmoC      MYIVCGVATYLYAMTRLPLFH-RGISFPLVMAIAGPLMILPNVGLNEWGH 211
NAV AmoC2       MYIVCGVASYLYAMTRLPLYA-RGTSFPLLMAIAGPLMILPNVGLNEWGH 210
NAV AmoC3       MYIVCGVASYLYAMTRLPLYA-RGTSFPLVMAIAGPLMILPNVGLNEWGH 210
NAV AmoC4       MYIVCGVASYLYAMTRLPLYA-RGTSFPLVMAIAGPLMILPNVGLNEWGH 210
NMU AmoC1       MYIIMGVSTFLYASTRLPLYN-KGTSFPLLMAIAGPLMSLPNVGLNEWGH 217
NMU AmoC2       MYIVCGIASYLYAMTRLPLYS-RGTSFPLVMAIAGPLMILPNVGLNEWGH 211
NOC AmoC        IYVMVGLGSFTYAKTRIPYFA-KGWSVPYLMLVFGPFMIFPNVGLNEWGH 206
                :* : . .   ** **:* :  :  *.  ::   **:* :**:.******
```

```
MCB PmoC1       TFWFMEELFVAPLHYGFVIFGWLALAVMGTLTQTFYRFAQGGLGQSLCEA 252
MCB PmoC2       TFWFMEELFVAPLHYGFVIFGWLALAVMGTLTQTFYSFAQGGLGQSLCEA 281
MCB PmoC3       TFWFMEELFVAPLHYGFVIFGWLALAVMGTLTQTFYSFSH-LFERDLCPD 251
MNI PmoC        TFWFMEELFVAPLHYGFVFFGWSALGVLGVINIELGALSK-LLKKDLA-- 250
MTR PmoC        TFWFMEELFVAPLHWGFVFFGWMALGVFGVVLQILMGVKRLIG--KDCVA 252
MCYS PmoC       TFWFMEELFVAPLHWGFVFFGWMALGVFGVVLQILGRIHALIG--KEGVA 252
SC2 PmoC1       TFWFMEELFVAPLHWGFVFFRWMALGVFGVVLQLLINIQRLIG--KEGVA 252
SC2 PmoC2       TFWFMEELFTAPLHWGFVFFGWFALAVFGVARQVLDRVIELSKEYEKDAL 256
GSC PmoC        TFWFMEELFVAPLHWGFVFFGWMALGVFGVVLQILARIHALVG--KEGVA 252
MAC PmoC        TFWFMEELFVAPLHWMFVFFGWFMLSVFGVSLQILGRIKELCTGYEDVVG 260
UNC PmoC        TFWFMEELFVEPLHWMFVFFGWFSLAVFGVTLQLIGRVVELAHGHEELLG 294
NEU AmoC2       AFWFMEELFSAPLHWGFVVLGWAGLFQGGVAAQIITRYSNLTDVVWNNQS 261
NEU AmoC3       AFWFMEELFSAPLHWGFVILAWAALFQGGLAIQLITRYSNLVDVEWNKQD 263
NET AmoC        AFWFMEELFSAPLHWGFVILAWAALFQGGLAVQIIARFSNLLDVEWNKQD 263
ENI11 AmoC2     AFWFMEELFSAPLHWGFVVLGWAGLFQGGVAAQIITRYSNLTDVIWNNQS 261
TK794 AmoC      AFWFMEELFSAPLHWGFVVLGWAGLFQGGVAAQIITRYSNLTDVVWNNQS 261
NAV AmoC2       AFWFMEELFSAPLHWGFVILGWSGLFAGGIAAQIITRYSSLTDVVWNGQS 260
NAV AmoC3       AFWFMEELFSAPLHWGFVILGWSGLFAGGIAAQIITRYSNLTDVVWNGQS 260
NAV AmoC4       AFWFMEELFSAPLHWGFVILGWSGLFAGGIAAQIITRYSNLTDVVWNGQS 260
NMU AmoC1       AFWFMEELFSAPLHWGFVVLAWAALFSGGIAVQVIARFSNLMDVQWNRQS 267
NMU AmoC2       AFWFMEELFSAPLHWGFVILGWSGLFAGGIAAQIITRYSNLTDVVWNGQS 261
NOC AmoC        TFWFMEELFVAPLHWGFVFFAWFILAVFGVFLQVQPRMKELIG--RELQQ 254
                :******** ***: **.: *  *   *

MCB PmoC1       VDEGLIAK------ 260
MCB PmoC2       VDEGLIAK------ 289
MCB PmoC3       IR------------ 253
MNI PmoC        --------------
MTR PmoC        ALVG---------- 256
MCYS PmoC       LLTE---------- 256
SC2 PmoC1       LLTE---------- 256
SC2 PmoC2       AL------------ 258
GSC PmoC        LLT----------- 255
MAC PmoC        LEPAE--------- 265
UNC PmoC        LEPAE--------- 299
NEU AmoC2       KEILNNRIVA---- 271
NEU AmoC3       RAILDDVVTTP--- 274
NET AmoC        RAILDDVITAP--- 274
ENI11 AmoC2     KEILNNRVVA---- 271
TK794 AmoC      KEILNNRVVA---- 271
NAV AmoC2       KVILNNRIVP---- 270
NAV AmoC3       KVILNNRIVP---- 270
NAV AmoC4       KVILNNRIVP---- 270
NMU AmoC1       RVILDNVV------ 275
NMU AmoC2       KVILNNRIVPYDKA 275
NOC AmoC        SEDYARS------- 261
```